

# Exact analysis of the subthreshold variability for conductance-based neuronal models with synchronous synaptic inputs

Logan A. Becker,<sup>1, 2</sup> Baowang Li,<sup>3, 4, 2, 5</sup> Nicholas J. Priebe,<sup>4, 1, 2</sup> Eyal Seidemann,<sup>3, 2, 5</sup> and Thibaud Taillefumier<sup>1, 6, 2, \*</sup>

<sup>1</sup>*Center for Theoretical and Computational Neuroscience, The University of Texas at Austin*

<sup>2</sup>*Department of Neuroscience, The University of Texas at Austin*

<sup>3</sup>*Center for Perceptual Systems, The University of Texas at Austin*

<sup>4</sup>*Center for Learning and Memory, The University of Texas at Austin*

<sup>5</sup>*Department of Psychology, The University of Texas at Austin*

<sup>6</sup>*Department of Mathematics, The University of Texas at Austin*

The spiking activity of neocortical neurons exhibits a striking level of variability, even when these networks are driven by identical stimuli. The approximately Poisson firing of neurons has led to the hypothesis that these neural networks operate in the asynchronous state. In the asynchronous state neurons fire independently from one another, so that the probability that a neuron experience synchronous synaptic inputs is exceedingly low. While the models of asynchronous neurons lead to observed spiking variability, it is not clear whether the asynchronous state can also account for the level of subthreshold membrane potential variability. We propose a new analytical framework to rigorously quantify the subthreshold variability of a single conductance-based neuron in response to synaptic inputs with prescribed degrees of synchrony. Technically we leverage the theory of exchangeability to model input synchrony via jump-process-based synaptic drives; we then perform a moment analysis of the stationary response of a neuronal model with all-or-none conductances that neglects post-spiking reset. As a result, we produce exact, interpretable closed forms for the first two stationary moments of the membrane voltage, with explicit dependence on the input synaptic numbers, strengths, and synchrony. For biophysically relevant parameters, we find that the asynchronous regime only yields realistic subthreshold variability (voltage variance  $\simeq 4 - 9 \text{mV}^2$ ) when driven by a restricted number of large synapses, compatible with strong thalamic drive. By contrast, we find that achieving realistic subthreshold variability with dense cortico-cortical inputs requires including weak but nonzero input synchrony, consistent with measured pairwise spiking correlations. We also show that without synchrony, the neural variability averages out to zero for all scaling limits with vanishing synaptic weights, independent of any balanced state hypothesis. This result challenges the theoretical basis for mean-field theories of the asynchronous state.

## I. INTRODUCTION

A common and striking feature of cortical activity is the high degree of neuronal spiking variability [1]. This high variability is notably present in sensory cortex and motor cortex, as well as in regions with intermediate representations [2–5]. The prevalence of this variability has led to it being a major constraint for modeling cortical networks as achieving high variability in biophysically relevant spiking networks poses a number of challenges. Cortical neurons are thought to receive a large number of synaptic contacts ( $\simeq 10^4$ ) [6], which are commonly thought to operate asynchronously [7–9]. In the asynchronous state, neurons fire independently from one another, so that the probability that a neuron experiences synchronous synaptic inputs is exceedingly low. Although the impact of such asynchronous inputs varies across synapses, the law of large numbers implies that variability should average out when integrated at the soma. In principle, this would lead to clock-like spiking responses, contrary to experimental observations [10].

A number of mechanisms have been proposed to explain how high spiking variability emerges in cortical net-

works [11]. The prevailing approach posits that excitatory and inhibitory inputs converge on cortical neurons in a balanced manner. In balanced models, the overall excitatory and inhibitory drives cancel each other so that transient imbalances in the drive can bring the neuron’s membrane voltage across the spike-initiation threshold. Such balanced models result in spiking statistics that match those found in the neocortex [12–16].

While the high spiking variability is an important constraint for generating cortical network modeling, there are other biophysical signatures that may be employed. We now have access to the subthreshold membrane voltage fluctuations that underlie spikes in awake, behaving animals (see Fig. 1). Membrane voltage recordings reveal two main deviations from the balanced hypothesis: first, in contrast to balanced models, membrane voltage does not hover near spiking threshold and is modulated by the synaptic drive; second, it exhibits non-Gaussian fluctuation statistics with positive skewness [17–19]. In this work, we further argue that membrane voltage recordings reveal much larger voltage fluctuations than predicted by balanced cortical models [20, 21].

How could such large subthreshold variations in membrane voltage emerge? One way that fluctuations could emerge, even for large numbers of input, is if there is synchrony in the driving inputs [22]. In practice, input synchrony is revealed by the presence of positive spik-

\* Corresponding author; ttaillef@austin.utexas.edu

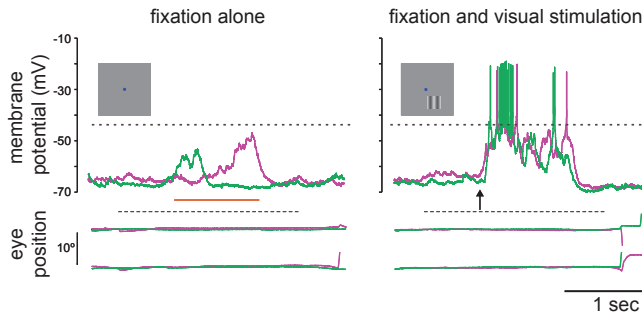


**FIG. 1. Large trial-by-trial membrane voltage fluctuations.** Membrane voltage responses are shown using whole cell recordings in awake behaving primates for both fixation alone trials (left) and visual stimulation trials (right). A drifting grating was presented for 1 second beginning at the arrow. Below the membrane voltage traces are records of horizontal and vertical eye movements, illustrating that the animal was fixating during the stimulus. Red and green traces indicate different trials under the same conditions. Adapted from [18].

ing correlations, which quantify the propensity of distinct synaptic inputs to co-activate. Measurements of spiking correlations between pairs of neurons vary across reports, but have generally been shown to be weak [7–9]. That said, even weak correlations can have a large impact when the population of correlated inputs is large [23, 24]. Further, the existence of input synchrony, supported by weak but persistent spiking correlations, is consistent with at least two other experimental observations. First, intracellular recordings from pairs of neurons in both anesthetized and awake animals reveal a high degree of membrane voltage correlations [25–27]. Second, excitatory and inhibitory conductance inputs are highly correlated with each other within the same neuron [27, 28]. These observations suggest that input synchrony could explain the observed level of subthreshold variability.

While our focus is on achieving realistic subthreshold variability, other challenges to asynchronous networks have been described. In particular, real neural networks exhibit distinct regimes of activity depending on the strength of their afferent drives [29]. In that respect, Zerlaut *et al.* showed that asynchronous networks can exhibit a spectrum of realistic regimes of activity if they have moderate recurrent connections and are driven by strong thalamic projections (see also [16]). Furthermore, it has been a challenge to identify the scaling rule that should apply to synaptic strengths for asynchrony to hold stably in idealized networks [30]. Recently, Sanzeni *et al.* proposed that a realistic asynchronous regime is achieved for a particular large-coupling rule, whereby synaptic strengths scale in keeping with the logarithmic size of the network. Both studies consider balanced networks with conductance-based neuronal models but neither include a role for synchrony, as it would challenge the asynchronous state hypothesis. The asynchronous state hypothesis is theoretically attractive because it represents

a naturally stable regime of activity in infinite-size, balanced networks of current-based neuronal models [13–16]. Such neuronal models, however, neglect the voltage dependence of conductances and it remains unclear whether the asynchronous regime is asymptotically stable for infinite-size, conductance-based network models.

Here, independent of the constraint of network stability, we ask whether biophysically relevant neuronal models can achieve the observed subthreshold variability under realistic levels of input synchrony. To answer this question, we derive exact analytical expressions for the stationary voltage variance of a single conductance-based neuron in response to synchronous shot-noise drives [31, 32]. We develop this analysis for a variant of classically considered neuronal models. We call this variant the all-or-none-conductance-based (AONCB) model for which synaptic activation occurs as an all-or-none process rather than as an exponentially relaxing process. To perform an exact treatment of these models, we develop original probabilistic techniques inspired from Marcus' work about shot-noise driven dynamics [33, 34]. To model shot-noise drives with synchrony, we develop a statistical framework based on the property of input exchangeability, which assumes that no synaptic inputs play a particular role. In this framework, we show that input drives with varying degree of synchrony can be rigorously modeled via jump processes, while synchrony can be quantitatively related to measures of pairwise spiking correlations.

Our main results are biophysically interpretable formulas for the voltage mean and variance in the limit of instantaneous synapses. Crucially, these formulas explicitly depend on the input numbers, weights, and synchrony, and hold without any forms of diffusion approximation. This is in contrast with analytical treatments which elaborate on the diffusion and effective-time-constant approximations [29, 30, 35, 36]. We leverage these exact, explicit formulas to determine under which synchrony conditions a neuron can achieve the experimentally observed subthreshold variability. For biophysically relevant synaptic numbers and weights, we find that achieving realistic variability is possible in response to a restricted number of large asynchronous connections, compatible with the dominance of thalamo-cortical projections in the input layers of the visual cortex. However, we find that achieving realistic variability in response to a large number of moderate cortical inputs, as in superficial cortical visual layers, necessitates nonzero input synchrony in amounts that are consistent with the weak levels of measured spiking correlations observed *in vivo*.

In practice, persistent synchrony may spontaneously emerge in large but finite neural networks, as nonzero correlations are the hallmark of finite-dimensional interacting dynamics. The network structural features responsible for the magnitude of such correlations remains unclear, and we do not address this question here (see [37, 38] for review). The persistence of synchrony is also problematic for theoretical approaches that consider

networks in the infinite-size limits. Indeed, our analysis supports that in the absence of synchrony and for all scaling of the synaptic weights, subthreshold variability must vanish in the limit of arbitrary large numbers of synapses. This suggests that independent of any balanced condition, the mean-field dynamics that emerge in infinite-size networks of conductance-based neurons will not exhibit Poisson-like spiking variability, at least in the absence of additional constraints on the network structure or on the biophysical properties of the neurons. In current-based neuronal models, however, variability is not damped by a conductance-dependent effective time constant. These findings therefore challenge the theoretical basis for the asynchronous state in conductance-based neuronal networks.

Our exact analysis, as well as its biophysical interpretations, is only possible at the cost of several caveats: First, we neglect the impact of the spike-generating mechanism (and of the post-spiking reset) in shaping the subthreshold variability. Second, we quantify synchrony under the assumption of input exchangeability, that is, for synapses having a typical strength as opposed to being heterogeneous. Third, we consider input drives that implement an instantaneous form of synchrony with temporally precise synaptic coactivations. Fourth, we do not consider slow temporal fluctuations in the mean synaptic drive. Fifth, and perhaps most concerning, we do not account for the stable emergence of a synchronous regime in network models. We argue in the discussion that all the above caveats but the last one can be addressed without impacting our findings. Addressing the last caveat remains an open problem.

## II. STOCHASTIC MODELING

In this section, we specify the modeling framework of our analysis. In Section II A, we define the conductance-based neuronal model that is subjected to synchronous inputs. In Section II B, we model synchronous input drives as compound Poisson processes for exchangeable sets of excitatory inputs. In Section II C, we extend our input model to include separately exchangeable sets of excitatory and inhibitory inputs. In Section II D, we recapitulate our modeling approach within Marcus theory about shot-noise driven systems.

### A. All-or-none-conductance-based neurons

We consider the subthreshold dynamics of an original neuronal model, which we called the all-or-none-conductance-based (AONCB) model. In this model, as for virtually all conductance-based models, the membrane voltage  $V$  obeys the first-order stochastic differential equation

$$C\dot{V} = G(V_L - V) + g_e(V_e - V) + g_i(V_i - V) + I, \quad (1)$$

where randomness arises from the stochastically activating excitatory and inhibitory conductances, respectively denoted by  $g_e$  and  $g_i$  (see Fig. 2a). We further consider that both conductances result from the action of  $K_e$  excitatory and  $K_i$  inhibitory synapses:  $g_e(t) = \sum_{k=1}^{K_e} g_{e,k}(t)$  and  $g_i(t) = \sum_{k=1}^{K_i} g_{i,k}(t)$ . In the absence of synaptic inputs, i.e., when  $g_e = g_i = 0$ , and of external current  $I$ , the voltage exponentially relaxes toward its leak reversal potential  $V_L$  with passive time constant  $\tau = C/G$ , where  $C$  denotes the cell's membrane capacitance and  $G$  denotes the cellular passive conductance [39]. In the presence of synaptic inputs, the transient synaptic currents  $I_e = g_e(V_e - V)$  and  $I_i = g_i(V_i - V)$  cause the membrane voltage to fluctuate. Conductance-based models account for the voltage-dependence of synaptic currents via the driving forces  $V_e - V$  and  $V_i - V$ , where  $V_e$  and  $V_i$  denotes the excitatory and inhibitory reversal potential, respectively. Without loss of generality, we assume in the following that  $V_L = 0$  and that  $V_i < V_L = 0 < V_e$ .

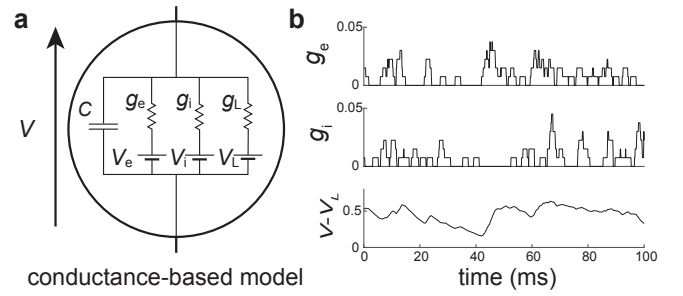


FIG. 2. **All-or-none-conductance-based models.** (a) Electrical diagram of conductance-based model for which the neuronal voltage  $V$  evolves in response to fluctuations of excitatory and inhibitory conductances  $g_e$  and  $g_i$ . (b) In all-or-none models, inputs delivered as Poisson processes transiently activate the excitatory and inhibitory conductances  $g_e$  and  $g_i$  during a finite, nonzero synaptic activation time  $\tau_s > 0$ . Simulation parameters:  $K_e = K_i = 50$ ,  $r_e = r_i = 10\text{Hz}$ ,  $\tau = 15\text{ms}$ ,  $\tau_s = 2\text{ms} > 0$ .

We model the spiking activity of the  $K_e + K_i$  upstream neurons as shot noise [31, 32], which can be generically modeled as a  $(K_e + K_i)$ -dimensional stochastic point process [40, 41]. Let us denote by  $\{N_{e,k}(t)\}_{1 \leq k \leq K_e}$  its excitatory component and by  $\{N_{i,k}(t)\}_{1 \leq k \leq K_i}$  its inhibitory component, where  $t$  denotes time and  $k$  is the neuron index. For each neuron  $k$ , the process  $N_{e/i,k}(t)$  is specified as the counting process registering the spiking occurrences of neuron  $k$  up to time  $t$ . In other words,  $N_i(t) = \sum_k \mathbb{1}_{\{T_{e/i,k,n} \leq t\}}$ , where  $\{T_{e/i,k,n}\}_{n \in \mathbb{Z}}$  denotes the full sequence of spiking times of neuron  $k$  and where  $\mathbb{1}_A$  denotes the indicator function of set  $A$  ( $\mathbb{1}_A(x) = 1$  if  $x$  is in  $A$  and  $\mathbb{1}_A(x) = 0$  if  $x$  is not in  $A$ ). Note that by convention, we label spikes so that  $T_{e/i,k,0} \leq 0 < T_{e/i,k,1}$  for all neuron  $k$ . Given a point-process model for the upstream spiking activity, classical conductance-based models consider that a single input to a synapse causes an instant-

taneous increase of its conductance, followed by an exponential decay with typical time scale  $\tau_s > 0$ . Here we depart from this assumption and consider that the synaptic conductances  $g_{e/i,k}$  operates all-or-none with a common activation time still referred to as  $\tau_s$ . Specifically, we assume that the dynamics of the conductance  $g_{e/i,k}$  follows

$$\dot{g}_{e/i,k}(t) = w_{e/i,k} \sum_n (\delta(t - T_{e/i,k,n}) - \delta(t - T_{e/i,k,n} - \tau_s)), \quad (2)$$

where  $w_{e/i,k} \geq 0$  is the dimensionless synaptic weight. The above equation prescribes that the  $n$ -th spike delivery to synapse  $k$  at time  $T_{e/i,k,n}$  is followed by an instantaneous increase of that synapse's conductance by an amount  $w_{e/i,k}$  for a period  $\tau_s$ . Thus, the synaptic response prescribed by Eq. (2) is all-or-none as opposed to being graded as in classical conductance-based models. However, just as in classical models, Eq. (2) allows synapses to multi-activate via linear superposition, thereby neglecting nonlinear synaptic saturation (see Fig. 2b).

To be complete, AONCB neurons must in principle include a spike-generating mechanism. In that regard, it is customary to consider an integrate-and-fire mechanism [42, 43]: a neuron emits a spike whenever its voltage  $V$  exceeds a threshold value  $V_T$ , and reset instantaneously to some value  $V_R$  afterwards. Such a mechanism impacts the neuronal subthreshold voltage dynamics via post-spiking reset, which implements a nonlinear form of feedback. However, in this work we focus on the variability that is generated by fluctuating, possibly synchronous, synaptic inputs. For this reason, we neglect the influence of the spiking reset in our analysis and actually, we ignore the spike-generating mechanism altogether.

## B. Synchronous input model via exchangeability

Our goal here is to rigorously model synchronous input via compound Poisson processes [40, 41], which in turn will serve as the drive to AONCB neurons. To do so in a principled way, we first consider a discrete model of excitatory synaptic inputs under the assumption of input exchangeability [44, 45]. Specifically, we suppose that the neuron under consideration receives inputs from  $K_e$  neurons, chosen from an arbitrary large—actually soon to be considered infinite—pool of  $N \gg K_e$  neurons. Adopting a discrete-time representation with elementary bin size  $\Delta t$ , we denote by  $\{x_{1,i}, \dots, x_{K_e,i}\}$  in  $\{0, 1\}^{K_e}$  the input state within the  $i$ -th bin. Our main simplifying assumption consists in modeling all  $N$  inputs as exchangeable random variables  $\{X_{1,i}, \dots, X_{N,i}\}$  that are distributed identically over  $\{0, 1\}^N$  and independently across time. Owing to the latter independence property, we drop the dependence on time index  $i$  in the following. By exchangeable, we mean that no combination of inputs plays a distinct role so that at all time,

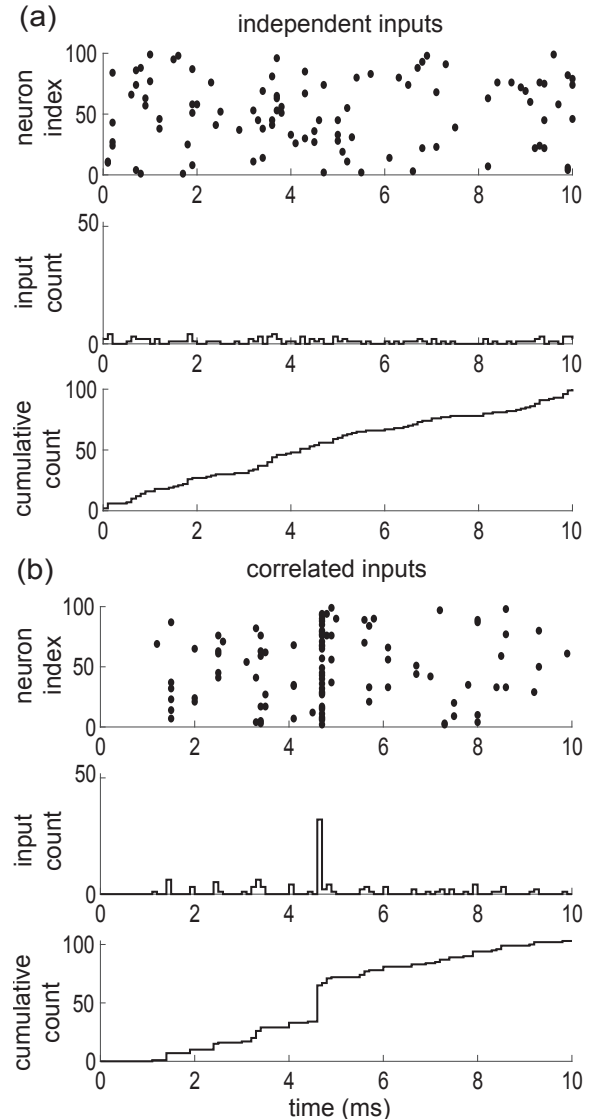


**FIG. 3. Parametrizing correlations via exchangeability.** The activity of  $K_e = 100$  exchangeable synaptic inputs collected over  $N$  consecutive time bins can be represented as  $\{0, 1\}$ -valued array  $\{X_{k,i}\}_{1 \leq k \leq K_e, 1 \leq i \leq N}$ , where  $X_{k,i} = 1$  if input  $k$  activates in time bin  $i$ . Under assumptions of exchangeability, the input spiking correlation is entirely captured by the count statistics of how many inputs coactivate within a given time bin. In the limit  $K_e \rightarrow \infty$ , the distribution of the fraction of coactivating inputs coincides with the directing de Finetti measure, which we consider as a parametric choice in our approach. In the absence of correlation, synapses tend to activate in isolation:  $\rho_e = 0$  in (a). In the presence of correlation, synapses tend to coactivate yielding disproportionately large synaptic activation event:  $\rho_e = 0.1$  in (b). Considering the associated cumulative counts specifies discrete-time jump processes that can be generalized to the continuous-time limit, i.e., for time bins of vanishing duration  $\Delta t \rightarrow 0^+$ .

the distribution of  $\{X_1, \dots, X_N\}$  is independent of the inputs labelling. In other words, for all permutations  $\sigma$  of  $\{1, \dots, N\}$ ,  $\{X_{\sigma(1)}, \dots, X_{\sigma(N)}\}$  and  $\{X_1, \dots, X_N\}$  have identical distribution [44, 45]. By contrast with independent random spiking variables, exchangeable ones can exhibit positive correlations, that is

$$\rho_e = \frac{\mathbb{C}[X_k, X_l]}{\sqrt{\mathbb{V}[X_k] \mathbb{V}[X_l]}} > 0,$$

where  $\rho_e$  denotes the constant pairwise correlation for all  $k \neq l$  and where  $\mathbb{C}[X_k, X_l]$  and  $\mathbb{V}[X_k]$  denote the covariance and the variance of the binary variables  $X_k$ , respectively.

Interestingly, a more explicit form of  $\rho_e$  can be obtained in the limit of an infinite size pool  $N \rightarrow \infty$ . This follows from de Finetti theorem [46], which states that the probability of observing a given input configuration for  $K_e$  neurons is given by

$$\mathbb{P}[X_1, \dots, X_{K_e}] = \int \prod_{k=1}^{K_e} \theta_e^{X_k} (1 - \theta_e)^{1-X_k} dF_e(\theta_e), \quad (3)$$

where  $F_e$  is the directing de Finetti probability measure supported on  $[0, 1]$ . In the equation above, the number  $\theta_e$  simply represents the (fluctuating) probability that a neuron spikes in a given time bin. The core message of de Finetti theorem is that the correlated spiking activity of neurons from an infinite exchangeable pool is obtained as a mixture of conditionally independent binomial laws. This mixture is specified by the directing measure  $F_e$ , which thus fully parametrizes our synchronous input model. Independent spiking corresponds to choosing  $F_e$  as a point-mass measure concentrated on some probability  $p_e = r_e \Delta t$ ,  $0 \leq p_e \leq 1$ , where  $r_e$  denotes the individual spiking rate of an excitatory neuron:  $dF_e(\theta) = \delta(\theta - p_e) d\theta$  (see Fig 3a). By contrast, a dispersed directing measure  $F_e$  corresponds to the existence of correlations among the inputs (see Fig 3b). Accordingly, we show in Appendix A that the spiking pairwise correlation takes the explicit form

$$\rho_e = \frac{\mathbb{V}[\theta_e]}{\mathbb{E}[\theta_e](1 - \mathbb{E}[\theta_e])},$$

where  $\mathbb{E}[\theta_e]$  and  $\mathbb{V}[\theta_e]$  denote the expectation and the variance of  $\theta_e \sim F_e$ , respectively. The above formula reveals that nonzero correlations corresponds to nonzero variance, as is always the case for dispersed distribution.

Observe that an infinity of measures  $F_e$  can achieve the same spiking correlation. This observation is the reason why one can argue that the correlation  $\rho_e$  is not a genuine modeling parameter. Considering  $\rho_e$  as a genuine parameter requires additional assumptions about the form of  $F_e$ . In our exchangeable setting, a reasonable parametric choice for  $F_e$  is given by beta distributions  $\text{Beta}(\alpha_e, \beta_e)$ , where  $\alpha_e$  and  $\beta_e$  denote shape parameters [47]. Practically, this choice is motivated by the ability of beta distributions to efficiently fit correlated spiking data generated by existing algorithms [48]. Formally, this choice is

motivated by the fact that beta distributions are conjugate priors for the binomial likelihood functions, so that the resulting probabilistic models can be studied analytically [49–51]. In particular, for  $F_e \sim \text{Beta}(\alpha_e, \beta_e)$ , the probability that  $k_e$  synapses among the  $K_e$  inputs are jointly active within the same time bin follows the beta-binomial distribution

$$P_{e,k} = \binom{K_e}{k} \frac{B(\alpha_e + k, \beta_e + K_e - k)}{B(\alpha_e, \beta_e)}. \quad (4)$$

Accordingly, the mean number of active excitatory inputs is  $\mathbb{E}[k_e] = K_e \alpha_e / (\alpha_e + \beta_e) = K_e r_e \Delta t$ . Utilizing Eq. (4), we also find that  $\rho_e = 1/(1 + \alpha_e + \beta_e)$  (see Fig. 4a).

Given a typical synaptic weight  $w_e$ , the overall synaptic drive to a neuron is determined by the number of active inputs at each discrete time step, while synchrony is encoded via the probability  $P_{e,k}$ . As AONCB dynamics unfolds in continuous time, we need to consider this discrete drive in the continuous-time limit as well, i.e., for vanishing time bins  $\Delta t \rightarrow 0^+$ . When  $\Delta t \rightarrow 0^+$ , we show in Appendix B that the overall synaptic drive specifies a compound Poisson process  $Y_e$  with variable jump size  $W_e$ , i.e.,

$$Y_e(t) = \sum_{n=0}^{N(t)} W_{e,n}, \quad (5)$$

where  $W_{e,n}$  are i.i.d. samples of  $W_e$  (see Fig. 4c). In the following, we denote the distribution of  $W_e$  as  $p_e$ . Moreover, given a fixed typical synaptic weight  $w_e$ , we show that the jumps are given as  $W_e = k w_e$ , with  $k$  distributed on  $\{1, \dots, K_e\}$  according to

$$p_{e,k} = \lim_{\Delta t \rightarrow 0^+} \frac{P_{e,k}}{1 - P_{e,0}} = \binom{K_e}{k} \frac{B(k, \beta_e + K_e - k)}{\psi(\beta_e + K_e) - \psi(\beta_e)}, \quad (6)$$

where  $\psi$  denotes the digamma function. Observe that the probability to find a spike within a bin is  $\mathbb{E}[X_i] = \alpha_e / (\alpha_e + \beta_e) = r_e \Delta t$ , so that for fixed excitatory spiking rate  $r_e$ ,  $\alpha_e \rightarrow 0^+$  when  $\Delta t \rightarrow 0^+$ . As a result, the continuous-time spiking correlation is  $\rho_e = 1/(1 + \beta_e)$ , so that we can interpret  $\beta_e$  as the parameter controlling correlations. To contrast with expectations with respect to the stationary expectation for  $V$ , denoted by  $\mathbb{E}[\cdot]$ , we denote expectations with respect to the excitatory jump distributions  $p_e$  or  $p_{e,k}$  by  $\mathbb{E}_e[\cdot]$ . In Appendix D, we show that the correlation  $\rho_e$  only depends on the jump distribution  $p_{e,k}$  in the limit  $\Delta t \rightarrow 0^+$  via

$$\rho_e = \frac{\mathbb{E}_e[k(k-1)]}{\mathbb{E}_e[k](K_e - 1)}. \quad (7)$$

This shows that zero spiking correlation corresponds to jump of fixed unit size, i.e., to an input drive modeled as a classical Poisson process, as opposed to a compound Poisson process. For classical Poisson-process models, the overall rate of synaptic events is necessarily equal to the sum of the individual spiking rate:  $b_e = K_e r_e$ . This is no longer the case in the presence of synchronous spiking, when nonzero input correlation  $\rho_e > 0$  arises from

coincidental synaptic activations. Indeed, as the limiting process  $\Delta t \rightarrow 0^+$  conserves the population spiking rate, the rate  $b_e$  of synaptic activation events satisfies  $K_e r_e = b_e \mathbb{E}_e [k]$  so that we have

$$b_e = \frac{K_e r_e}{\mathbb{E}_e [k]} = r_e \beta_e (\psi(\beta_e + K_e) - \psi(\beta_e)). \quad (8)$$

Let us stress for clarity, that if  $k_e$  synapses activate synchronously, this only count as one synaptic event, which can come in variable size  $k$ . Consistently, we have in general  $r_e \leq b_e \leq K_e r_e$ . Further inspection confirms that when  $\beta_e \rightarrow 0$ , we have perfect synchrony with  $\rho_e = 1$  and  $b_e \rightarrow r_e$ , whereas the independent spiking regime with  $\rho_e = 0$  is attained for  $\beta_e \rightarrow \infty$ , for which we have  $b_e \rightarrow K_e r_e$ .

The above parametrization in term of beta distributions offers a principled way to model spiking correlations via the compound Poisson process  $Y_e$  with discrete jump distribution given by  $p_{e,k}$ . There are other possible parametrizations and our result will hold for arbitrary jump distribution  $p_e$ . When considering an arbitrary  $p_e$ , the main caveat is understanding how such a distribution may correspond to a given input number  $K_e$  and spiking correlation  $\rho_e$ . For this reason, we will always consider that  $k_e = W_e/w_e$  follows the distribution  $p_{e,k}$  given in Eq. (6) when discussing the roles of  $w_e$ ,  $K_e$ , and  $\rho_e$  in shaping the voltage response of a neuron.

### C. Correlation between excitation and inhibition via partial exchangeability

One can generalize the modeling of synchronous inputs via compound Poisson processes to include inhibition in addition to excitation. Such a generalization leverages representations akin to Eq. (3) but for the joint probability distributions of  $K_e$  exchangeable excitatory inputs and  $K_i$  exchangeable inhibitory inputs. Accordingly, let us assume that the inputs specify a  $(K_e + K_i)$ -dimensional random variable  $\{X_1, \dots, X_{K_e}, Y_1, \dots, Y_{K_i}\}$  on  $\{0, 1\}^{K_e + K_i}$ . Let us further assume that the excitatory inputs  $X_i$ ,  $1 \leq i \leq K_e$  and the inhibitory inputs  $X_j$ ,  $1 \leq j \leq K_i$  are separately exchangeable. Here, we can only assume partial exchangeability as excitatory and inhibitory inputs are distinguishable [52]. As a result, the directing measure must be chosen as a bivariate distribution  $F_{ei}(\theta_e, \theta_i)$  over the unit square  $[0, 1] \times [0, 1]$ , so that we have

$$\mathbb{P}[X_1, \dots, X_{K_e}, Y_1, \dots, Y_{K_i}] = \int \prod_{k=1}^{K_e} \theta_e^{X_k} (1 - \theta_e)^{1-X_k} \prod_{l=1}^{K_i} \theta_i^{X_l} (1 - \theta_i)^{1-X_l} dF_{ei}(\theta_e, \theta_i).$$

In this setting, we show in Appendix A that the spiking correlation between excitatory and inhibitory inputs is given by

$$\rho_{ei} = \frac{\mathbb{C}[\theta_e, \theta_i]}{\sqrt{\mathbb{E}[\theta_e] \mathbb{E}[\theta_i] (1 - \mathbb{E}[\theta_e])(1 - \mathbb{E}[\theta_i])}} \geq 0, \quad (9)$$

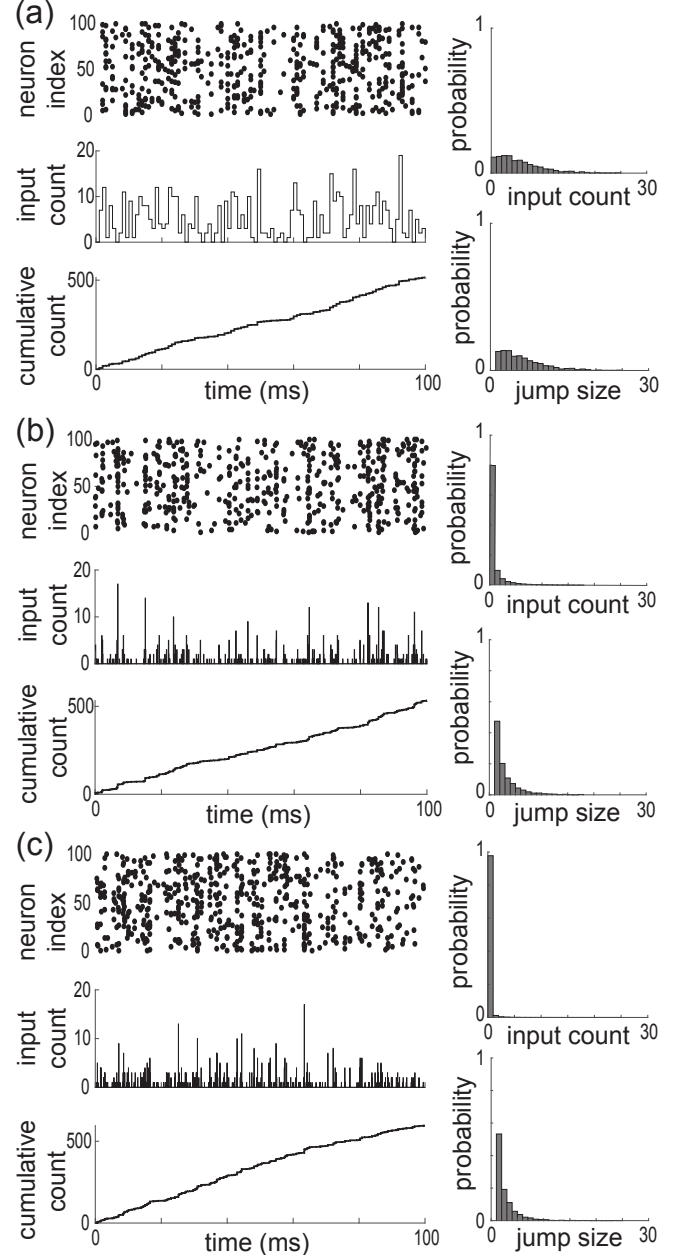


**FIG. 4. Limit compound Poisson process.** (a) Modeling synaptic inputs for a bin size  $\Delta t = 1\text{ms}$  specifies an input count process and a cumulative count process (left) as in Fig. 3. Correlations are parametrized via the distribution  $P_{e,k}$  of the input count  $k_e = \sum_{k=1}^{K_e} X_k$  (top right). Alternatively, the discrete-time cumulative count process encodes correlations via its jump distribution (bottom right):  $P_{e,k}/(1 - P_{e,0})$ . (b) Taking a smaller bin size  $\Delta t = 0.1\text{ms}$  yields similarly looking raster plots and cumulative counts, but an increasing proportion of bins become empty, with zero count. Accordingly, the input-count distribution increasingly concentrates on zero. In the presence of correlation, however, the jump distribution remains dispersed. (c) In the limit  $\Delta t \rightarrow 0$ , the input-count distribution is concentrated on zero. By contrast, the distribution of jump sizes converges toward a well-defined distribution:  $p_{e,k} = \lim_{\Delta t \rightarrow 0^+} P_{e,k}/(1 - P_{e,0})$ . This distribution characterizes the jumps of a limit compound Poisson process.

where  $\mathbb{C}[\theta_e, \theta_i]$  denotes the covariance of  $\theta_e$  and  $\theta_i$ . Thus, independence between excitation and inhibition for which  $\rho_{ei} = 0$  corresponds to directing measure  $F_{ei}$  with product form, i.e.,  $F_{ei}(\theta_e, \theta_i) = F_e(\theta_e)F_i(\theta_i)$ , where  $F_e$  and  $F_i$  denote the marginal distributions. Alternative forms of the directed measure  $F_{ei}$  lead to nonzero cross correlation  $\rho_{ei}$ , which necessarily satisfies  $0 < |\rho_{ei}| \leq \sqrt{\rho_e \rho_i}$ .

Eq. (9) shows that, in principle,  $F_{ei}$  can be chosen as to achieve negative correlations between excitation and inhibition in the discrete setting. However, when shifting to a continuous-time representation, our exchangeability-based modeling approach can only capture nonnegative correlations  $\rho_{ei} \geq 0$ . This is because in the limit of vanishing bin size  $\Delta t \rightarrow 0^+$ , nonzero correlations between excitation and inhibition amounts to having simultaneously activating excitatory and inhibitory synapses. To see this, let us consider a particular case for which the marginals of  $F_{ei}$  are given by the same beta distribution:  $F_e = F_i = F \sim \text{Beta}(\alpha, \beta)$ . Let us further consider two particular coupling for  $\theta_e$  and  $\theta_i$ : (i) the case of maximum positive correlation for  $\theta_e = \theta_i$  and (ii) the case of zero correlation for which  $\theta_e$  and  $\theta_i$  are independent. Note that albeit symmetric, cases (i) and (ii) are not fully exchangeable due to excitation and inhibition being associated to distinct reversal potentials  $V_i < 0 < V_e$ . For the maximally correlated case (i), the probability that  $k$ ,  $1 \leq k \leq K_e$ , excitatory synapses and  $l$ ,  $1 \leq l \leq K_i$ , inhibitory synapses are jointly active within the same time bin follows the modified beta-binomial distribution

$$P_{ei,kl} = \binom{K_e}{k} \binom{K_i}{l} \frac{B(\alpha + k + l, \beta + 2K - k - l)}{B(\alpha, \beta)},$$

whereas for the independent case (ii), this probability is  $P_{ei,kl} = P_{e,k}P_{i,l}$  where  $P_{e,k}$  and  $P_{i,l}$  refers to the same beta-binomial distribution defined by (4) for the parameter  $\alpha$ ,  $\beta$ ,  $K_e$ , and  $K_i$  (see Fig. 5a for  $\rho_e = \rho_i = \rho_{ei}$ ).

As we still have  $r_{e/i}\Delta t = K_{e/i}\alpha/(\alpha + \beta)$ , the derivation of the continuous-time limit proceeds similarly as for the case of excitation alone, by considering vanishing time bins  $\Delta t \rightarrow 0^+$ , which amounts to  $\alpha \rightarrow 0^+$  (see Appendix B). This implies that the excitatory- and inhibitory-specific correlations are both equal to  $\rho_e = \rho_i = 1/(1 + \beta)$  in this limit. However, owing to considering both excitation and inhibition, the continuous-time limit  $\Delta t \rightarrow 0^+$  actually defines two coupled Poisson processes  $(N_e, N_i)$  with associated rates of synaptic events  $b_e$  and  $b_i$  satisfying Eq. (8) for the parameters  $\alpha$ ,  $\beta$ ,  $K_e$  and  $K_i$ , respectively. The key observation is to realize that the coupling between these Poisson processes is mediated by simultaneous excitatory and inhibitory activations. As a result, the continuous-time limit depicting the excitatory and inhibitory drives is specified via a compound Poisson process  $Y$  with bivariate jumps  $(W_e, W_i)$ :

$$Y(t) = \left( \sum_n^{N(t)} W_{e,n}, \sum_n^{N(t)} W_{i,n} \right), \quad (10)$$

where the overall driving Poisson process  $N$  registers the number of synaptic activations without double counts.

Note that this implies that  $\max(N_e(t), N_i(t)) \leq N(t) \leq N_e(t) + N_i(t)$  with  $\max(b_e, b_i) \leq b \leq b_e + b_i$ . For the maximally correlated case (i), we show in Appendix C that the jumps are given as  $(W_e, W_i) = (kw_e, lw_i)$ , with  $(k, l)$  distributed on  $\{0, \dots, K\} \times \{0, \dots, K\} \setminus \{0, 0\}$  (see Fig. 5b and c) according to

$$p_{ei,kl} = \lim_{\alpha \rightarrow 0^+} \frac{P_{ei,kl}}{1 - P_{ei,00}} = \binom{K_e}{k} \binom{K_i}{l} \frac{B(k + l, \beta + K_e + K_i - k - l)}{\psi(\beta + K_e + K_i) - \psi(\beta)}. \quad (11)$$

Incidentally, the driving Poisson process  $N$  has a rate  $b$  determined by adapting Eq. (8)

$$b = r\beta(\psi(\beta + K_e + K_i) - \psi(\beta)),$$

for which one can check that  $r \leq b \leq (K_e + K_i)r$ . By contrast, for the independent case (ii), in the limit  $\alpha \rightarrow 0^+$ , jumps are either excitatory alone or inhibitory alone. In Appendix C, we actually show that

$$p_{ei,kl} = \lim_{\alpha \rightarrow 0^+} \frac{P_k P_l}{1 - P_{e,0} P_{i,0}} = \frac{1}{2} (p_{e,k} \mathbb{1}_{\{l=0\}} + p_{i,l} \mathbb{1}_{\{k=0\}}),$$

where  $p_{e,k}$  and  $p_{i,l}$  are specified by (6) for the parameters  $\alpha$ ,  $\beta$ ,  $K_e$ , and  $K_i$ . Incidentally, the driving process is such that  $N = N_e + N_i$  with rate  $b = b_e + b_i$ .

The two considered cases (i) and (ii) above are only examples of compound Poisson processes modeling jointly excitation and inhibition within AONCB models. In general, such models will be determined by the choice of an overall rate of synaptic events  $b$  and a bivariate jump distribution  $p_{ei}$  for the excitatory jumps  $W_e$  and the inhibitory jumps  $W_i$ . Correlation between excitation and inhibition corresponds to those choices of  $p_{ei}$  for which  $W_e W_i > 0$  with nonzero probability, which indicates the presence of synchronous excitatory and inhibitory inputs. Incidentally, synchrony restricts nonzero correlations to be positive. Then, when  $\rho_{ei} > 0$ , the overall rate of synaptic events  $b$  must be such that  $b < b_e + b_i$  owing to synchronization of excitatory and inhibitory inputs. In the following, we refer to expectations with respect to the joint jump distribution  $p_{ei}$  as  $\mathbb{E}_{ei}[\cdot]$ . This is by contrast with  $\mathbb{E}_e[\cdot]$  which denotes expectation with respect to the distribution of the excitatory jumps alone  $p_e$ .

Ideally, this distribution  $p_{ei}$  should be such that its conditional marginals  $p_e$  and  $p_i$ , with support on  $\{W_e > 0\}$  and  $\{W_i > 0\}$ , respectively, are distributed according to the previously introduced and biophysically interpretable distributions given by Eq. (6) (see Appendix B). Unfortunately, there does not seem to be a simple low-dimensional parametrization for distributions  $p_{ei}$  with such conditional marginals and a varying degree of correlations, except in particular cases such as (i) and (ii). To address this point, one can resort to a variety of methods including copulas [53, 54]. However, these are beyond the scope of the present work. For these reasons, we will perform all our calculations for arbitrary jump joint distribution  $p_{ei}$  on the positive orthant  $(0, \infty) \times (0, \infty)$ . We

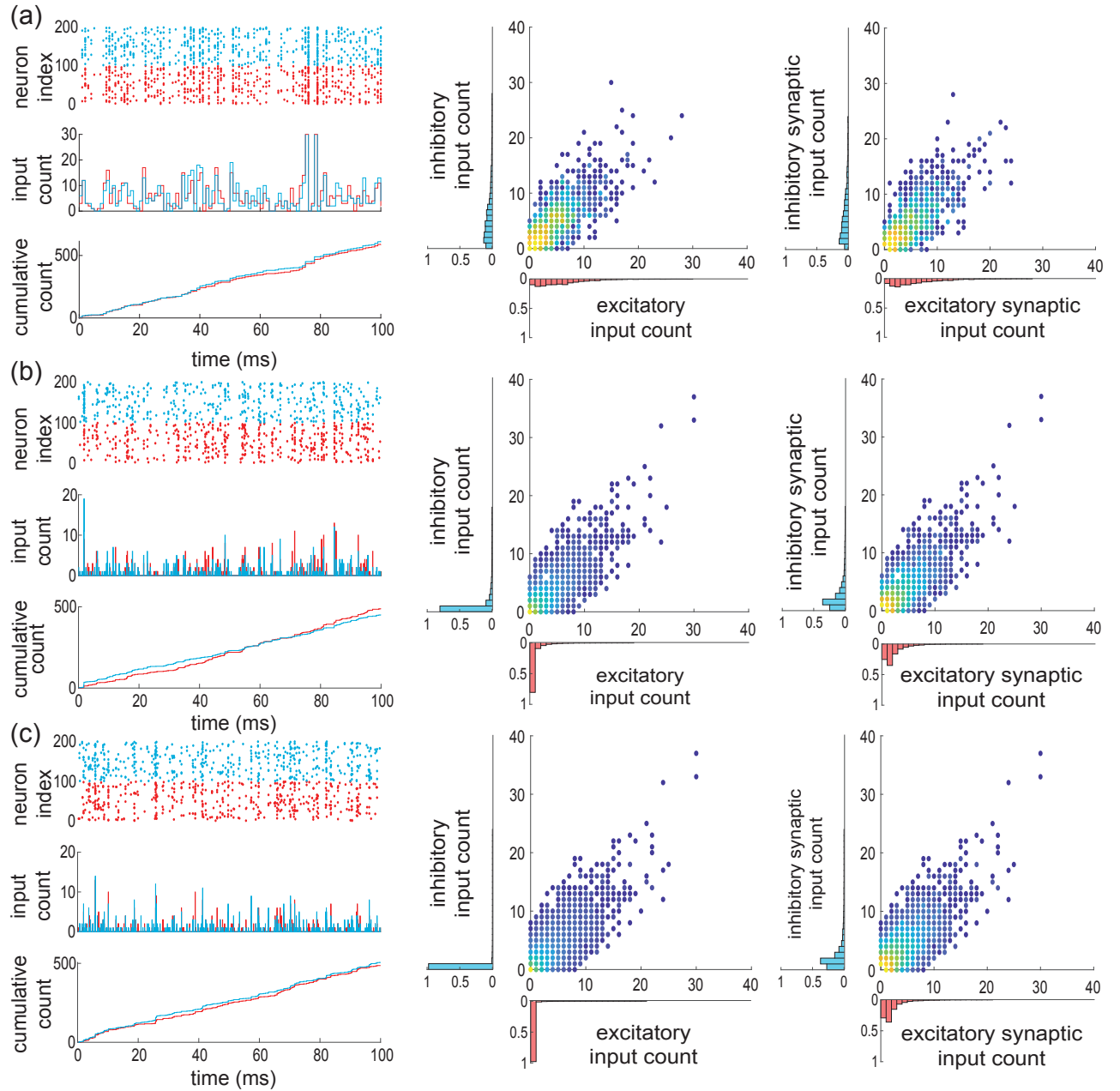


**FIG. 5. Limit compound Poisson process with excitation and inhibition.** The continuous-time limit procedure depicted in Fig. 4 generalizes to the case of joint excitatory and inhibitory inputs, which breaks the assumption of exchangeability. (a) Under assumption of partial exchangeability, synaptic inputs can only be distinguished by the fact that they are either excitatory or inhibitory, which is marked by being colored in red or blue in the discrete representation of correlated synaptic inputs with bin size  $\Delta t = 1\text{ms}$ . Accordingly, considering excitation and inhibition separately specifies two associated input-count processes and two cumulative counting processes. For nonzero spiking correlation  $\rho = 0.03$ , these processes are themselves correlated as captured by the joint distribution of excitatory and inhibitory input counts  $P_{ei,kl}$  (center) and by the joint distribution of excitatory and inhibitory jumps  $P_{ei,kl}/(1 - P_{00})$  (right). (b) The input count distribution  $P_{ei,kl}$  is a finite-size approximation of the bivariate directing de Finetti measure  $F_{ei}$ , which we consider as a parameter as usual. For a smaller bin size  $\Delta t = 0.1\text{ms}$ , this distribution concentrates in  $(0,0)$ , as an increasing proportion of time bins does not register any synaptic events, be they excitatory or inhibitory. In the presence of correlation however, the conditioned jump distribution remains correlated but also dispersed. (c) In the limit  $\Delta t \rightarrow 0$ , the input-count distribution is concentrated in  $(0,0)$ , consistent with the fact that the average number of synaptic activations remains constant while the number of bins diverges. By contrast, the distribution of synaptic event size conditioned to distinct from  $(0,0)$  converges toward a well-defined distribution:  $p_{ei,k} = \lim_{\Delta t \rightarrow 0^+} P_{ei,k}/(1 - P_{ei,00})$ . This distribution characterizes the jumps of a bivariate compound Poisson process, obtained as the limit of the cumulative count process when considering  $\Delta t \rightarrow 0^+$ .

will only restrict ourselves to particular parametric forms for  $p_{ei}$  when discussing the role of  $\rho_{ei}$ , whose specification via (9) requires modeling assumptions about  $F_{ei}$ . In that respect, we show in Appendix D that the coefficient  $\rho_{ei}$  can always be deduced from the knowledge of a discrete distribution  $p_{ei,kl}$  on  $\{0, \dots, K_e\} \times \{0, \dots, K_i\} \setminus \{0,0\}$  via

$$\rho_{ei} = \frac{\mathbb{E}_{ei}[k_e k_i]}{\sqrt{K_e \mathbb{E}_{ei}[k_e] K_i \mathbb{E}_{ei}[k_i]}},$$

where the expectations are with respect to  $p_{ei,kl}$ .

#### D. Itō, Stratonovich, and Marcus integrals

We are now in a position to formulate the mathematical problem at stake within the framework developed by Marcus to study shot-noise driven systems [33, 34]. Our goal is quantifying the subthreshold variability of an AONCB neuron subjected to synchronous inputs. Mathematically, this amounts to computing the first two moments of the stationary process solving the following stochastic dynamics

$$\dot{V} = -V/\tau + h_e(V_e - V) + h_i(V_i - V) + I/C, \quad (12)$$

where  $V_i < 0 < V_e$  are constants and where the reduced conductances  $h_e = g_e/C$  and  $h_i = g_i/C$  follows stochastic processes defined in terms of a compound Poisson process  $Y$  with bivariate jumps. Formally, the compound Poisson process  $Y$  is specified by  $b$ , the rate of its governing Poisson process  $N$ , and by the joint distribution of its jumps  $p_{ei}$ . Each point of the Poisson process  $N$  represents a synaptic activation time  $T_k$ , where  $k$  is in  $\mathbb{Z}$  with the convention that  $T_0 \leq 0 \leq T_1$ . At all these times, the synaptic input sizes are drawn as i.i.d. random variables  $(W_{e,k}, W_{i,k})$  in  $\mathbb{R}^+ \times \mathbb{R}^+$  with probability distribution  $p_{ei}$ . In order to understand how our approach fits in Marcus framework, it is important to remark that the driving process  $Y$  is distinct from the conductance process  $h = (h_e, h_i)$ . The latter process is formally defined for AONCB neurons as

$$\begin{aligned} h(t) &= \frac{Y(t) - Y(t - \epsilon\tau)}{\epsilon\tau}, \\ &= \frac{1}{\epsilon\tau} \left( \sum_{n=N(t-\epsilon\tau)+1}^{N(t)} W_{e,n}, \sum_{n=N(t-\epsilon\tau)+1}^{N(t)} W_{i,n} \right), \end{aligned}$$

where the dimensionless parameter  $\epsilon = \tau_s/\tau > 0$  is the ratio of the duration of synaptic activation relative to the passive membrane time constant. The simplifying limit of instantaneous synapses corresponds to infinitely fast synaptic activation, i.e.,  $\epsilon = \tau_s/\tau \rightarrow 0^+$ . Thus-defined, the conductance processes of AONCB neurons have the dimension of a rate and are well-behaved in the sense that for  $\epsilon > 0$ , these processes are almost-surely bounded for finitely supported distributions  $p_{ei}$ . This well-behaved behavior is the key allowing us to leverage Marcus framework to analyze shot-noise driven systems.

Shot noise processes are defined as temporal derivative of compound Poisson processes, i.e., as collections of randomly weighted Dirac-delta masses. One can show that the conductance processes  $(h_e, h_i)$  actually become shot noises in the limit  $\epsilon \rightarrow 0^+$ .

A general problem of stochastic analysis is solving equations akin to Eq. (12), where the stochastic process  $h$  is interpreted as a shot noise, as in the limit of instantaneous synapses. Even when neglecting the spike-generating mechanism, obtaining closed-form expressions for the moments of  $V$  is hindered by the multiplicative nature of the conductance shot noises. In principle, one might expect to address this problem via stochastic calculus, as for diffusion-based models. Solving such models with multiplicative diffusive noise involves addressing the Itō-Stratonovich dilemma, whereby one has to carefully interpret the meaning of the stochastic integral representations of solutions [55, 56]. For physical systems, dynamical equations such as Eq. (12) are interpreted as Langevin equations, for which Stratonovich calculus applies. The major caveat to taking such an approach in conductance-based models is that Stratonovich calculus is not well-defined for shot-noise drives, including those derived from compound Poisson processes [57]. To remedy this point, Marcus has proposed to study stochastic dynamical equations subjected to regularized versions of shot noises, whose regularity is controlled by a nonnegative parameter  $\epsilon$  [33, 34]. For  $\epsilon > 0$ , the dynamical equations admit classical solutions, whereas the shot-noise-driven regime is recovered in the limit  $\epsilon \rightarrow 0^+$ . The hope is to be able to characterize analytically the shot-noise-driven solution, or at least some of its moments, by considering regular solutions in the limit  $\epsilon \rightarrow 0^+$ . We choose to refer to the control parameter as  $\epsilon$  by design in the above. This is because we will show that AONCB models represent Marcus-type regularizations that are amenable to analysis in the limit of instantaneous synapses, i.e., when  $\epsilon = \tau_s/\tau \rightarrow 0^+$ , for which the conductance processes  $h$  converge toward a form of shot noise.

Finally, it is important to note that the Marcus interpretation of stochastic integration has practical implications for numerical simulations with shot noise. Indeed, according to this interpretation, shot-noise-driven solutions shall be conceived as limits of regularized solutions for which standard numerical scheme applies. Correspondingly, shot-noise-driven solutions to Eq. (12) can be simulated via a limit numerical scheme (see Fig. 6a). We derive such a limit scheme in Appendix E. Specifically, we show that the voltage of shot-noise-driven AONCB neurons exponentially relaxes toward the leak reversal potential  $V_L = 0$ , except when subjected to synaptic impulses at times  $\{T_n\}_{n \in \mathbb{Z}}$ . At these times, the voltage  $V$  updates discontinuously according to  $V(T_n) = V(T_n^-) + J_n$ , where the jumps are given in Appendix E via the Marcus rule

$$\begin{aligned} J_n &= \\ &\left( \frac{W_{e,n} V_e + W_{i,n} V_i}{W_{e,n} + W_{i,n}} - V(T_n^-) \right) \left( 1 - e^{-(W_{e,n} + W_{i,n})} \right). \end{aligned} \quad (13)$$

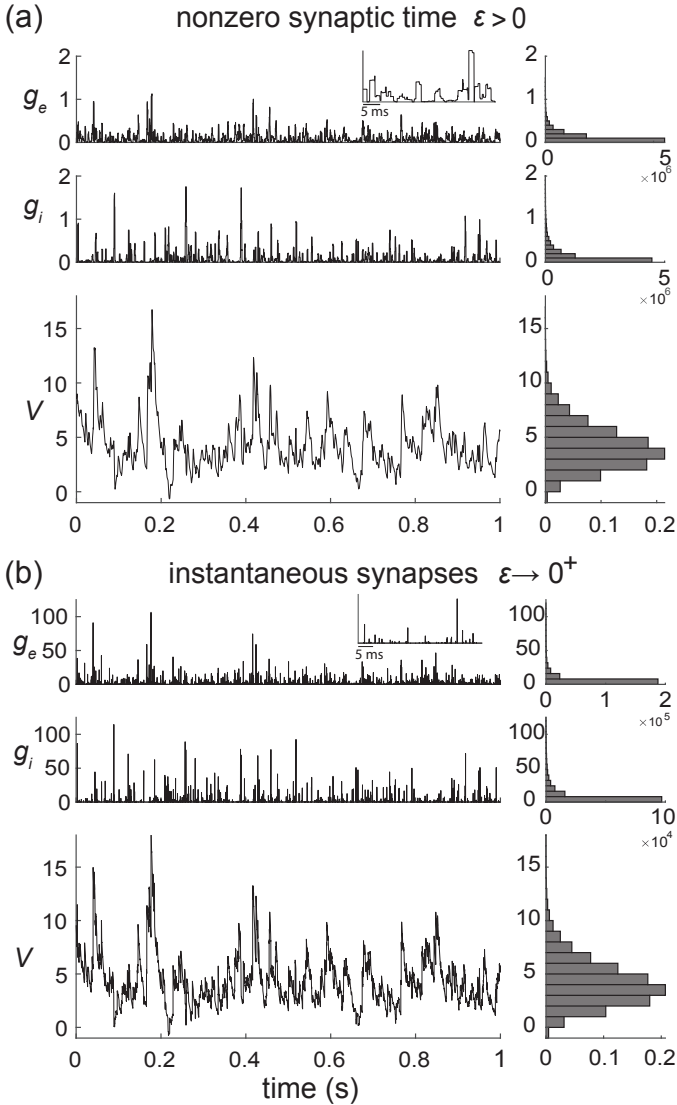


**FIG. 6. Limit of instantaneous synapses within the Marcus framework.** (a) Simulation of the conductance processes  $g_e$  and  $g_i$  as all-or-none conductance process with nonzero synaptic time constant  $\tau_s = 2\text{ms}$ . We consider Poisson-process drive without cross-population correlation  $\rho_{ei} = 0$ , but with nonzero correlations within the excitatory and inhibitory synaptic inputs:  $\rho_e = 0.03$  and  $\rho_i = 0.06$ . For  $\tau_s > 0$ , the membrane voltage  $V$  is simulated via a standard Euler discretization scheme. The corresponding empirical conductance and voltage distributions are shown on the right. The later voltage distribution asymptotically determines the stationary moments of  $V$ . (b) In the limit of instantaneous synapses  $\epsilon = \tau_s/\tau \rightarrow 0^+$ , the conductance processes  $g_e$  and  $g_i$  converge toward the increments of compound Poisson processes, which are determined as a collection of Dirac delta functions with i.i.d. weights. Simulating the limit process  $V$  obtained when  $\epsilon = \tau_s/\tau \rightarrow 0^+$  requires to adopt the framework of Marcus integrals, which generalize Stratonovich integrals to the case of point-process drives, when possible. Importantly, for the same sequence of activation time, the voltage trace and the empirical voltage distribution are only marginally altered in the limit  $\epsilon \rightarrow 0^+$ , at least compared with  $\epsilon = 0.2$  in (a).

Observe that the above Marcus rule directly implies that no jump can cause the voltage to exit  $(V_i, V_e)$ , the allowed range of variation for  $V$ . Moreover, note that this rule specifies an exact even-driven simulation scheme given knowledge of the synaptic activation times and sizes  $\{T_n, W_{e,n}, W_{i,n}\}_{n \in \mathbb{Z}}$  [58]. We adopt the above Marcus-type numerical scheme in all the simulations that involved instantaneous synapses (see Fig. 6b).

### III. MOMENT CALCULATIONS

In this section, we derive our two main exact results for AONCB neurons driven by synchronous synaptic inputs. Specifically, we derive the stationary mean voltage Eq. (19) in III A and the stationary voltage variance Eq. (30) in III B. These results are obtained by probabilistic treatment exploiting the properties of compound Poisson processes, which yields interpretable formulas in the limit of instantaneous synapses  $\epsilon = \tau_s/\tau \rightarrow 0^+$ . Readers who have no interest in the method of derivation for these results may skip the content of this section, aside from Eq. (19) and Eq. (30).

#### A. Stationary voltage mean

For a positive synaptic activation time  $t > 0$ , the classical method of the variation of the constant applies to solve Eq. (1). This yields an expression for  $V_\epsilon(t)$  in terms of regular Riemann-Stieltjes integrals where the conductance traces  $h_e(t)$  and  $h_i(t)$  are treated as a form of deterministic quenched disorder. Specifically, given an initial condition  $V_\epsilon(0)$ , we have

$$V_\epsilon(t) = V_\epsilon(0) e^{- \int_0^t \frac{1}{\tau} + h_e(u) + h_i(u) \, du} + \int_0^t (V_e h_e(u) + V_i h_i(u) + I/C) e^{- \int_u^t \frac{1}{\tau} + h_e(v) + h_i(v) \, dv} \, du.$$

where  $V_\epsilon(t)$  depends on  $\epsilon$  via the all-or-none-conductance processes  $h_e$  and  $h_i$ . As usual, the stationary dynamics of the voltage  $V_\epsilon$  is recovered by considering the limit of arbitrary large times  $t \rightarrow \infty$ , for which one can neglect the influence of the initial condition  $V_\epsilon(0)$ . Introducing the cumulative input processes  $H = (H_e, H_i)$  defined by

$$(H_e(t), H_i(t)) = \left( \int_0^t h_e(u) \, du, \int_0^t h_i(u) \, du \right).$$

and satisfying  $\tau dH_e(t) = h_e(t) \, dt$  and  $\tau dH_i(t) = h_i(t) \, dt$ , we have

$$V_\epsilon = \int_{-\infty}^0 e^{\frac{t}{\tau} + H_e(t) + H_i(t)} \left( d[V_e H_e(t) + V_i H_i(t)] + \frac{I}{G} \frac{dt}{\tau} \right). \quad (14)$$

In turn, expanding the integrand above yields the following expression for the stationary expectation of the

voltage

$$\begin{aligned}\mathbb{E}[V_\epsilon] &= V_e \int_{-\infty}^0 e^{\frac{t}{\tau}} \mathbb{E} \left[ e^{H_e(t) + H_i(t)} dH_e(t) \right] \\ &+ V_i \int_{-\infty}^0 e^{\frac{t}{\tau}} \mathbb{E} \left[ e^{H_e(t) + H_i(t)} dH_i(t) \right] \\ &+ \frac{I}{G} \int_{-\infty}^0 e^{\frac{t}{\tau}} \mathbb{E} \left[ e^{H_e(t) + H_i(t)} \right] \frac{dt}{\tau}.\end{aligned}\quad (15)$$

Our primary task is to evaluate the various stationary expectations appearing in the above formula. Such a goal can be achieved analytically for AONCB models. As the involved calculations tend to be cumbersome, we only give a detailed account in Appendix. Here we account for the key steps of the calculation, which ultimately produces an interpretable compact formula for  $\mathbb{E}[V_\epsilon]$  in the limit of instantaneous synapses, i.e., when  $\epsilon \rightarrow 0$ .

In order to establish this compact formula, it is worth introducing the stationary bivariate function

$$Q_\epsilon(t, s) = \mathbb{E} \left[ e^{H_e(t) + H_i(s)} \right], \quad (16)$$

which naturally depends on  $\epsilon$  via  $H_e(t)$  and  $H_i(s)$ . The function  $Q_\epsilon$  is of great interest because all the stationary expectations at stake in Eq. (15) can be derived from it. Before justifying this point, an important observation is that the expectation defining  $Q_\epsilon(t, s)$  only bears on the cumulative input processes  $H_e$  and  $H_i$ , which specify bounded, piecewise continuous functions with probability one, independent of  $\epsilon$ . As a result of this regular behavior, the expectation commute with the limit of instantaneous synapses allowing one to write

$$\begin{aligned}Q(t, s) &= \lim_{\epsilon \rightarrow 0^+} Q_\epsilon(t, s) \\ &= \mathbb{E} \left[ e^{\lim_{\epsilon \rightarrow 0} H_e(t) + H_i(s)} \right], \\ &= \mathbb{E} \left[ e^{-Y_e(t) - Y_i(t)} \right],\end{aligned}$$

where we exploit the fact that the cumulative input processes  $H_e$  and  $H_i$  converge toward the coupled compound Poisson processes  $Y_e$  and  $Y_i$  when  $\epsilon \rightarrow 0^+$ . The above remark allows one to compute the term due to current injection  $I$  in Eq. (15), where the expectation can be identified to  $Q_\epsilon(t, t)$ . Indeed, utilizing the standard form for the moment-generating function for compound Poisson processes [40], we find that

$$Q(t, t) = e^{a_{ei,1} t / \tau},$$

where we introduce the first-order aggregate efficacy

$$a_{ei,1} = b\tau \left( 1 - \mathbb{E}_{ei} \left[ e^{-(W_e + W_i)} \right] \right).$$

Remember that in the above definition,  $\mathbb{E}_{ei}[\cdot]$  denotes the expectation with respect to the joint probability of the conductance jumps, i.e.,  $p_{ei}$ .

It remains to evaluate the expectations associated to excitation and inhibition reversal potentials in Eq. (15).

These terms differ from the current-associated term in that they involve expectations of stochastic integrals with respect to the cumulative input processes  $H_{e/i}$ . This is by contrast with evaluating Eq. (16), which only involves expectations of functions that depends on  $H_{e/i}$ . In principle, one could still hope to adopt a similar route as for the current associated term, exploiting the compound Poisson process  $Y$  obtained in the limit of instantaneous synapses. However, such an approach would require that the operations of taking the limit of instantaneous synapses and evaluating the stationary expectation still commute. This is a major caveat as such a commuting relation generally fails for point-process-based stochastic integrals. Therefore, one has to analytically evaluate the expectations at stake for positive synaptic activation time  $\epsilon > 0$ , without resorting to the simplifying limit of instantaneous synapses. This analytical requirement is the primary motivation to consider AONCB models.

The first step in the calculation is to realize that for  $\epsilon > 0$ , the conductance traces  $h_e(t) = \tau dH_e(t)/dt$  and  $h_i(t) = \tau dH_i(t)/dt$  are bounded, piecewise continuous functions with probability one. Under these conditions, it then holds that

$$\begin{aligned}\lim_{s \rightarrow t} \partial_t Q_\epsilon(t, s) &= \mathbb{E} \left[ \frac{dH_e(t)}{dt} e^{H_e(t) + H_i(t)} \right], \\ \lim_{s \rightarrow t} \partial_s Q_\epsilon(t, s) &= \mathbb{E} \left[ \frac{dH_i(t)}{dt} e^{H_e(t) + H_i(t)} \right],\end{aligned}$$

so that the sought-after expectations can be deduced from the closed-form knowledge of  $Q_\epsilon(t, s)$  for positive  $\epsilon > 0$ . The analytical expression of  $Q_\epsilon(t, s)$  can be obtained via careful manipulation of the processes  $H_e$  and  $H_i$  featured in the exponent of Eq. (16) (see Appendix F). In a nutshell, these manipulations hinge on splitting the integrals defining  $H_e(t)$  and  $H_i(s)$  into independent contributions arising from spiking events occurring in the five nonoverlapping, contiguous intervals bounded by the times  $0 \geq -\epsilon\tau \geq t \geq s \geq t - \epsilon\tau \geq s - \epsilon\tau$ . There is no loss of generality in assuming the latter ordering and from the corresponding analytical expression, we can compute

$$\lim_{\epsilon \rightarrow 0^+} \lim_{s \rightarrow t} \partial_t Q_\epsilon(t, s) = b a_{ei,1} e^{a_{ei,1} t / \tau},$$

$$\lim_{\epsilon \rightarrow 0^+} \lim_{s \rightarrow t} \partial_s Q_\epsilon(t, s) = b a_{ei,1} e^{a_{ei,1} t / \tau},$$

where we define the effective first-order synaptic efficacies

$$a_{e,1} = b\tau \mathbb{E}_{ei} \left[ \frac{W_e}{W_e + W_i} \left( 1 - e^{-(W_e + W_i)} \right) \right], \quad (17)$$

$$a_{i,1} = b\tau \mathbb{E}_{ei} \left[ \frac{W_i}{W_e + W_i} \left( 1 - e^{-(W_e + W_i)} \right) \right]. \quad (18)$$

Observe that by definition,  $a_{e,1}$  and  $a_{i,1}$  satisfy  $a_{e,1} + a_{i,1} = a_{ei,1}$ .

Altogether, upon evaluation of the integrals featured in Eq. (15), these results allow one to produce a compact expression for the stationary voltage mean in the limit of instantaneous synapses:

$$\mathbb{E}[V] = \lim_{\epsilon \rightarrow 0^+} \mathbb{E}[V_\epsilon] = \frac{a_{e,1} V_e + a_{i,1} V_i + I/G}{1 + a_{e,1} + a_{i,1}}. \quad (19)$$

The above formula is the same as the one obtained for fixed asynchronous conductances set to values  $a_{e,1}$  and  $a_{i,1}$ . Thus, the impact of synchrony entirely lies in the definition of the first-order synaptic efficacies via Eq. (17) and Eq. (18). Technically, the exponential form of the efficacies follows from the shot-noise nature of the synaptic conductances. At the same time, the expectation form of the efficacies follows from the stochastic nature of the conductance jumps ( $W_e, W_i$ ), which captures input synchrony.

### B. Stationary voltage variance

The calculation of the stationary voltage variance is more challenging than that of the stationary voltage

$$\begin{aligned} V_\epsilon^2 &= \left( \int_{-\infty}^0 e^{\frac{t}{\tau} + H_e(t) + H_i(t)} \left( d(V_e H_e(t) + V_i H_i(t)) + \frac{I}{G} \frac{dt}{\tau} \right) \right)^2, \\ &= \iint_{\mathbb{R}^2} e^{\frac{t+s}{\tau} + H_e(t) + H_i(t) + H_e(s) + H_i(s)} \left( d(V_e H_e(t) + V_i H_i(t)) + \frac{I}{G} \frac{dt}{\tau} \right) \left( d(V_e H_e(s) + V_i H_i(s)) + \frac{I}{G} \frac{ds}{\tau} \right). \end{aligned} \quad (20)$$

Our main goal is to compute the stationary expectation of the above quantity. As for the stationary voltage mean, our strategy is (i) to derive the exact stationary expectation of the integrands for finite synaptic activation time, (ii) to evaluate these integrands in the simplifying limit of instantaneous synapses, and (iii) to rearrange the terms obtained after integration into an interpretable final form. Enacting the above strategy is a rather tedious task, and as for the calculation of the mean voltage, we only present the key steps of the calculation in the following.

The integrand terms at stake are obtained by expanding Eq. (20), which yields the following quadratic expression for the stationary second moment of the voltage

$$\begin{aligned} \mathbb{E}[V_\epsilon^2] &= A_{e,\epsilon} V_e^2 + B_{ei,\epsilon} V_e V_i + A_{i,\epsilon} V_i^2 \\ &\quad + (V_e B_{eI,\epsilon} + V_i B_{iI,\epsilon}) (I/G) + A_{I,\epsilon} (I/G)^2, \end{aligned} \quad (21)$$

whose various coefficients needs to be evaluated. These coefficients are conveniently specified in terms of the following symmetric random function

$$\mathcal{E}_{ei}(t, s) = e^{H_e(t) + H_i(t) + H_e(s) + H_i(s)}.$$

which features prominently in Eq. (20). Moreover, drawing on the calculation of the stationary mean voltage, we anticipate that the quadrivariate version of  $\mathcal{E}_{ei}(t, s)$  will play a central role in the calculation via its stationary expectation. Owing to this central role, we denote this expectation as

$$R_\epsilon(t, u, s, v) = \mathbb{E} \left[ e^{H_e(t) + H_i(u) + H_e(s) + H_i(v)} \right].$$

mean. However, in the limit of instantaneous synapses, this calculation produces a compact, interpretable formula as well. Adopting a similar approach as for the stationary mean calculation, we start by expressing  $V_\epsilon^2$  in the stationary limit in terms of a stochastic integrals involving the cumulative input processes  $H_e$  and  $H_i$ . Specifically, using Eq. (14), we have

where we make the  $\epsilon$ -dependence explicit. As a mere expectation with respect to the cumulative input processes  $(H_e, H_i)$ , the expectation can be evaluated in closed form for AONCB models. This again requires careful manipulations of the processes  $H_e$  and  $H_i$ , which need to split into independent contributions arising from spiking events occurring in nonoverlapping intervals. By contrast with the bivariate case, the quadrivariate case requires to consider nine contiguous intervals. There is no loss of generality to consider these interval bounds to be determined by the two following time orderings:

**O-order:**  $0 \geq -\epsilon\tau \geq t \geq u \geq t - \epsilon\tau \geq u - \epsilon\tau \geq s \geq v \geq s - \epsilon\tau \geq v - \epsilon\tau$ ,

**D-order:**  $0 \geq -\epsilon\tau \geq t \geq u \geq s \geq v \geq t - \epsilon\tau \geq u - \epsilon\tau \geq s - \epsilon\tau \geq v - \epsilon\tau$ .

where  $O$  stands for off-diagonal ordering and  $D$  for diagonal ordering.

The reason to only consider the  $O/D$ -orders is that all the relevant calculations will be made in the limit  $(u, v) \rightarrow (t, s)$ . By symmetry of  $R_\epsilon(t, u, s, v)$ , it is then enough to restrict our consideration to the limit  $(u, v) \rightarrow (t^-, s^-)$ , which leaves the choice of  $t, s \leq 0$  to be determined. By symmetry, one can always choose  $t > s$ , so that the only remaining alternative is to decide whether  $(t, s)$  belong to the diagonal region  $\mathcal{D}_\epsilon = \{t, s \leq 0 \mid \epsilon\tau \geq |t - s|\}$  or the off-diagonal region  $\mathcal{O}_\epsilon = \{t, s \leq 0 \mid \epsilon\tau < |t - s|\}$ . For the sake of completeness, we give the two expressions of  $R_\epsilon(t, u, s, v)$  on the regions  $\mathcal{O}_\epsilon$  and  $\mathcal{D}_\epsilon$  in Appendix G. Owing to their tediousness, we do not give the detailed calculations

leading to these expressions, which are lengthy but straightforward elaborations on those used in Appendix F. Here we stress that for  $\epsilon > 0$ , these expressions reveal that  $R_\epsilon(t, u, s, v)$  is defined as a twice-differentiable quadrivariate function.

With these remarks in mind, the coefficients featured in Eq. (21) can be categorized in three classes:

1. There is a single current-dependent inhomogeneous coefficient

$$A_{I,\epsilon} = \iint_{\mathbb{R}^2} e^{\frac{t+s}{\tau}} \mathbb{E}[\mathcal{E}_{\text{ei}}(t, s)] \frac{dt ds}{\tau^2},$$

where we recognize that  $\mathbb{E}[\mathcal{E}_{\text{ei}}(t, s)] = R_\epsilon(t, t, s, s) \stackrel{\text{def}}{=} R_\epsilon(t, s)$ . As  $R_\epsilon(t, s)$  is merely a stationary expectation with respect to the cumulative input processes  $(H_e, H_i)$ , it can be directly evaluated in the limit of instantaneous synapses. In other word, step (ii) can be performed before step (i), similarly as for the stationary voltage mean calculation. However, having a general analytical expression for  $R_\epsilon(t, u, s, v)$  on  $\mathcal{O}_\epsilon$  (see Appendix G), we can directly evaluate for all  $t \neq s$  that

$$\begin{aligned} R(t, s) &= \lim_{\epsilon \rightarrow 0^+} R_\epsilon(t, s) \\ &= e^{(2a_{\text{ei},2} \max(t, s) - a_{\text{ei},1}|t-s|)/\tau}, \end{aligned} \quad (22)$$

where we define the second-order aggregate efficacy

$$a_{\text{ei},2} = \frac{b\tau}{2} \left( 1 - \mathbb{E}_{\text{ei}} \left[ e^{-2(W_e + W_i)} \right] \right).$$

It is clear that the continuous function  $R(t, s)$  is smooth everywhere except on the diagonal where it admits a slope discontinuity. As we shall see, this slope discontinuity is the reason why one needs to consider the  $\mathcal{D}_\epsilon$  region carefully, even when only concerned with the limit  $\epsilon \rightarrow 0^+$ . That being said, the diagonal behavior plays no role here and straightforward integration of  $R(t, s)$  on the negative orthant gives

$$A_I = \lim_{\epsilon \rightarrow 0^+} A_{I,\epsilon} = \frac{1}{(1 + a_{\text{ei},1})(1 + a_{\text{ei},2})}.$$

2. There are two current-dependent linear coefficients

$$\begin{aligned} B_{eI,\epsilon} &= 2 \iint_{\mathbb{R}^2} e^{\frac{t+s}{\tau}} \mathbb{E}[\mathcal{E}_{\text{ei}}(t, s) dH_e(t)] \frac{ds}{\tau}, \\ B_{iI,\epsilon} &= 2 \iint_{\mathbb{R}^2} e^{\frac{t+s}{\tau}} \mathbb{E}[\mathcal{E}_{\text{ei}}(t, s) dH_i(t)] \frac{ds}{\tau}, \end{aligned}$$

where the coefficient 2 above comes from the fact that  $B_{eI,\epsilon}$  and  $B_{iI,\epsilon}$  are actually resulting from the contributions of two symmetric terms in the expansion of Eq. (20). Both  $B_{eI,\epsilon}$  and  $B_{iI,\epsilon}$  involve expectations of stochastic integrals akin to those evaluated for the stationary mean calculation. Therefore, these terms can be treated similarly by implementing step (i) and (ii) sequentially. The

trick is to realize that for positive  $\epsilon$  and  $t \neq s \leq 0$ , it holds that

$$\mathbb{E} \left[ \mathcal{E}_{\text{ei}}(t, s) \frac{dH_e(t)}{dt} \right] = \lim_{u \rightarrow t} \partial_t R_\epsilon(t, u, s, s),$$

$$\mathbb{E} \left[ \mathcal{E}_{\text{ei}}(t, s) \frac{dH_i(t)}{dt} \right] = \lim_{v \rightarrow s} \partial_s R_\epsilon(t, t, s, v),$$

Thus for any  $(t, s)$  in the off-diagonal region  $\mathcal{O}_\epsilon$ , the analytical knowledge of  $R_\epsilon(t, u, s, v)$  (see Appendix G) allows one to evaluate

$$\lim_{u \rightarrow t^-} \tau \frac{\partial_t R_\epsilon(t, u, s, s)}{R_\epsilon(t, s)} = \begin{cases} a_{\text{e},1} & \text{if } t > s, \\ a_{\text{e},2} - a_{\text{e},1} & \text{if } t < s, \end{cases} \quad (23)$$

$$\lim_{v \rightarrow s^-} \tau \frac{\partial_s R_\epsilon(t, u, s, s)}{R_\epsilon(t, s)} = \begin{cases} a_{\text{i},1} & \text{if } t > s, \\ a_{\text{i},2} - a_{\text{i},1} & \text{if } t < s, \end{cases} \quad (24)$$

where the second-order synaptic efficacies are defined as

$$a_{\text{e},2} = \frac{b\tau}{2} \mathbb{E}_{\text{ei}} \left[ \frac{W_e}{W_e + W_i} \left( 1 - e^{-2(W_e + W_i)} \right) \right], \quad (25)$$

$$a_{\text{i},2} = \frac{b\tau}{2} \mathbb{E}_{\text{ei}} \left[ \frac{W_i}{W_e + W_i} \left( 1 - e^{-2(W_e + W_i)} \right) \right]. \quad (26)$$

Observe that these efficacies satisfy the familiar relation  $a_{\text{e},2} + a_{\text{i},2} = a_{\text{ei},2}$ . Taking the limits of Eq. (23) and Eq. (24) when  $\epsilon \rightarrow 0^+$  specify two bivariate functions that are continuous everywhere, except on the diagonal  $t = s$ , where these functions present a jump discontinuity. This behavior is still regular enough to discard any potential contributions from diagonal terms, so that we can restrict ourselves to the region  $\mathcal{O}_\epsilon$ . Then, taking the limit  $\epsilon \rightarrow 0^+$  after integration of over  $\mathcal{O}_\epsilon$ , we find that

$$\begin{aligned} B_{eI} &= \lim_{\epsilon \rightarrow 0^+} B_{eI,\epsilon} = \frac{a_{\text{e},2}}{(1 + a_{\text{ei},1})(1 + a_{\text{ei},2})}, \\ B_{iI} &= \lim_{\epsilon \rightarrow 0^+} B_{iI,\epsilon} = \frac{b\tau a_{\text{i},2}}{(1 + a_{\text{ei},1})(1 + a_{\text{ei},2})}. \end{aligned}$$

3. There are four quadratic coefficients associated to the reversal-potential  $V_e$  and  $V_i$ , including two diagonal terms

$$A_{e,e} = \iint_{\mathbb{R}^2} e^{\frac{t+s}{\tau}} \mathbb{E}[\mathcal{E}_{\text{ei}}(t, s) dH_e(t) dH_e(s)],$$

$$A_{i,i} = \iint_{\mathbb{R}^2} e^{\frac{t+s}{\tau}} \mathbb{E}[\mathcal{E}_{\text{ei}}(t, s) dH_i(t) dH_i(s)],$$

and two symmetric cross terms contributing

$$B_{ei,\epsilon} = 2 \iint_{\mathbb{R}^2} e^{\frac{t+s}{\tau}} \mathbb{E}[\mathcal{E}_{\text{ei}}(t, s) dH_e(t) dH_i(s)].$$

Notice that it is enough to compute only one diagonal term as the other term can be deduced by symmetry. Following the same method as for the linear terms, we start by remarking that for all  $(t, s)$  in the off-diagonal region  $\mathcal{O}_\epsilon$ , it holds that

$$\mathbb{E} \left[ \mathcal{E}_{\text{ei}}(t, s) \frac{dH_e(t)}{dt} \frac{dH_e(s)}{ds} \right] = \lim_{(u,v) \rightarrow (t,s)} \partial_t \partial_s R_\epsilon(t, u, s, v),$$

$$\mathbb{E} \left[ \mathcal{E}_{\text{ei}}(t, s) \frac{dH_i(t)}{dt} \frac{dH_i(s)}{ds} \right] = \lim_{(u,v) \rightarrow (t,s)} \partial_t \partial_v R_\epsilon(t, u, s, v),$$

As before, the analytical knowledge of  $R_\epsilon(t, u, s, v)$  on the  $O_\epsilon$  region (see Appendix G) allows one to evaluate

$$\begin{aligned} \lim_{(u,v) \rightarrow (t,s)^-} \tau^2 \frac{\partial_t \partial_u R_\epsilon(t, u, s, s)}{R_\epsilon(t, s)} &= a_{e,1}(2a_{e,2} - a_{e,1}), \\ \lim_{(u,v) \rightarrow (t,s)^-} \tau^2 \frac{\partial_t \partial_s R_\epsilon(t, u, s, v)}{R_\epsilon(t, s)} &= \\ &\frac{1}{2}(a_{e,1}(2a_{i,2} - a_{i,1}) + a_{i,1}(2a_{e,2} - a_{e,1})). \end{aligned}$$

The above closed-form expressions allow one to compute  $A'_{e,\epsilon}$  and  $B'_{ei,\epsilon}$ , the part of the coefficients  $A_{e,\epsilon}$  and  $B_{ei,\epsilon}$  resulting from integration over the off-diagonal region  $O_\epsilon$ , which admit well-defined limit values  $A'_e = \lim_{\epsilon \rightarrow 0^+} A'_{e,\epsilon}$  and  $B'_{ei} = \lim_{\epsilon \rightarrow 0^+} B'_{ei,\epsilon}$  with:

$$\begin{aligned} A'_e &= \lim_{\epsilon \rightarrow 0^+} \iint_{O_\epsilon} e^{\frac{t+s}{\tau}} \mathbb{E} [\mathcal{E}_{ei}(t, s) dH_e(t) dH_e(s)], \\ &= \frac{a_{e,1}(2a_{e,2} - a_{e,1})}{(1 + a_{ei,1})(1 + b\tau a_{ei,2})}, \\ B'_{ei} &= 2 \lim_{\epsilon \rightarrow 0^+} \iint_{O_\epsilon} e^{\frac{t+s}{\tau}} \mathbb{E} [\mathcal{E}_{ei}(t, s) dH_e(t) dH_i(s)], \\ &= \frac{a_{e,1}(2a_{i,2} - a_{i,1}) + a_{i,1}(2a_{e,2} - a_{e,1})}{(1 + a_{ei,1})(1 + a_{ei,2})}. \end{aligned}$$

However, for quadratic terms, one also needs to include the contributions arising from the diagonal region  $\mathcal{D}_\epsilon$ , as suggested by the first-order jump discontinuity of  $R(t, s) = \lim_{\epsilon \rightarrow 0^+} R_\epsilon(t, s)$  on the diagonal  $t = s$ . To confirm this point, one can show from the analytical expression of  $R_\epsilon(t, u, s, v)$  on  $\mathcal{D}_\epsilon$  (see Appendix G), that all relevant second-order derivative terms scale as  $1/\epsilon$  over  $\mathcal{D}_\epsilon$ . This scaling leads to the nonzero contributions  $A''_{e,\epsilon}$  and  $B''_{ei,\epsilon}$  resulting from the integration of these second-order derivative terms over the diagonal region  $\mathcal{D}_\epsilon$ , even in the limit  $\epsilon \rightarrow 0^+$ . Actually, we find that these contributions also admit well-defined limit values  $A''_e = \lim_{\epsilon \rightarrow 0^+} A''_{e,\epsilon}$  and  $B''_{ei} = \lim_{\epsilon \rightarrow 0^+} B''_{ei,\epsilon}$  with: (see Appendix H)

$$\begin{aligned} A''_e &= \lim_{\epsilon \rightarrow 0^+} \iint_{\mathcal{D}_\epsilon} e^{\frac{t+s}{\tau}} \mathbb{E} [\mathcal{E}_{ei}(t, s) dH_e(t) dH_e(s)], \\ &= \frac{a_{e,12} - c_{ei}}{1 + a_{ei,2}}, \\ B''_{ei} &= 2 \lim_{\epsilon \rightarrow 0^+} \iint_{\mathcal{D}_\epsilon} e^{\frac{t+s}{\tau}} \mathbb{E} [\mathcal{E}_{ei}(t, s) dH_e(t) dH_i(s)], \\ &= \frac{2c_{ei}}{1 + a_{ei,2}}. \end{aligned}$$

Remembering that the expression of  $A''_i$  can be deduced from that of  $A''_e$  by symmetry, Eq. (27) defines  $A''_e$ , and thus  $A''_i$ , in terms of the useful auxiliary second-order efficacies  $a_{e,12} = a_{e,1} - a_{e,2}$  and  $a_{i,12} = a_{i,1} - a_{i,2}$ . These efficacies will feature prominently in the final variance expression and it is worth mentioning their explicit defi-

nitions as

$$a_{e,12} = \frac{b\tau}{2} \mathbb{E}_{ei} \left[ \frac{W_e}{W_e + W_i} \left( 1 - e^{-(W_e + W_i)} \right)^2 \right], \quad (27)$$

$$a_{i,12} = \frac{b\tau}{2} \mathbb{E}_{ei} \left[ \frac{W_i}{W_e + W_i} \left( 1 - e^{-(W_e + W_i)} \right)^2 \right]. \quad (28)$$

The other quantity of interest is the coefficient  $c_{ei}$ , which appears in both Eq. (27) and Eq. (27). This nonnegative coefficient, defined as

$$c_{ei} = \frac{b\tau}{2} \mathbb{E}_{ei} \left[ \frac{W_e W_i}{(W_e + W_i)^2} \left( 1 - e^{-(W_e + W_i)} \right)^2 \right], \quad (29)$$

entirely captures the (nonnegative) correlation between excitatory and inhibitory inputs and shall be seen as an efficacy as well. Keeping these definitions in mind, the full quadratic coefficients are finally obtained as  $A_e = A'_e + A''_e$ ,  $A_i = A'_i + A''_i$ , and  $B_{ei} = B'_{ei} + B''_{ei}$ .

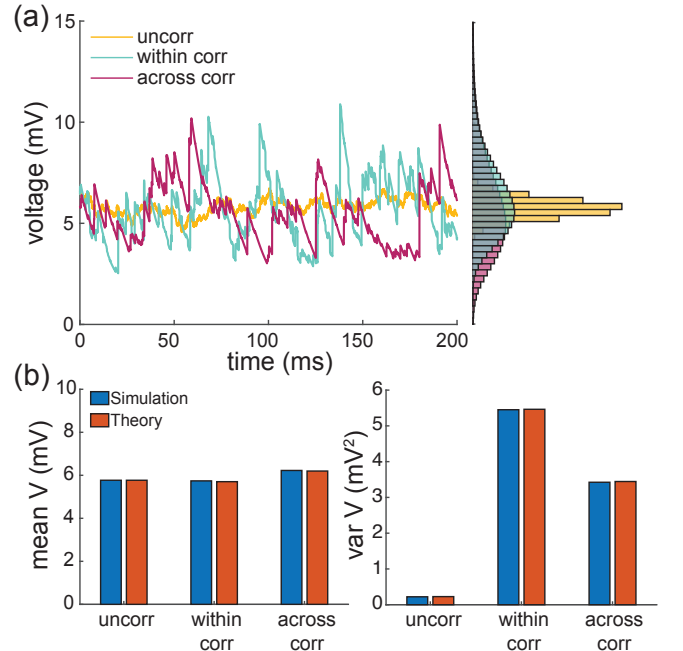


FIG. 7. **Comparison of simulation and theory.** (a) Examples of voltage traces obtained via Monte-Carlo simulations of an AONCB neuron for various types of synchrony-based input correlations: uncorrelated  $\rho_e = \rho_i = \rho_{ei} = 0$  (uncorr, yellow), within correlation  $\rho_e, \rho_i > 0$  and  $\rho_{ei} = 0$  (within corr, cyan), within and across correlation  $\rho_e, \rho_i, \rho_{ei} > 0$  (across corr, magenta). (b) Comparison of the analytically derived expressions (19) and (30) with numerical estimates obtained via Monte-Carlo simulations for the synchrony conditions considered in (a).

From there, injecting the analytical expressions of the various coefficients in the quadratic form Eq. (21) leads to an explicit formula for the stationary voltage variance in the limit of instantaneous synapses. Then, one is only left

with step (iii), which aims at exhibiting a compact, interpretable form for this formula. We show in Appendix I that lengthy but straightforward algebraic manipulations lead to the following simplified form

$$\mathbb{V}[V] = \frac{1}{1 + a_{ei,2}} \times (a_{e,12}(V_e - \mathbb{E}[V])^2 + a_{i,12}(V_i - \mathbb{E}[V])^2 - c_{ei}(V_e - V_i)^2). \quad (30)$$

Note that for AONCB models, establishing the above exact expression does not require any approximation other than taking the limit of instantaneous synapses. In particular, we neither resort to any diffusion approximations [29, 30] nor invoke the effective-time-constant approximation [59, 60]. We give in Appendix J an alternative factorized form  $\mathbb{V}[V]$  to justify the nonnegativity of expression Eq. (30). In Fig. 7, we illustrate the excellent agreement of the analytically derived expressions (19) and (30) with numerical estimates obtained via Monte-Carlo simulations of the AONCB dynamics for various input synchrony conditions. Discussing and interpreting quantitatively (30) within a biophysically relevant context will be the main focus of the remaining of this work.

#### IV. COMPARISON WITH EXPERIMENTAL DATA

In this section, we leverage the biophysically interpretable formulas (19) and (30) to determine under which synchrony conditions a neuron can achieve the experimentally observed subthreshold variability. In IV A, we show that for biophysically relevant parameters, asynchronous drives only yields realistic subthreshold variability for a restricted number of large synaptic inputs. In IV B, we show that realistic subthreshold variability can also be achieved with moderate synaptic inputs by including input synchrony in amounts compatible with measured pairwise spiking correlation. In IV C, we demonstrate that the asynchronous state hypothesis is incompatible with the persistence of variability in mean-field dynamics, independent of any scaling assumptions about the synaptic weights.

##### A. Independent inputs yield exceedingly small neural variability

Cortical activity typically exhibits a high degree of trial-to-trial variability in response to identical stimuli [61, 62], with individual neuronal spiking exhibiting Poisson-process characteristics [3, 63]. Such variability is striking because neurons are thought to typically receive a large number ( $\simeq 10^4$ ) of synaptic contacts [6]. As a result, in the absence of correlations, neuronal variability should average out, leading to quasi-deterministic neuronal voltage dynamics [64]. To explain how variability seemingly defeats averaging in large neural networks, it has been proposed that neurons operate in a

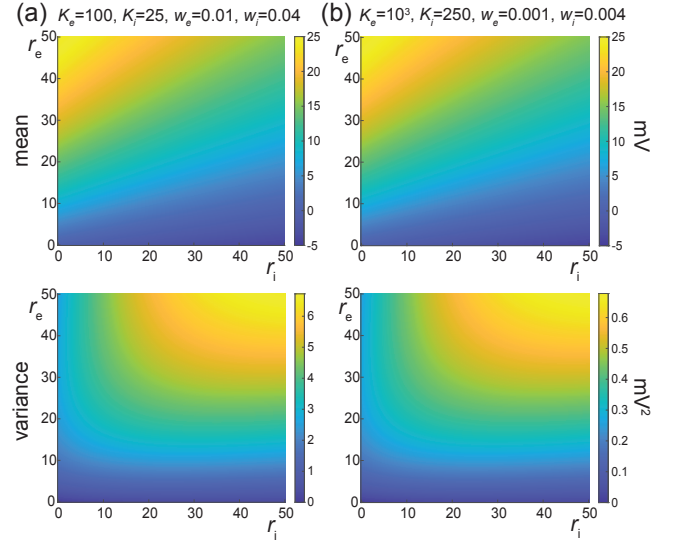


FIG. 8. **Voltage mean and variance in the absence of input correlations.** Column (a) depicts the stationary subthreshold response of an AONCB neurons driven by  $K_e = 100$  and  $K_i = 25$  synapses with typical dimensionless weights  $w_e = 0.01$  and  $w_i = 0.04$ . Column (b) depicts the stationary subthreshold response of an AONCB neurons driven by  $K_e = 10^3$  and  $K_i = 250$  synapses with moderate weights  $w_e = 0.001$  and  $w_i = 0.004$ . For synaptic weights  $w_e, w_i \ll 1$ , the mean voltage response is identical as  $K_e w_e = K_i w_i = 1$  for (a) and (b). By contrast, for  $\rho_e = \rho_i = \rho_{ei} = 0$ , the voltage variance is at least an order-of-magnitude smaller than that experimentally observed ( $4 - 9 \text{mV}^2$ ) for typical weights as shown in (a). Reaching the lower range of realistic neural variability requires driving the cell via large synaptic weights as shown in (b).

special regime, whereby inhibitory and excitatory drive nearly cancel one another [12–16]. In such balanced networks, the voltage fluctuations become the main determinant of the dynamics, yielding a Poisson-like spiking activity [12–16]. Here, we exploit the analytical framework of AONCB neurons to argue that this fluctuation-dominated picture predicts voltage fluctuations that are order of magnitudes smaller than experimental observations [1, 17–19]. Such observations indicate that the variability of the neuronal membrane voltage exhibits typical variance values of  $\simeq 4 - 9 \text{mV}^2$ . [14, 16].

Balanced models, as virtually all mean-field models, assume that neuronal inputs have zero correlation structure, for which synapses are driven by independent Poisson processes. In particular, excitation and inhibition act independently. Within the framework of AONCB neurons, this latter assumption corresponds to choosing a joint jump distribution of the form

$$p_{ei}(W_e, W_i) = \frac{b_e}{b} p_e(W_e) \delta(W_i) + \frac{b_i}{b} p_i(W_i) \delta(W_e).$$

where  $\delta(\cdot)$  denotes the Dirac delta function so that  $W_e W_i = 0$  with probability one. In other words, there

is no synchrony between excitatory and inhibitory inputs. Moreover,  $b_e$  and  $b_i$  are independently specified via Eq. (8) and the overall rate of synaptic events is purely additive:  $b = b_e + b_i$ . Consequently, the crosscorrelation efficacy  $c_{ei}$  in Eq. (30) vanishes and the dimensionless efficacies simplify to

$$a_{e,1} = b_e \tau \mathbb{E}_e [1 - e^{-W_e}] \quad \text{and} \quad a_{i,1} = b_i \tau \mathbb{E}_i [1 - e^{-W_i}],$$

where the expectations are with respect to the excitatory and inhibitory jump distributions  $p_e$  and  $p_i$ . Further assuming that individual excitatory and inhibitory synapses act independently leads to considering that  $p_e$  and  $p_i$  depict the size of individual synaptic inputs, as opposed to aggregate events. This corresponds to taking  $\beta_e \rightarrow \infty$  and  $\beta_i \rightarrow \infty$  in our parametric model based on beta distributions. Then, as intuition suggests, the overall rates of excitation and inhibition activation are recovered as  $b_e = K_e r_e$  and  $b_i = K_i r_i$ , where  $r_e$  and  $r_i$  are the individual spiking rates.

In order to investigate our findings numerically, we consider that excitatory and inhibitory synaptic weights have typical values denoted by  $w_e$  and  $w_i$ , respectively, so that  $p_e(W_e) = \delta(W_e - w_e)$  and  $p_i(W_i) = \delta(W_i - w_i)$ . Such typical weights can be estimated via biophysical considerations within the framework of AONCB neurons. In order to develop these considerations, we assume the values  $V_i = -10\text{mV} < V_L = 0 < V_e = 60\text{mV}$  for reversal potentials and  $\tau = 15\text{ms}$  for the passive membrane time constant. Given these values, we set the upper range of excitatory synaptic weights so that when delivered to a neuron close to its resting state, unitary excitatory inputs cause peak membrane fluctuations of  $\simeq 0.5\text{mV}$  at the soma, attained after a peak time of  $\simeq 5\text{ms}$ . Such fluctuations correspond to typically large *in-vivo* synaptic activations of thalamo-cortical projections in rats [65]. Although activations of similar amplitude have been reported for cortico-cortical connections [66, 67], recent large-scale *in vivo* studies have revealed that cortico-cortical excitatory connections are typically much weaker [68, 69]. At the same time, these studies have shown that inhibitory synaptic conductances are about fourfold larger than excitatory ones, but with similar timescales. Fitting these values within the framework of AONCB neurons for  $\epsilon = \tau_s/\tau \simeq 1/4$  reveals that the largest possible synaptic inputs correspond to dimensionless weights such that  $w_e \simeq 0.01$  and  $w_i \simeq 0.04$ . Furthermore, we will assume that the more numerous but comparatively moderate cortico-cortical recurrent connections are an order of magnitude weaker than typical thalamo-cortical projections, i.e.,  $w_e \simeq 0.001$  and  $w_i \simeq 0.004$ . Such a range is in keeping with estimates used in [30].

Thus, independent individual synaptic weights are small in the sense that  $w_e, w_i \ll 1$ , which warrants neglecting exponential corrections for the evaluation of the synaptic efficacies, at least in the absence of synchrony-based correlations. Accordingly, we have

$$a_{e,1} \simeq K_e r_e \tau w_e \quad \text{and} \quad a_{e,12} \simeq K_e r_e \tau w_e^2 / 2,$$

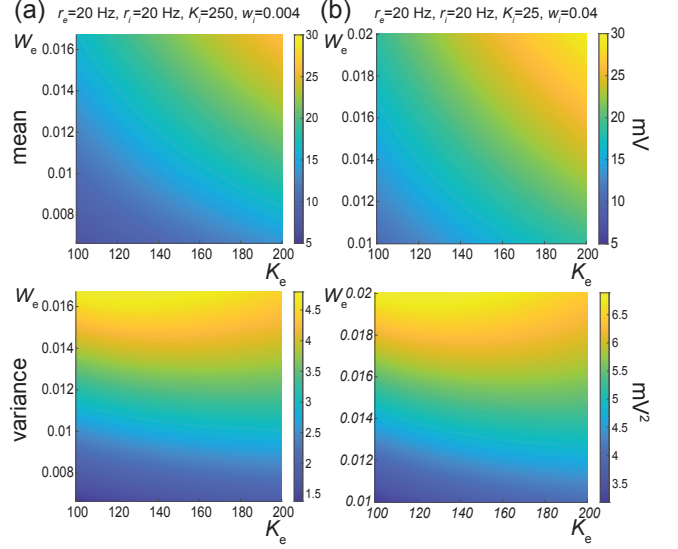


FIG. 9. **Dependence on the number of inputs and the synaptic weights in the absence of correlations.** Column (a) depicts the stationary subthreshold response of an AONCB neurons driven by a varying number of excitatory synapses  $K_e$  with varying weight  $w_e$  at rate  $r_e = 20\text{Hz}$ , with background inhibitory drive given by  $K_i = 250$  with moderate weights  $w_i = 0.004$  and  $r_i = 20\text{Hz}$ . Column (b) depicts the same as in column (a) but for a background inhibitory drive given by  $K_i = 25$  with large weights  $w_i = 0.04$  and  $r_i = 20\text{Hz}$ . For both conditions, achieving realistic level of variance, i.e.,  $\mathbb{V}[V] \simeq 4 - 9\text{mV}^2$ , while ensuring a biophysically relevant mean range of variation, i.e.,  $\Delta \mathbb{E}[V] \simeq 10-20\text{mV}$ , is only possible for large synapses:  $w_e \geq 0.015$  for moderate inhibitory synapses in Fig. 9a and  $w_e \geq 0.01$  for large synapses.

as well as symmetric expressions for inhibitory efficacies. Plugging these values in Eq. (30) yields the classical mean-field estimate for the stationary variance

$$\mathbb{V}[V] \simeq \frac{K_e r_e w_e^2 (V_e - \mathbb{E}[V])^2 + K_i r_i w_i^2 (V_i - \mathbb{E}[V])^2}{2(1/\tau + K_e r_e w_e + K_i r_i w_i)},$$

which is exactly the same expression as that derived via the diffusion and effective-time-constant approximations in [35, 36]. However, observe that the only approximation we made in obtaining the above expression is to neglect exponential corrections due to the relative weakness of biophysically relevant synaptic weights, which we hereafter refer to as the small-weight approximation.

In Fig. 8, we represent the stationary mean  $\mathbb{E}[V]$  and variance  $\mathbb{V}[V]$  as a function of the neuronal spiking input rates  $r_e$  and  $r_i$ , but for distinct values of synaptic weights  $w_e$  and  $w_i$ . In Fig. 8a, we consider synaptic weights as large as biophysically admissible based on recent *in-vivo* studies [68, 69], i.e.,  $w_e = 0.01$  and  $w_i = 0.04$ . By contrast, in Fig. 8b, we consider moderate synaptic weights  $w_e = 0.001$  and  $w_i = 0.004$ , which yield somatic postsynaptic deflections of typical amplitudes. In both cases, we consider input numbers  $K_e$  and  $K_i$  such that the mean voltage  $\mathbb{E}[V]$  covers the same biophysical range of val-

ues as  $r_e$  and  $r_i$  varies between 0Hz and 50Hz. Given a zero resting potential, we set this biophysical range to be bounded by  $\Delta\mathbb{E}[V] \leq 20\text{mV}$  as typically observed experimentally in electrophysiological recordings. These conditions correspond to constant aggregate weights set to  $K_e w_e = K_i w_i = 1$  so that

$$K_e r_e w_e = K_i r_i w_i \leq 50\text{Hz} \simeq 1/\tau.$$

This implies that the AONCB neurons under consideration do not reach the high-conductance regime for which the passive conductance can be neglected, i.e.,  $K_e r_e w_e + K_e r_i w_i \gg 1/\tau$  [70]. Away from the high-conductance regime, the variance magnitude is controlled by the denominator of Eq. (31). Accordingly, the variance in both cases is primarily dependent on the excitatory rate  $r_e$  since for  $K_e w_e = K_i w_i = 1$ , the effective excitatory driving force  $F_e = K_e w_e^2 (V_e - \mathbb{E}[V])^2$  dominates the effective inhibitory driving force  $F_i = K_i w_i^2 (V_i - \mathbb{E}[V])^2$ . This is because the neuronal voltage typically sits close to the inhibitory reversal potential but far from the excitatory reversal potential  $V_e - \mathbb{E}[V] > \mathbb{E}[V] - V_i$ . For instance, when close to rest  $\mathbb{E}[V] \simeq 0$ , the ratio of the effective driving forces is  $(K_e w_e^2 V_e^2)/(K_i w_i^2 V_i^2) \simeq 9$  fold in favor of excitation. Importantly, the magnitude of the variance is distinct for moderate synapses and for large synapses. This is because for constant aggregate weights  $K_e w_e = K_i w_i = 1$ , the ratio of effective driving forces for large and moderate synapses scales in keeping with the ratio of the weights, and so does the ratio of variances away from the high conductance regime. Thus we have

$$F_e|_{w_e=10^{-2}}/F_e|_{w_e=10^{-3}} = F_i|_{w_i=10^{-2}}/F_i|_{w_i=10^{-3}} = 10,$$

and the variance decreases by one order of magnitude from large weights in Fig. 8a to moderate weights in Fig. 8b.

The above numerical analysis reveals that achieving realistic levels of subthreshold variability for a biophysical mean range of variation requires AONCB neurons to be exclusively driven by large synaptic weights. This is confirmed by considering the voltage mean  $\mathbb{E}[V]$  and variance  $\mathbb{V}[V]$  in Fig. 9 as a function of the number of inputs  $K_e$  and of the synaptic weights  $w_e$  for a given level of inhibition. We choose this level of inhibition to be set by  $K_i = 250$  moderate synapses  $w_i = 0.004$  with  $r_i = 20\text{Hz}$  in Fig. 9a and by  $K_i = 25$  large synapses  $w_i = 0.04$  with  $r_i = 20\text{Hz}$  in Fig. 9b. As expected, assuming that  $r_e = 20\text{Hz}$  in the absence of input correlations, the voltage mean  $\mathbb{E}[V]$  only depends on the product  $K_e w_e$ , which yields similar mean range of variations for  $K_e$  varying up to 2000 in Fig. 9a and up to 200 in Fig. 9b. Thus, it is possible to achieve the same range of variations as with moderate synaptic with a fewer number of larger synaptic weights. By contrast, the voltage variance  $\mathbb{V}[V]$  only achieves realistic levels for large synaptic weights in both conditions, with  $w_e \geq 0.015$  for moderate inhibitory background synapses in Fig. 9a and  $w_e \geq 0.01$  for large inhibitory background synapses in Fig. 9b.

## B. Including input correlations yields realistic subthreshold variability

With zero correlation structure, achieving the experimentally observed variability necessitates an excitatory drive mediated via synaptic weights  $w_e \simeq 0.01$ , which corresponds to the upper bounds of the biophysically admissible range and is in agreement with numerical results presented in [30]. Given such synaptic weights, every single excitatory synaptic activation would cause a post-synaptic potential with a peak amplitude larger or equal to 0.5mV. Albeit possible, this is unrealistic given the wide distribution of amplitudes observed experimentally, whereby the vast majority of synaptic events are small to moderate, at least for cortico-cortical connections [68, 69]. In principle, one can remedy this issue by allowing for synchronous activation of, say,  $k_e = 10$  synapses with moderate weight  $w_e = 0.001$ , as it amounts to the activation of a single synapse with large weight  $k_e w_e = 0.01$ . A weaker assumption that yields a similar increase in neural variability is to only ask for synapses to tend to synchronize probabilistically, which amounts to require  $k_e$  to be a random variable with some distribution mass on  $\{k_e > 1\}$ . This exactly amounts to model the input drive via a jump process as presented in Section II, with a jump distribution  $p_e$  that probabilistically captures this degree of input synchrony. In turn, this distribution  $p_e$  corresponds to a precise input correlation  $\rho_e$  via Eq. (7).

With these preliminary remarks in mind, we explore the role of input correlations in shaping the voltage variability of AONCB neurons with instantaneous synapses. Experimental estimates of the spiking correlations are typically thought as weak with coefficients ranging from 0.01 to 0.04 [7–9]. However, it is important to note that such weak values do not warrant the neglect of correlations owing to the typically high number of synaptic connections. Actually, if  $K_e$  denotes the number of excitatory inputs, all assumed to play exchangeable roles, an empirical criterion to decide whether a correlation coefficient  $\rho_e$  is weak is that  $\rho_e < 1/K_e$  [23, 24]. Assuming the lower estimate of  $\rho_e \simeq 0.01$ , this criterion is achieved for  $\simeq 100$  inputs, which is well below the typical number of excitatory synapses for cortical neurons. We confirm the impact of nonzero correlation in Fig. 10 where we consider the cases of moderate weights  $w_e = 0.001$  and  $w_e = 0.004$  and large weights  $w_e = 0.01$  and  $w_i = 0.04$  as in Fig. 8 but for  $\rho_e = \rho_i = 0.03$ . Specifically, we assume in both cases that the AONCB neuron is subjected to two independent beta-binomial-derived compound Poisson process drives with rate  $b_e$  and  $b_i$ , respectively. We compute both rate of synaptic events  $b_e$  and  $b_i$  via (8) by setting  $\beta_e = \beta_i = 1/\rho_e - 1 = 1/\rho_i - 1$  and for the corresponding number of inputs  $K_e$  and  $K_i$  and spiking rates  $r_e$  and  $r_i$ . This ensures that the mean number of synaptic activations  $b_e \mathbb{E}_{ei}[k_e] = K_e r_e$  and  $b_i \mathbb{E}[k_i] = K_i r_i$  remains constant when compared with Fig. 8. As a result, the mean response of the AONCB

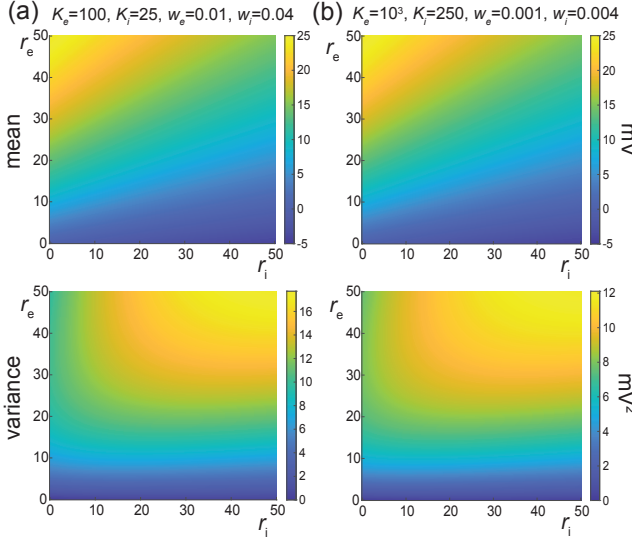


**FIG. 10. Voltage mean and variance in the presence of excitatory and inhibitory input correlations but without correlation across excitation and inhibition:**  $\rho_e = \rho_i > \rho_{ei} = 0$ . Column (a) depicts the stationary subthreshold response of an AONCB neurons driven by  $K_e = 100$  and  $K_i = 25$  synapses with typical dimensionless weights  $w_e = 0.01$  and  $w_i = 0.04$ . Column (b) depicts the stationary subthreshold response of an AONCB neurons driven by  $K_e = 10^3$  and  $K_i = 250$  synapses with atypically large dimensionless weights  $w_e = 0.001$  and  $w_i = 0.004$ . For synaptic weights  $w_e, w_i \ll 1$ , the mean voltage response is identical as  $K_e w_e = K_i w_i = 1$  for (a) and (b). By contrast with the case of no correlation in Fig. 8, for  $\rho_e = \rho_i = 0.03$  and  $\rho_{ei} = 0$ , the voltage variance achieved similar level as experimentally observed ( $4 - 9 \text{mV}^2$ ) for typical weight as shown in (a), but slightly too large levels for large synaptic weight as shown in (b).

neuron is essentially left unchanged by the presence of correlations, with virtually identical biophysical range of variations  $\Delta \mathbb{E}_{ei} [V] \simeq 10-20 \text{mV}$ . This is because for correlation  $\rho_e = \rho_i \simeq 0.03$ , the aggregate weights still satisfy  $k_e w_e, k_i w_i < 1$  with probability close to one given that  $K_e w_e = K_i w_i = 1$ . Then, in the absence of crosscorrelation, i.e.,  $\rho_{ei} = 0$ , we still have

$$a_{e,1} = b_e \tau \mathbb{E}_e [1 - e^{-k_e w_e}] \simeq b_e \tau w_e \mathbb{E}_e [k_e] = K_e r_e \tau w_e ,$$

as well as  $a_{i,1} \simeq K_i r_i \tau w_i$  by symmetry. However, for both moderate and large synaptic weights, the voltage variance  $\mathbb{V}[V]$  now exhibits similar or slightly larger magnitudes than observed experimentally. This is because the second-order efficacies involved in the denominator of Eq. (30) with  $c_{ei} = 0$  satisfy

$$a_{e,12} = \frac{b_e \tau}{2} \mathbb{E}_e [(1 - e^{-k_e w_e})^2] \simeq \frac{b_e \tau w_e^2}{2} \mathbb{E}_e [k_e^2] ,$$

and a symmetric relation for  $a_{i,2}$ . In turn, using the parametric form Eq. (6) for  $p_{e,k}$ , one can show that

$$a_{e,12} \simeq (1 + \rho_e (K_e - 1)) \frac{K_e r_e \tau w_e^2}{2} ,$$

where we recognize  $K_e r_e \tau w_e^2 / 2 = a_{e,12}|_{\rho_e=0}$  as the second-order efficacy in the absence of correlations from Fig. 8. A similar statement holds for the inhibition-related second-order efficacy  $a_{i,12}$ . This shows that correlations increase neural variability whenever  $\rho_e > 1/K_e$  or  $\rho_i > 1/K_i$ , which exactly coincides with the empirical criterion given previously to assess the relative weakness of correlations.

Recapitulating all these statements shows that including correlation separately in the excitatory and inhibitory inputs yields an increase in the neural variability. Specifically, when excitation and inhibition act independently, i.e.,  $\rho_{ei} = 0$ , we find in Appendix K that

$$\mathbb{V}[V]|_{\rho_{ei}=0} - \mathbb{V}[V]|_{\rho_{e/i}=\rho_{ei}=0} \simeq \frac{\rho_e (K_e - 1) K_e r_e w_e^2 (V_e - \mathbb{E}[V])^2 + \rho_i (K_i - 1) K_i r_i w_i^2 (V_i - \mathbb{E}[V])^2}{2(1/\tau + K_e r_e w_e + K_i r_i w_i)} , \quad (31)$$

which follows from the fact that the small-weight approximation for  $\mathbb{E}[V]$  is independent of correlations and from neglecting the exponential corrections due to the nonzero size of the synaptic weights. In particular, the above formula remains valid as long as the correlations  $\rho_e$  and  $\rho_i$  are weak enough so that the aggregate weights satisfy  $k_e w_e, k_i w_i < 1$  with probability close to one. To inspect the relevance of exponential corrections, we estimate in Appendix L the error incurred by neglecting exponential corrections. Focusing on the case of excitatory inputs, we find that for correlation coefficients  $\rho_e \leq 0.05$ , neglecting exponential corrections incurs less than a 3% error if the number of inputs is smaller than  $K_e \leq 1000$  for moderate

synaptic weight  $w_e = 0.001$  or than  $K_e \leq 100$  for large synaptic weight  $w_e = 0.01$ .

The voltage variance shown in Fig. 10 for  $\rho_e = \rho_i = 0.03$  and  $\rho_{ei} = 0$  exceeds the typical levels measured *in vivo*, i.e.,  $4 - 9 \text{mV}^2$ , for large synaptic weights. The inclusion of correlations between excitation and inhibition, i.e.,  $\rho_{ei} > 0$  can reduce the voltage variance to more realistic levels. We confirm this point in Fig. 11 where we consider the cases of moderate weights  $w_e = 0.001$  and  $w_e = 0.004$  and large weights  $w_e = 0.01$  and  $w_i = 0.04$  as in Fig. 10 but for  $\rho_e = \rho_i = \rho_{ei} = 0.03$ . Positive crosscorrelation between excitation and inhibition only marginally impacts the mean voltage response. This is due to the fact

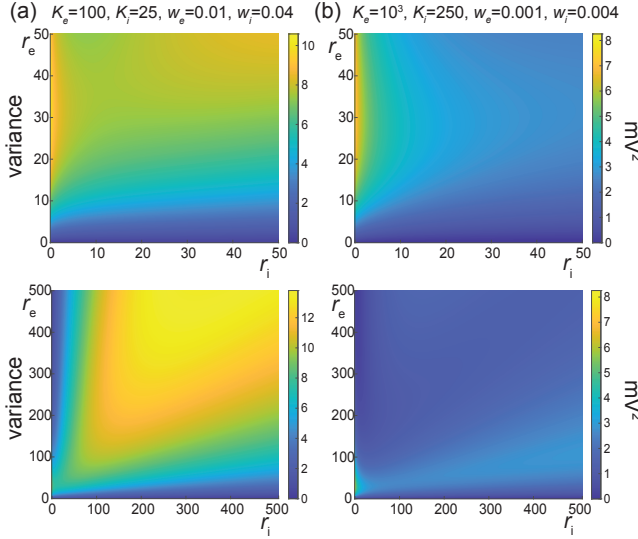


**FIG. 11. Voltage mean and variance in the presence of excitatory and inhibitory input correlations and with correlation across excitation and inhibition:**  $\rho_e = \rho_i = \rho_{ei} > 0$ . Column (a) depicts the stationary subthreshold response of an AONCB neurons driven by  $K_e = 100$  and  $K_i = 25$  synapses with typical dimensionless weights  $w_e = 0.01$  and  $w_i = 0.04$ . Column (b) depicts the stationary subthreshold response of an AONCB neurons driven by  $K_e = 10^3$  and  $K_i = 250$  synapses with atypically large dimensionless weights  $w_e = 0.001$  and  $w_i = 0.004$ . For synaptic weights  $w_e, w_i \ll 1$ , the mean voltage response is identical as  $K_e w_e = K_i w_i = 1$  for (a) and (b). Compared with the case of no crosscorrelation in Fig. 10, for  $\rho_e = \rho_i = \rho_{ei} = 0.03$ , the voltage variance is reduced to a biophysical range similar to that experimentally observed ( $4 - 9 \text{mV}^2$ ) for typical weight as shown in (a), as well as for atypically large synaptic weight as shown in (b).

that exponential corrections become slightly more relevant as the presence of crosscorrelation leads to larger aggregate weights:  $W_e + W_i$  with  $W_e$  and  $W_i$  possibly being jointly positive. By contrast with this marginal impact on the mean response, the voltage variance is significantly reduced when excitation and inhibition are correlated. This is in keeping with the intuition that the net effect of such crosscorrelation is to cancel excitatory and inhibitory synaptic inputs with one another, before they can cause voltage fluctuations. The amount by which the voltage variance is reduced can be quantified in the small-weight approximation. In this approximation, we show in Appendix K that the efficacy  $c_{ei}$  capturing the impact of crosscorrelations simplifies to

$$c_{ei} \simeq \frac{b\tau}{2} \mathbb{E}_{ei} [W_e W_i] = (\rho_{ei} \sqrt{r_e r_i} \tau / 2) (K_e w_e) (K_i w_i).$$

Using the above simplified expression and invoking the fact that the small-weight approximation for  $\mathbb{E}[V]$  is independent of correlations show a decrease in the voltage

variance in the amount

$$\begin{aligned} \mathbb{V}[V] - \mathbb{V}[V] |_{\rho_{ei}=0} &\simeq \\ -\frac{\rho_{ei} \sqrt{r_e r_i} (K_e w_e) (K_i w_i) (V_e - \mathbb{E}[V]) (\mathbb{E}[V] - V_i)}{1/\tau + K_e r_e w_e + K_i r_i w_i} &\leq 0. \end{aligned} \quad (32)$$

Despite the above reduction in variance, we show in Appendix K that positive correlations always cause an overall increase of neural variability:

$$0 \leq \mathbb{V}[V] |_{\rho_{e/i}=\rho_{ei}=0} \leq \mathbb{V}[V] \leq \mathbb{V}[V] |_{\rho_{ei}=0}.$$

### C. Variability-preserving scaling limits

Numerical analysis reveals that the correlations must significantly impact the voltage variability whenever the number of inputs are such that  $K_e > 1/\rho_e$  or  $K_i > 1/\rho_i$ . Spiking correlations are typically measured *in vivo* to be larger than 0.01. Therefore, synchrony must shape the response of neurons that are driven by more than 100 active inputs, which is presumably allowed by the typically high number of synaptic contacts ( $\simeq 10^4$ ) in cortex [6]. In practice, we find that synchrony can explain the relatively high level of neural variability observed in the subthreshold neuronal responses. Beyond these practical findings, we predict that input synchrony also have significant theoretical implications with respect to modeling spiking networks. Analytically tractable models for cortical activity are generally obtained by considering spiking networks in the infinite-size limit. Such infinite-size networks are tractable because the neurons they comprise only interact via population averages, erasing any role for nonzero correlation structure. Distinct mean-field models assume that synaptic weights vanish according to distinct scalings with respect to the number of synapses, i.e.,  $w_{e/i} \rightarrow 0$  as  $K_{e/i} \rightarrow \infty$ . In particular, classical mean-field limits consider the scaling  $w_{e/i} \sim 1/K_{e/i}$ , balanced mean-field limits consider the scaling  $w_{e/i} \sim 1/\sqrt{K_{e/i}}$ , with  $K_e w_e - K_i w_i = O(1)$ , and strong coupling limits consider the scaling  $w_{e/i} \sim 1/\ln K_{e/i}$ , with  $K_e w_e - K_i w_i = O(1)$  as well. Importantly, all these mean-field limits assume no correlation, and in particular, no synchrony.

Our analysis of AONCB neurons shows that the neglect of synchrony-based correlations is incompatible with the maintenance of neural variability in the infinite-size limit. Indeed, Eq. (31) shows that for any scaling with  $1/w_e = o(K_e)$  and  $1/w_i = o(K_i)$ , as for all the mean-field limits mentioned above, we have

$$\mathbb{V}[V] = O(w_e) + O(w_i) \xrightarrow{K_e, K_i \rightarrow \infty} 0.$$

Thus, in the absence of correlation and independent of the synaptic weight scaling, the subthreshold voltage variance of AONCB neurons must vanish in the limit of arbitrary large numbers of synapses. We expect such decay of the voltage variability to be characteristic of conductance-based models in the absence of input correlation. Indeed, dimensional analysis suggests that volt-

age variance for both current-based and conductance-based models are generically obtained via normalization by the reciprocal of the membrane time constant. However, by contrast with current-based models, the reciprocal of the membrane time constant for conductance-based models, i.e.,  $1/\tau + K_e w_e r_e + K_i w_i r_i$ , involves contributions from synaptic conductances. Thus, to ensure nonzero asymptotic variability, the denominator scaling  $O(K_e w_e) + O(K_i w_i)$  must be balanced by the natural scaling of the Poissonian input drives, i.e.,  $O(K_e w_e^2) + O(K_i w_i^2)$ . In the absence of input correlations, this is only possible for fixed-size weights, which is incompatible with any scaling assumptions. Assuming fixed-size weights and taking the limit  $K_{e/i} \rightarrow \infty$  with fixed rate-input ratio  $\gamma_{ei} = (K_e r_e)/(K_i r_i)$ , yields

$$\frac{\mathbb{V}[V]}{(V_e - \mathbb{E}[V])(\mathbb{E}[V] - V_i)} = \frac{1 + \gamma_{ei}}{\left(\frac{1 + e^{-w_i}}{1 - e^{-w_e}}\right) + \gamma_{ei} \left(\frac{1 + e^{-w_e}}{1 - e^{-w_i}}\right)} \leq 1, \quad (33)$$

which follows from neglecting the passive leak in the high-conductance regime [70]. As for  $0 < \gamma_{ei} < \infty$ , we necessarily have  $V_i < \mathbb{E}[V] < V_e$ , this shows that variability is preserved in the infinite-size limit for fixed synaptic weights in the absence of correlations. This observation is by contrast with current-based models for which variability diverges, while holding independent of any balance conditions. Moreover observe that equality in (33) is achieved for  $w_{e/i} \rightarrow \infty$ . This indicates that even in the limit of arbitrary large weights, variability is maintained but the voltage distribution becomes bimodal with support on  $\{V_e, V_i\}$ . For small weights  $4w_e = w_i \ll 1$ , the voltage distribution remains unimodal around its mean value  $\mathbb{E}[V]$ . Actually, one can check that maximum variance is attained for  $\gamma_{ei} \simeq 6.6$ , which corresponds to a depolarization of  $\mathbb{E}[V] \simeq 27.5\text{mV}$  above resting potential. This value yields the upper bound estimate  $\mathbb{V}[V] \leq 1200w_e\text{mV}^2$ , which amounts to  $\simeq 1.2\text{mV}^2$  for moderate synaptic weight ( $w_e = 0.001$ ) and  $\simeq 12\text{mV}^2$  for large synaptic weights ( $w_e = 0.01$ ). Thus, as expected the neglect of the passive conductance compared to synaptic conductances incurs a moderate but significant increase of neural variability.

The above discussion shows that naive infinite-size limits with fixed-size synaptic weights preserve neural variability in conductance-based models, at least for AONCB neurons. However, these naive limits are problematic for restricting modeled neurons to operate in the high-conductance regime, whereby the passive conductance properties of the cell plays no role. Such a regime is biophysically unrealistic as it implies that the cell would respond to perturbations infinitely fast. We propose to address this issue by considering a new type of variability-preserving limit models obtained with for the classical scaling but in the presence of synchrony-based correlations. For simplicity, let us consider our correlated input model with excitation alone in the limit of an arbi-

trary large number of inputs  $K_e \rightarrow \infty$ . When  $\rho_e > 0$ , the small-weight approximation Eq. (31) suggests that adopting the scaling  $w_e \sim \Omega_e/K_e$ , where  $\Omega_e$  denotes the aggregate synaptic weight, yields a nonzero contribution when  $K_e \rightarrow \infty$  as the numerator scales as  $O(K_e^2 w_e^2)$ . It turns out that this choice can be shown to be valid without resorting to any approximations. Indeed, under the classical scaling assumption, we show in Appendix M that the discrete jump distribution  $p_{e,k}$  weakly converges to the continuous density  $d\nu_e/dw$  in the sense that

$$b_e \sum_{k=1}^{K_e} p_{e,k} \delta\left(\frac{w}{\Omega_e} - \frac{k}{K_e}\right) dw \xrightarrow{K_e \rightarrow \infty} \nu_e(dw) = \frac{r_e \beta_e}{w} \left(1 - \frac{W_e}{w}\right)^{\beta_e - 1} dw. \quad (34)$$

The above density has infinite mass over  $[0, \Omega_e]$  owing to its diverging behavior in zero and is referred to as a degenerate beta distribution. In spite of its degenerate nature, it is known that densities of the above form define well-posed processes, the so-called beta processes, which have been studied extensively in the field of nonparametric Bayesian inference [50, 51].

Originally introduced by Hjort for survival analysis [49], beta processes are examples of positive completely random measures  $Z$  on  $\mathbb{R}$ . Completely random measures  $Z$  on  $\mathbb{R}$  are set-indexed processes such that the masses  $Z(S_1), \dots, Z(S_k)$  assigned to disjoint subsets  $S_1, \dots, S_k$  in  $\mathbb{R}$  specify independent random variables, whose laws are uniquely characterized by a positive measure  $\nu$  on  $\mathbb{R} \times \mathbb{R}^+$ , called the Lévy measure [71, 72]. Beta processes  $Z \sim \text{BetaP}(\beta_e)$  correspond to Lévy measures on  $\mathbb{R} \times [0, \Omega_e]$  that are precisely of the form  $\nu(dt, dw) = \nu_e(dw) dt$ , where  $\nu_e$  is given by Eq. (34). Owing to the degeneracy of the Lévy measure  $\nu_e(dw) dt$ , beta processes  $Z$  can only be represented over a time interval  $[0, T]$  as countably infinite sums of Dirac delta masses

$$Z = \sum_k w_{e,k} \delta_{t_{e,k}},$$

where the pairs  $(t_{e,k}, w_{e,k})$  are defined as points from a bivariate Poisson process over  $\mathbb{R} \times [0, \Omega_e]$  with intensity given by the Lévy measure  $\nu_e(dw) dt$ , [50, 51]. Within our modeling framework,  $\{t_{e,k}\}$  represents the infinite set of synaptic activation times obtained in the limit of an arbitrary large number of inputs  $K_e \rightarrow \infty$ , whereas  $\{w_{e,k}\}$  represents the associated jump size amplitudes, whose fluctuating size captures correlations via  $\rho_e = 1/(1 + \beta_e)$ . Importantly, notice that although there is of infinite number of jumps, the overall mass  $Z([0, T])$ , i.e., the cumulative jump size, remains finite with probability one. Actually, one can check that

$$\mathbb{E}[Z([0, T])] = \int_{[0, T] \times [0, \Omega_e]} w \nu_e(dw) dt = r_e T \Omega_e,$$

thereby showing that  $\Omega_e$  can be interpreted as an effective mean jump size.

The point of the above discussion is to justify that taking the infinite-size limit  $K_e \rightarrow \infty$  with classical scaling  $w_e \sim 1/K_e$  specifies well-defined input drives as jump processes, at least when considering excitation alone. By contrast with the compound Poisson processes obtained for finite input numbers  $K_e < \infty$ , these processes admit a countably infinite, dense set of activation times  $\{t_{e,k}\}$ , as intuition suggests for  $K_e \rightarrow \infty$ . Rather than being defined by a probability distribution as for compound Poisson processes, the statistics of the positive jumps  $\{w_{e,k}\}$  occurring at  $\{t_{e,k}\}$  is specified by a Lévy measure  $\nu_e$ . This Lévy measure typically exhibits a nonintegrable degeneracy in zero but are such that all moments are finite, allowing one to specify the corresponding spiking correlation via

$$\rho_e = \frac{\int_0^{\Omega_e} w^2 \nu_e(dw)}{\Omega_e \int_0^{\Omega_e} w \nu_e(dw)},$$

which directly generalizes Eq. (7) to processes with a countable infinity of positive jumps. This shows that the Lévy measure  $\nu_e$  fully parametrizes our correlated excitation input model in the infinite-size limit with classical synaptic scaling. Then, the key observation is that these generalized input models can serve as the drive of AONCB neurons, just as compound Poisson processes do. Moreover, as processes parametrized via Lévy measures can be obtained as limits of compound Poisson processes, all our analytical results will remain valid for this more generic class of processes. Concretely, for excitation alone, our results generalize by replacing all expectations of the form  $b_e \mathbb{E}_e[\cdot]$  by integral with respect to the Lévy measure  $\nu_e$ . One can easily check that these expectations, which feature prominently in the definition of the various synaptic efficacies, all remain finite under the condition of moments integrability listed above. Thus, the voltage mean and variance of AONCB neurons remain finite with

$$\begin{aligned} \mathbb{E}[V] &= \frac{V_e \int_0^{\Omega_e} (1 - e^{-w}) \nu_e(dw)}{1/\tau + \int_0^{\Omega_e} (1 - e^{-w}) \nu_e(dw)}, \\ \mathbb{V}[V] &= \frac{(V_e - \mathbb{E}[V])^2 \int_0^{\Omega_e} (1 - e^{-w})^2 \nu_e(dw)}{2/\tau + \int_0^{\Omega_e} (1 - e^{-2w}) \nu_e(dw)}. \end{aligned}$$

Observe that as  $(1 - e^{-w})^2 \leq w^2$  for all  $w \geq 0$ , the definition of the spiking correlation in Eq. (35) implies that we have  $\mathbb{V}[V] = O(\rho_e)$  so that neural variability consistently vanishes in the absence of correlations.

## V. DISCUSSION

### A. Synchrony modeling

We have presented a parametric representation of the neuronal drives resulting from a finite number of asynchronous or (weakly) synchronous synaptic inputs. Several parametric statistical models have been proposed for

generating correlated spiking activities in a discrete setting [48, 73–75]. Such models have been used to analyze the activity of neural populations via Bayesian inference methods [76–78], as well as maximum entropy methods [79, 80]. Our approach is not to simulate or analyze complex neural dependencies but rather to derive from first principles the synchronous input models that could drive conductance-based neuronal models. This approach primarily relies on extending the definition of discrete-time correlated spiking models akin to [48] to the continuous-time setting. To do so, the main tenet of our approach is to realize that input synchrony and spiking correlation represent equivalent measures under the assumption of input exchangeability.

Input exchangeability posits that the driving inputs form a subset of an arbitrarily large pool of exchangeable random variables [44, 45]. In particular, this implies that the main determinant of the neuronal drive is the number of active inputs, as opposed to the magnitude of these synaptic inputs. Then, de Finetti theorem [46] states that the probability of observing a given input configuration can be represented in the discrete setting under an integral form (see Eq. (3)) involving a directing probability measure  $F$ . Intuitively,  $F$  represents the probability distribution of the fraction of coactivating inputs at any discrete time. Our approach identifies the directing measure  $F$  as a free parameter that captures input synchrony. The more dispersed the distribution  $F$ , the more synchronous the inputs, as previously noted in [81, 82]. Our work elaborates on this observation to develop computationally tractable statistical models for synchronous spiking in the continuous-time limit, i.e., for vanishing discrete time step  $\Delta t \rightarrow 0^+$ .

We derive our results using a discrete-time directing measure chosen as beta distribution  $F \sim B(\alpha, \beta)$ , where the parameters  $\alpha$  and  $\beta$  can be related to the individual spiking rate  $r$  and the spiking correlation  $\rho$  via  $r\Delta t = \alpha/(\alpha + \beta)$  and  $\rho = 1/(1 + \alpha + \beta)$ . For this specific choice of distribution, we are able to construct statistical models of the correlated spiking activity as generalized beta-binomial processes [49], which play an important role in statistical Bayesian inference [50, 51]. This construction allows us to fully parametrize the synchronous activity of a finite number of inputs via the jump distribution of a compound Poisson process, which depends explicitly on the spiking correlation. For being continuously indexed in time, stationary compound Poisson processes can naturally serve as the drive to biophysically relevant neuronal models. The idea to utilize compound Poisson processes to model input synchrony was originally proposed in [83, 84], but without constructing these processes as limits of discrete spiking models and without providing explicit functional form for their jump distributions.

We expect our framework to apply to any exchangeable spiking models for which the directing probability measure  $F$  is such that  $\mathbb{E}[\theta] \sim \Delta t$  and  $\mathbb{V}[\theta] \sim \Delta t$  in the vanishing timescale limit  $\Delta t \rightarrow 0^+$ . Moreover, our frame-

work generalizes to multidimensional compound Poisson process when applied to partially exchangeable neural populations [52], which is necessary to account for the distinction between excitatory and inhibitory neuronal populations. Generic dependencies between distinct populations can be achieved via classical statistical techniques such as copulas [53, 54], supporting the flexibility of our exchangeability-based modeling approach. That being said, it is worth mentioning that such approaches also suffer from a range of limitations that we will discuss later.

### B. Moment analysis

We also present an analytical characterization of the subthreshold variability of a tractable conductance-based neuronal model, the AONCB neurons, when driven by synchronous synaptic inputs. The analytical characterization of a neuron's voltage fluctuations has been the focus of intense research [35, 36, 85–87]. These attempts have considered neuronal models that already incorporate some diffusion scaling hypotheses [88, 89], formally obtained by assuming an infinite number of synaptic inputs. The primary benefit of these diffusion approximations is that one can treat the corresponding Fokker-Planck equations to quantify neuronal variability in conductance-based integrate-and-fire models, while also including the effect of post-spiking reset [29, 30]. In practice, subthreshold variability is often estimated in the effective-time-constant approximation, while neglecting the multiplicative noise contributions due to considering voltage-dependent membrane fluctuations [35, 85, 86], although an exact treatment is also possible without this simplifying assumption [30]. By contrast, the analysis of conductance-based models has resisted exact treatments when driven by shot noise, as for compound Poisson input processes, rather than by Gaussian white noise, as in the diffusion approximation [59, 60].

The exact treatment of shot-noise-driven neuronal dynamics is primarily hindered by the limitations of the Ito/Stratonovich integrals [55, 56] to capture the effects of point-process-based noise sources, even without including a reset mechanism. These limitations were originally identified by Marcus, who proposed to approach the problem via a new type of stochastic equation [33, 34]. The key to Marcus equation is to define shot noise as limits of regularized, well-behaved approximations of that shot noise, for which classical calculus applies [57]. In practice, these approximations are canonically obtained as the solutions of shot-noise-driven Langevin equations with relaxation time scale  $\tau_s$ , and shot noise is formally recovered in the limit  $\tau_s \rightarrow 0^+$ . Our assertion here is that all-or-none conductances implement such a form of shot-noise regularization for which a natural limiting process can be defined when synapses operate instantaneously, i.e.,  $\tau_s \rightarrow 0^+$ . The main difference with the canonical

Marcus approach is that our regularization is all-or-none, substituting each Dirac delta impulse with a finite step-like impulse of duration  $\tau_s$  and magnitude  $1/\tau_s$ , thereby introducing a synaptic timescale but without any relaxation mechanism.

The above assertion is the basis for introducing AONCB neurons, which is supported by our ability to obtain exact formulas for the first two moments of their stationary voltage dynamics (see Eq. (19) and Eq. (30)). For  $\tau_s > 0$ , these moments can be expressed in terms of synaptic efficacies that takes exact but rather intricate integral forms. Fortunately, these efficacies drastically simplify in the instantaneous synapse limit  $\tau_s \rightarrow 0^+$ , for which the canonical shot-noise drive is recovered. These resulting formulas mirror those obtained in the diffusion and effective-time-constant approximations [35, 36], except that the featured dimensionless coefficients are specified as the first-order efficacies  $a_{e/i,1}$  for the mean (see Eq. (17) and Eq. (18)), and as the second-order efficacies  $a_{e/i,2}$ ,  $a_{e/i,12}$ , and  $c_{ei}$  for the variance (see Eq. (25), Eq. (26), Eq. (27), Eq. (28), and Eq. (29)). These synaptic efficacies differ from the coefficients obtained in the diffusion and effective-time-constant approximations in three ways: First, independent of input synchrony, these efficacies all have exponential forms and saturate in the limit of large synaptic weights  $w_e, w_i \rightarrow \infty$ , with  $a_{e/i,1} \leq b\tau$  and  $a_{e/i,2}, a_{e/i,12}, c_{ei} \leq b\tau/2$ . Such saturation is a general characteristic of shot-noise-driven, continuously-relaxing systems [90–92]. Second, these efficacies are defined as expectations with respect to the jump distribution  $p_{ei}$  of the driving compound Poisson process (see Eq. (11) and Appendix B). A nonzero dispersion of  $p_{ei}$ , indicating that synaptic activation is truly modeled via random variables  $W_e$  and  $W_i$ , is the hallmark of input synchrony [83, 84]. Third, these efficacies involve the overall rate of synaptic activation  $b$  (see (12)), which also depends on input synchrony. Such dependence can be naturally understood within the framework of Palm calculus [93], a form of calculus specially developed for stationary point processes (see Appendix C).

Finally, note that our approach is distinct from those adopted in recent computational and theoretical works [94–97] as our focus is on the derivation of exact formulas with explicit dependence on inputs numbers, sizes and correlations. Importantly, the moment expressions obtained in the diffusion and effective-time-constant approximations can be recovered within our framework by making the two independent assumptions that (i) synaptic weights are small, i.e.,  $w_{e,1}, w_{i,1} \ll 1$  and that (ii) input synchrony can be neglected, i.e.  $\rho_e = \rho_i = \rho_{ei} = 0$ . Moreover, observe that our exact results are obtained for shot-noise drives without any approximation, including for nonzero synaptic time constant  $\tau_s > 0$ , and only take an interpretable form in the instantaneous synapse limit  $\tau_s \rightarrow 0^+$ . Our moment formulas, derived for compound Poisson processes, directly generalize to the larger mathematical class of Lévy processes with positive jumps [40, 41], which may be useful

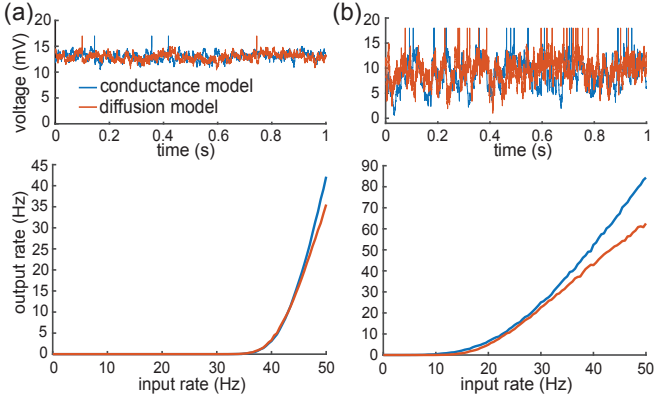


FIG. 12. **Diffusion approximations in the presence of synchrony.** (a) Comparison of an asynchronously driven integrate-and-fire AONCB neuron (blue trace) with its diffusion approximation obtained via the effective-time-constant approximation (red trace). (b) Comparison of a synchronously driven integrate-and-fire AONCB neuron (blue trace) with its diffusion approximation obtained by our exact analysis (red trace). Parameters:  $K_e = 1000$ ,  $K_i = 350$ ,  $\tau = 15$  ms,  $w_e = 0.001$ ,  $w_i = 0.004$ ,  $r_e = r_i = 25$  Hz,  $\rho_e = \rho_i = 0.03$ ,  $\rho_{ei} = 0$ ,  $V_T = 15$  mV, and  $V_R = 12$  mV.

to define new scaling limits for neuronal activity.

### C. Biophysical relevance

Our analysis allows us to investigate quantitatively how subthreshold variability depends on the numbers and strength of the synaptic contacts. This approach requires that we infer synaptic weights from the typical peak time and peak amplitude of the somatic membrane fluctuations caused by post-synaptic potentials [65, 68, 69]. Within our modeling framework, these weights are dimensionless quantities that we estimate by fitting the AONCB neuronal response to a single all-or-none synaptic activation at rest. For biophysically relevant parameters, this yields typically small synaptic weights in the sense that  $w_e, w_i \ll 1$ . These small values warrant adopting the small-weight approximation, for which expressions Eq. (19) and Eq. (30) simplify.

In the small-weight approximation, the mean voltage becomes independent of input synchrony, whereas the simplified voltage variance Eq. (31) only depends on input synchrony via the spiking correlation coefficients  $\rho_e$ ,  $\rho_i$ , and  $\rho_{ei}$ , as opposed to depending on a full jump distribution. Spike-count correlations have been experimentally shown to be weak in cortical circuits [7–9] and for this reason, virtually all theoretical approaches assume no spiking correlation structure [16, 98–101] and argued for asynchronous activity [102]. A putative role for correlations in neural computations remains a matter of debate [103–105]. When distributed over large networks, weak correlations can still give rise to precise synchrony,

once information is pooled from a large enough number of synaptic inputs [23, 24]. In this view, and assuming that distinct inputs play comparable roles, correlations measure the propensity of distinct synaptic inputs impinging on a neuron to co-activate, which represents a clear form of synchrony. Our analysis shows that considering input synchrony in amounts consistent with the weak level of observed spiking correlation is enough to account for the surprisingly large magnitude of subthreshold neuronal variability [1, 17–19]. In contrast, the asynchronous regime yields unrealistically low variability, an observation that challenges the basis for the asynchronous state hypothesis.

Recent theoretical works [29, 30] have also noted that the asynchronous state hypothesis seems at odds with certain features of the cortical activity such as the emergence of spontaneous activity or the maintenance of significant average polarization during evoked activity. Zerlaut *et al.* have analyzed under which conditions conductance-based networks can achieve a spectrum of asynchronous states with realistic neural features. In their work, a key variable to achieve this spectrum is a strong afferent drive that modulates a balanced network with moderate recurrent connections. Moderate recurrent conductances are inferred from allowing for up to 2mV somatic deflections at rest, whereas the afferent drive is provided via even stronger synaptic conductances that can activate synchronously. These inferred conductances appear large in light of recent *in-vivo* measurements [65, 68, 69], and the corresponding synaptic weights all satisfy  $w_e, w_i \geq 0.01$  within our framework. Correspondingly, the typical connectivity numbers considered are small with  $K_e = 200$ ,  $K_i = 50$  for recurrent connections and  $K_e = 10$  for the co-activating afferent projections. Thus, results from [29] appear consistent with our observation that realistic subthreshold variability can only be achieved asynchronously for a restricted number of large synaptic weights. Our findings, however, predict that these results follow from connectivity sparseness and will not hold in denser networks, for which the pairwise spiking correlation will exceed the empirical criteria for asynchrony, e.g.,  $\rho_e > 1/K_e$  ( $\rho_e < 0.005 \leq 1/K_e$  in [29]). Sanzeni *et al.* have pointed out that implementing the effective-time-constant approximation in conductance-based models suppresses subthreshold variability, especially in the high-conductance state [70]. As mentioned here, this suppression causes the voltage variability to decay as  $O(w_e) + O(w_i)$  in any scaling limit with vanishing synaptic weights. Sanzeni *et al.* observe that such decay is too fast to yield realistic variability for the balanced scaling, which assumes  $w_e \sim 1/\sqrt{K_e}$  and  $w_i \sim 1/\sqrt{K_i}$ . To remedy this point, these authors propose to adopt a slower scaling of the weights, i.e.,  $w_e \sim 1/\ln K_e$  and  $w_i \sim 1/\ln K_i$ , which can be derived from the principle of rate conservation in neural networks. Such a scaling is sufficiently slow for variability to persist in networks with large connectivity number ( $\simeq 10^5$ ). However, as any scaling with vanishing weights,

our exact analysis shows that such scaling must eventually lead to decaying variability, thereby challenging the basis for the synchronous state hypothesis.

Both of these studies focus on the network dynamics of conductance-based networks under the diffusion and effective-time-constant approximations. The effective-time-constant approximation follows the prior assumption that the diffusion approximation is valid [35, 36, 85–87]. In turn, diffusive behaviors only rigorously emerge under some scaling limit with vanishing weights [88, 89]. By focusing on the single-cell level rather than the network level, we are able to demonstrate that the effective-time-constant approximation holds exactly for shot-noise driven, conductance-based neurons, without any diffusive approximations. Consequently, suppression of variability must occur independent of any scaling choice, except in the presence of input synchrony. Although this observation poses a serious theoretical challenge to the asynchronous state hypothesis, observe that it does not invalidate the practical usefulness of the diffusion approximation. For instance, we show in Fig. 12 that the mean spiking response of an a shot-noise driven AONCB neuron with an integrate-and-fire mechanism can be satisfactorily captured via the diffusion approximation. In addition, our analysis allows one to extend the diffusion approximation to include input synchrony.

One can address the above theoretical challenge by recognizing that albeit large, neural networks are finite and never operate in the idealized regime obtained in a scaling limit. Adopting biophysically relevant parameters shows that even in finite networks, stationary asynchronous regimes produce unrealistically low subthreshold variability. In that respect, we find that achieving a realistic range of mean voltage variation for moderate synaptic weights requires  $\simeq 10^3$  driving synapses. This is lower than the upper range for synaptic contact numbers ( $\simeq 10^4$ ), but consistent with the idea that only a subset of synaptic contacts share the same tuning specificities during evoked activity [106]. More generally, our analysis suggests that large but finite networks are such that they operate with weak but significant spiking correlations. Such spiking correlations amount to a form of input synchrony, which in turn can explain the observed level of subthreshold variability. That said, by focusing on the single-cell level, our analysis makes no predictions about the origin of such correlations and about how correlation may differ in the spontaneous or evoked regime [17, 18, 107].

#### D. Limitations of the approach

A first limitation of our analysis is that we neglect the spike-generating mechanism as a source of neural variability. Most diffusion-based approaches model spike generation via the integrate-and-fire mechanism, whereby the membrane voltages reset to fixed value upon reaching a spike-initiation threshold [29, 30, 35, 36, 85–

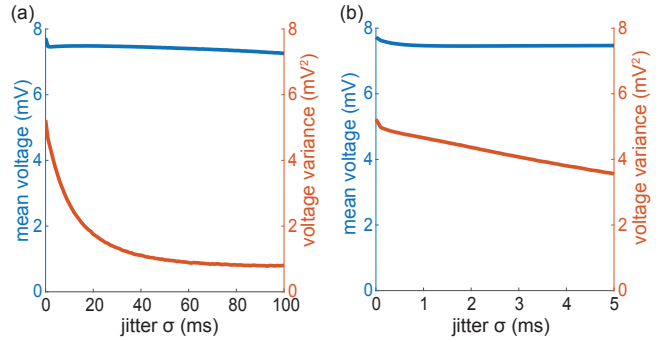


**FIG. 13. Impact of jittering synchronous inputs.** Voltage mean and variance of AONCB neurons in response to synchronous inputs that have been jittered for parameters:  $K_e = 1000$ ,  $w_e = 0.001$ ,  $\rho_e = 0.03$ . Specifically, each input timing has been independently shifted in time by a centered Gaussian random variable with standard deviation  $\sigma$ . (a) If the mean response is largely independent of jittering, the variance steadily decreases with the jittering, which erases synchrony-based correlation over the timescale  $\sigma$ . Accordingly, for large timescale,  $\sigma \geq \tau$ , we recover variance values obtained for asynchronous drive with  $\rho_e = \rho_i = \rho_{ei} = 0$ . (b) Variability estimates are reliable for jittering at timescales  $\sigma \leq 2\text{ms}$ .

87]. Accounting for such a mechanism can impact our findings in two ways: (i) By confining voltage below the spiking threshold, the spiking mechanism may suppress the mean response enough for the neuron to operate well in the high-conductance regime for large input drives. Such a scenario will still produce exceedingly low variability due to variability quenching in the high-conductance regime, consistent with [1]. (ii) The additional variability due to post-spiking resets may dominate the synaptic variability, so that a large overall subthreshold variability can be achieved in spite of low synaptic variability. This possibility also seems unlikely as dominant yet stereotypical resets would imply a quasi-deterministic neural response [64]. Addressing the above limitations quantitatively requires extending our exact analysis to include the integrate-and-fire mechanism using technique from queueing theory [93]. This is beyond the scope of this work. We note, however, that implementing a post-spiking reset to a fixed voltage level yields simulated trajectories that markedly differ from physiological ones (see Fig. 1), for which the post-spiking voltage varies across conditions [17–19]. The limitations due to the spike-generating mechanism can be circumvented experimentally by studying the spontaneous and evoked subthreshold responses in artificially silenced, through the injection of hyperpolarizing current neurons. Our analysis can then be used to infer the correlation regime of the synaptic inputs by fitting our voltage moment formulas.

A second limitation of our analysis is our assumption of exchangeability, which is the lens through which we operate a link between spiking correlations and input drives. Taken literally, the exchangeability assumption

states that synapses all have a typical strength and that conductance variability primarily stems from the variable numbers of co-activating synapses. This is certainly an oversimplification as synapses exhibit heterogeneity [108], which likely plays a role in shaping neural variability [95]. Distinguishing between heterogeneity and correlation contributions, however, is a fundamentally ambiguous task [109]. For instance, considering  $K_e$  synchronous inputs with weight  $w_e$  at rate  $b_e$  and with jump probability  $p_{e,k}$  (see Eq. (4) and Eq. (8)) is indistinguishable from considering  $K_e$  independent inputs with heterogeneous weights  $\{w_e, 2w_e, \dots, K_e w_e\}$  and rates  $K_e b_e p_{e,k}$ . Within our modeling approach, accounting for synaptic heterogeneity, with dispersed distribution for synaptic weights  $q_e(w)$ , can be done by taking the jump distribution  $p_e$  as

$$p_e(w) = \sum_{k=1}^K q_e^{(k)}(w) p_{e,k},$$

where  $q_e^{(k)}$  refers to the  $k$ -fold convolution of  $q_e(w)$ . This leads to an overdispersion of the jump distribution  $p_e$ , and thus increased subthreshold neural variability. Therefore, while we have assumed exchangeability, our approach can accommodate weight heterogeneity. The interpretation of our results in term of synchrony rather than heterogeneity follows from the knowledge that cortical activity displays weak but nonzero spiking correlations [25–28] and from recent experimental evidence that cortical response selectivity derives from strength in numbers of synapses, rather than difference in synaptic weights [106].

A third limitation of our analysis is to consider a perfect form of synchrony, with exactly simultaneous synaptic activations. Although seemingly unrealistic, we argue that perfect input synchrony can still yield biologically relevant estimates of the voltage variability. This is because voltage fluctuations result from the integration of inputs over a time scale set by the passive membrane time constant  $\tau \sim 20\text{ms}$ . As a result, synaptic activation times that differ by significantly less than  $\tau$  can be considered as synchronous inputs. To illustrate this point, we show in Fig. 13 the dependence of the voltage variance on the degree of synchrony by gradually jittering initially synchronous synaptic inputs. Assuming  $K_e = 1000$  excitatory inputs alone with spiking correlation  $\rho_e = 0.03$ , one can check that the neural variability is left unchanged by jittering synaptic activations over time scales  $\sigma \leq 2\text{ms}$ . One can also check that jittering over larger timescales than the synaptic time constant yields neural variability similar to that obtained in the absence of correlation in the inputs. This supports that our finding are robust to including temporal variability on timescales  $\sigma \leq 2\text{ms}$ , which is consistent with typical heterogeneities with axonal or dendritic conduction delays. A functional role for precise timing in cortical activity remains a matter of debate [110]. Here, we point out that weakened forms of synchrony will yield lower variability, so that our chal-

lenge to the asynchronous state will remain. One remaining limitation of our synchrony modeling is that our analysis can only account for instantaneous correlations between excitation and inhibition, while in reality such correlations are expected to peak at a non-zero time lag.

A fourth limitation of our analysis is that it is restricted to a form of synchrony that ignores temporal heterogeneity. This is a limitation because a leading hypothesis for the emergence of variability is that neurons generate spikes as if through a doubly stochastic process, i.e., as a Poisson process with temporally fluctuating rate [111]. To better understand this limitation, let us interpret our exchangeability-based modeling approach within the framework of doubly stochastic processes [40, 41]. This can be done most conveniently by reasoning on the discrete correlated spiking model specified by Eq. (3). Specifically, given fixed bin size  $\Delta t > 0$ , one can interpret the collection of *i.i.d.* variables  $\theta \sim F$  as an instantaneously fluctuating rate. In this interpretation, nonzero correlations can be seen as emerging from a doubly stochastic process for which the rate fluctuates as uncorrelated noise, i.e., with zero correlation time. This zero correlation time is potentially a serious limitation as it has been argued that shared variability is best modeled by a low-dimensional latent process evolving with slow, or even smooth, dynamics [75]. Addressing this limitation will require developing limit spiking model with nonzero correlation time using probabilistic techniques that are beyond the scope of this work [45]. Obtaining exact results for such input will represent another open challenge as the resulting driving processes may not be well-approximated by compound Poisson processes. We expect rate temporal heterogeneities to only play a significant role for the spontaneous regime of activity so that our analysis should remain valid in the evoked regime [18].

A final limitation of our analysis is that it does not explain the consistent emergence of synchrony in network dynamics. It remains conceptually unclear how synchrony can emerge and persist in neural networks that are fundamentally plagued by noise and exhibit large degrees of temporal and cellular heterogeneity. It may well be that carefully taking into account the finite-size of networks will be enough to produce the desired level of synchrony-based correlation, which is rather weak after all. Still, one would have to check whether achieving a given degree of synchrony requires the tuning of certain network features, such as the degree of shared input or the propensity of certain recurrent motifs [107] or the relative width of recurrent connections with respect to feedforward projections [112]. From a theoretical standpoint, the asynchronous state hypothesis answers the consistency problem by assuming no spiking correlations, and thus no synchrony. One can justify this assumption in idealized mathematical models by demonstrating the so-called “propagation-of-chaos” property [113], which rigorously holds for certain scaling limits with vanishing weights and under the assumption

of exchangeability [99–101]. In this light, the main theoretical challenge posed by our analysis is extending the latter exchangeability-based property to include nonzero correlations [114], and hopefully characterize irregular synchronous state in some scaling limits.

## ACKNOWLEDGMENTS

This work was supported by the CRCNS program of the National Science Foundation under award number

DMS-2113213 and by the Vision Research program of the National Institutes of Health under award number R01EY024071. We would like to thank François Baccelli, David Hansel, and Nicholas Brunel for insightful discussions.

## Appendix A: Discrete-time spiking correlation

In this appendix, we consider first the discrete-time version of our model for possibly correlated excitatory synaptic inputs. In this model, we consider that observing  $K_e$  synaptic inputs during  $N$  time steps specifies a  $\{0, 1\}$ -valued matrix  $\{X_{k,i}\}_{1 \leq k \leq K_e, 1 \leq i \leq N}$ , where 1 indicates that an input is received and 0 indicates an absence of inputs. For simplicity, we further assume that the inputs are independent across time

$$\mathbb{P} \left[ \{X_{k,i}\}_{1 \leq k \leq K_e, 1 \leq i \leq N} \right] = \prod_{i=1}^N \mathbb{P} \left[ \{X_{k,i}\}_{1 \leq k \leq K_e} \right],$$

so that we can drop the time index and consider the population vector  $\{X_k\}_{1 \leq k \leq K_e}$ . Consequently, given the individual spiking rate  $r_e$ , we have  $\mathbb{E}[X_k] = \mathbb{P}[X_k = 1] = r_e \Delta t$ , where  $\Delta t$  is the duration of the time step where a spike may or may not occur. Under the assumptions that  $\{X_k\}_{1 \leq k \leq K_e}$  belongs to an infinitely exchangeable set of random variables, de Finetti theorem states that there exists a probability measure  $F_e$  on  $[0, 1]$  such that

$$\mathbb{P} \left[ \{X_k\}_{1 \leq k \leq K_e} \right] = \int \prod_{k=1}^{K_e} \theta_e^{X_k} (1 - \theta_e)^{1 - X_k} dF_e(\theta_e).$$

Assuming the directing measure  $F_e$  known, we can compute the spiking correlation attached to our model. To see this, first observe that specifying the above probabilistic model for  $K_e = 1$ , we have

$$\mathbb{E}[X_k] = \mathbb{E}[\mathbb{E}[X_k | \theta_e]] = \mathbb{E}[\theta_e] = \int \theta_e dF_e(\theta_e).$$

Then, using the total law of covariance and specifying the above probabilistic model for  $K = 2$ , we have

$$\begin{aligned} \mathbb{C}[X_k, X_l] &= \mathbb{E}[\mathbb{C}[X_k, X_l | \theta_e]] + \mathbb{C}[\mathbb{E}[X_k | \theta_e], \mathbb{E}[X_l | \theta_e]], \\ &= \mathbb{1}_{\{k=l\}} \mathbb{E}[\mathbb{V}[X_k | \theta_e]] + \mathbb{C}[\theta_e, \theta_e], \\ &= \mathbb{1}_{\{k=l\}} \mathbb{E}[\theta_e(1 - \theta_e)] + \mathbb{V}[\theta_e], \\ &= \mathbb{1}_{\{k=l\}} \mathbb{E}[\theta_e] (1 - \mathbb{E}[\theta_e]) + \mathbb{1}_{\{k \neq l\}} \mathbb{V}[\theta_e]. \end{aligned}$$

This directly yields that the spiking correlation reads

$$\rho_e = \frac{\mathbb{C}[X_k, X_l]}{\mathbb{V}[X_k]} = \frac{\mathbb{V}[\theta_e]}{\mathbb{E}[\theta_e] (1 - \mathbb{E}[\theta_e])} \quad (\text{A1})$$

The exact same calculations can be performed for the partially exchangeable case of mixed excitation and inhibition. The assumption of partial exchangeability requires that when considered separately, the  $\{0, 1\}$ -valued vectors  $\{X_1, \dots, X_{K_e}\}$  and  $\{Y_1, \dots, Y_{K_i}\}$  each belong to an infinitely exchangeable sequence of random variables. Then, de Finetti's theorem states that the probability to find the full vector of inputs  $\{X_1, \dots, X_{K_e}, Y_1, \dots, Y_{K_i}\}$  in any particular configuration is given by

$$\mathbb{P}[X_1, \dots, X_{K_e}, Y_1, \dots, Y_{K_i}] = \int \prod_{k=1}^{K_e} \theta_e^{X_k} (1 - \theta_e)^{1 - X_k} \prod_{l=1}^{K_i} \theta_i^{Y_l} (1 - \theta_i)^{1 - Y_l} dF_{ei}(\theta_e, \theta_i), \quad (\text{A2})$$

where the directing measure  $F_{ei}$  fully parametrizes our probabilistic model. Performing similar calculations as for the case of excitation alone within this partially exchangeable setting yields

$$\rho_{ei} = \frac{\mathbb{C}[X_k, Y_l]}{\sqrt{\mathbb{V}[X_k] \mathbb{V}[Y_l]}} = \frac{\mathbb{C}[\theta_e, \theta_i]}{\sqrt{\mathbb{E}[\theta_e](1 - \mathbb{E}[\theta_e])\mathbb{E}[\theta_i](1 - \mathbb{E}[\theta_i])}}. \quad (\text{A3})$$

## Appendix B: Compound Poisson processes as continuous-time limits

Let us consider the discrete-time model specified by Eq. (A2), which is obtained under the assumption of partial infinite exchangeability. Under this assumption, the probability laws of the inputs is entirely determined by the distribution of  $(k_e, k_i)$ , where  $k_e$  denotes the number of active excitatory inputs and  $k_i$  denotes the number of inhibitory inputs. This distribution can be computed as

$$P_{ei,kl} = \mathbb{P}[k_e = k, k_i = l] = \binom{K_e}{k} \binom{K_i}{l} \int \theta_e^k (1 - \theta_e)^{K_e - k} \theta_i^l (1 - \theta_i)^{K_i - l} dF_{ei}(\theta_e, \theta_i).$$

It is convenient to choose the directing measure as beta distributions since these are conjugate to the binomial distributions. Such a choice yields a class of probabilistic models referred to as beta-binomial models, which have been studied extensively [50, 51]. In this appendix, we always assume that the marginals  $F_e$  and  $F_i$  have the form  $F_e \sim \text{Beta}(\alpha_e, \beta_e)$  and  $F_i \sim \text{Beta}(\alpha_i, \beta_i)$ . Then, direct integrations shows that the marginal distributions for the number of excitatory inputs and inhibitory inputs are

$$P_{e,k} = \sum_{l=0}^{K_i} P_{ei,kl} = \binom{K_e}{k} \frac{B(\alpha_e + k, \beta_e + K_e - k)}{B(\alpha_e, \beta_e)} \quad \text{and} \quad P_{i,l} = \sum_{k=0}^{K_e} P_{ei,kl} = \binom{K_i}{l} \frac{B(\alpha_i + l, \beta_i + K_i - l)}{B(\alpha_i, \beta_i)}.$$

Moreover, given individual spiking rates  $r_e$  and  $r_i$  within a time step  $\Delta t$ , we have

$$r_e \Delta t = \mathbb{E}[X_k] = \mathbb{P}[X_k = 1] = \mathbb{E}[\theta_e] = \frac{\alpha_e}{\alpha_e + \beta_e} \quad \text{and} \quad r_i \Delta t = \mathbb{E}[Y_l] = \mathbb{P}[Y_l = 1] = \mathbb{E}[\theta_i] = \frac{\alpha_i}{\alpha_i + \beta_i}.$$

The continuous-time limit is obtained by taking  $\Delta t \rightarrow 0^+$ , which implies that the parameters  $\alpha_e$  and  $\alpha_i$  jointly vanish. When  $\alpha_e, \alpha_i \rightarrow 0^+$ , the beta distributions  $F_e$  and  $F_i$  becomes deficient and we have  $P_{e,0}, P_{i,0} \rightarrow 1$ . In other words, time bins of size  $\Delta t$  almost surely have no active inputs in the limit  $\Delta t \rightarrow 0^+$ . Actually, one can show that

$$1 - P_{e,0} \sim (\psi(K_e + \beta_e) - \psi(\beta_e)) \alpha_e \quad \text{and} \quad 1 - P_{i,0} \sim (\psi(K_i + \beta_i) - \psi(\beta_i)) \alpha_i,$$

where  $\psi$  denotes the digamma function. This indicates in the limit  $\Delta t \rightarrow 0^+$ , the times at which some excitatory inputs or some inhibitory inputs are active define a point process. Moreover, owing to the assumption of independence across time, this point process will actually be a Poisson point process. Specifically, consider a time  $T > 0$  and set  $\Delta t = T/N$  for some large integer  $N$ . Define the sequence of times

$$T_{e,n} = \frac{T}{N} \cdot \inf \{i > NT_{e,n-1}/T \mid k_{e,i} \geq 1\} \quad \text{with} \quad T_{e,1} = \frac{T}{N} \cdot \inf \{i \geq 0 \mid k_{e,i} \geq 1\},$$

$$T_{i,n} = \frac{T}{N} \cdot \inf \{i > NT_{i,n-1}/T \mid k_{i,i} \geq 1\} \quad \text{with} \quad T_{i,1} = \frac{T}{N} \cdot \inf \{i \geq 0 \mid k_{i,i} \geq 1\}.$$

Considered separately, the sequences of times  $\{T_{e,n}\}_{n \geq 1}$  and  $\{T_{i,n}\}_{n \geq 1}$  constitute binomial approximations of Poisson processes which we denote by  $N_e$  and  $N_i$ , respectively. It is a classical result that these limit Poisson processes are recovered exactly when  $N \rightarrow \infty$  and that their rates are respectively given by

$$b_e = \lim_{\Delta t \rightarrow 0^+} \frac{1 - P_{e,0}}{\Delta t} = (\psi(K_e + \beta_e) - \psi(\beta_e)) \left( \lim_{\Delta t \rightarrow 0^+} \frac{\alpha_e}{\Delta t} \right) = (\psi(K_e + \beta_e) - \psi(\beta_e)) \beta_e r_e,$$

$$b_i = \lim_{\Delta t \rightarrow 0^+} \frac{1 - P_{i,0}}{\Delta t} = (\psi(K_i + \beta_i) - \psi(\beta_i)) \left( \lim_{\Delta t \rightarrow 0^+} \frac{\alpha_i}{\Delta t} \right) = (\psi(K_i + \beta_i) - \psi(\beta_i)) \beta_i r_i.$$

For all integer  $K > 1$ , the function  $\beta \mapsto \beta(\psi(K + \beta) - \psi(\beta))$  is an increasing analytic functions on the domain  $\mathbb{R}^+$  with range  $[1, K]$ . Thus, we always have  $r_e \leq b_e \leq K_e r_e$  and  $r_i \leq b_i \leq K_i r_i$  and the extreme cases are achieved for perfect or zero correlations. Perfect correlations are achieved when  $\rho_e = 1$  or  $\rho_i = 1$ , which corresponds to  $\beta_e \rightarrow 0$  or  $\beta_i \rightarrow 0$ . This implies that  $b_e = r_e$  and  $b_i = r_i$ , consistent with all synapses activating simultaneously. Zero correlations are achieved when  $\rho_e = 0$  or  $\rho_i = 0$ , which corresponds to  $\beta_e \rightarrow \infty$  or  $\beta_i \rightarrow \infty$ . This implies that  $b_e = K_e r_e$  and  $b_i = K_i r_i$ , consistent with all synapses activating asynchronously, so that no inputs simultaneously activate. Observe

that in all generality, the rates  $b_e$  and  $b_i$  are such that the mean number of spikes over the duration  $T$  is conserved in the limit  $\Delta t \rightarrow 0^+$ . For instance, one can check that

$$K_e r_e T = \mathbb{E} \left[ \sum_{T_{e,n} \leq T} k_{e,NT_{e,n}/T} \right] = \mathbb{E} \left[ \sum_{n=1}^{N_e(T)} k_{e,n} \right] = \mathbb{E} [N_e(T)] \mathbb{E} [k_e] = b_e T \mathbb{E} [k_e]$$

When excitation and inhibition are considered separately, the limit process  $\Delta t \rightarrow 0^+$  specifies two compound Poisson processes

$$t \mapsto \sum_{n=1}^{N_e(t)} k_{e,n} \quad \text{and} \quad t \mapsto \sum_{n=1}^{N_i(t)} k_{i,n},$$

where  $N_e$  and  $N_i$  are Poisson processes with rate  $b_e$  and  $b_i$  and where  $\{k_{e,n}\}_{n \geq 1}$  are i.i.d according to  $p_{e,k}$  and  $\{k_{i,n}\}_{n \geq 1}$  are i.i.d according to  $p_{i,k}$ . Nonzero correlations between excitation and inhibition emerge when the Poisson processes  $N_e$  and  $N_i$  are not independent. This corresponds to the processes  $N_e$  and  $N_i$  sharing times, so excitation and inhibition occur simultaneously at these times. To understand this point intuitively, let us consider the limit Poisson process  $N$  obtained by considering synaptic events without distinguishing excitation and inhibition. For perfect correlation, i.e.,  $\rho_{ei} = 1$ , all synapses activate synchronously and we have  $N = N_e = N_i$ : all times are shared. By contrast, for zero correlation, i.e.,  $\rho_{ei} = 0$ , no synapses activate simultaneously and we have  $N = N_e + N_i$ : no times are shared. For intermediary regime of correlations, a nonzero fraction of times will be shared resulting in a driving Poisson process  $N$  with overall rate  $b$  satisfying  $\min(b_e, b_i) \leq b < b_e + b_i$ . We investigate the above intuitive statements quantitatively in Appendix C by inspecting two key examples.

Let us conclude this appendix by recapitulating the general form of the limit compound process  $Y$  obtained in the continuous-time limit  $\Delta t \rightarrow 0^+$  when jointly considering excitation and inhibition. This compound Poisson process can be represented as

$$t \mapsto Y(t) = \left( \sum_n^{N(t)} W_{e,n}, \sum_n^{N(t)} W_{i,n} \right),$$

where  $N$  is that Poisson process registering all synaptic events without distinguishing excitation and inhibition and where the pairs  $(W_{e,n}, W_{i,n})$  are i.i.d. random jumps in  $\mathbb{R} \times \mathbb{R} \setminus \{0,0\}$ . Formally, such a process is specified by the rate of  $N$ , denoted by  $b$ , and the bivariate distribution of the jumps  $(W_{e,n}, W_{i,n})$ , denoted by  $p_{ei,kl}$ . These are defined as

$$b = \lim_{\Delta t \rightarrow 0^+} \frac{1 - P_{ei,00}}{\Delta t} \quad \text{and} \quad p_{ei,kl} = \lim_{\Delta t \rightarrow 0^+} \frac{P_{ei,kl}}{1 - P_{ei,00}} \quad \text{for } (k,l) \neq (0,0), \quad (\text{B1})$$

where  $P_{ei,00}$  is the probability to register no synaptic activation during a time step  $\Delta t$ . According to these definitions,  $b$  is the infinitesimal likelihood that an input is active within a time bin, whereas  $p_{ei,kl}$  is the probability that  $k$  excitatory inputs and  $l$  inhibitory inputs are active given that at least one input is active. One can similarly define the excitatory and inhibitory rates of events  $b_e$  and  $b_i$ , as well as the excitatory jump distribution  $p_{e,k}$  and the inhibitory jump distribution  $p_{i,l}$ . Specifically, we have

$$\begin{aligned} b_e &= \lim_{\Delta t \rightarrow 0^+} \frac{1 - P_{e,0}}{\Delta t} \quad \text{and} \quad p_{e,k} = \lim_{\Delta t \rightarrow 0^+} \frac{P_{e,k}}{1 - P_{e,0}} \quad \text{for } k \neq 0, \\ b_i &= \lim_{\Delta t \rightarrow 0^+} \frac{1 - P_{i,0}}{\Delta t} \quad \text{and} \quad p_{i,l} = \lim_{\Delta t \rightarrow 0^+} \frac{P_{i,l}}{1 - P_{i,0}} \quad \text{for } l \neq 0, \end{aligned} \quad (\text{B2})$$

with  $P_{e,k} = \sum_{l=0}^{K_i} P_{ei,k,l}$  and  $P_{i,k} = \sum_{k=0}^{K_e} P_{ei,k,l}$ . Observe that thus defined, the jump distribution  $p_{e,k}$  and  $p_{i,k}$  are specified as conditional marginal distributions of the joint jump distribution  $p_{ei,kl}$  on the events  $\{k_e > 0\}$  and  $\{k_i > 0\}$ , respectively. These are such that  $p_{e,k} = (b/b_e) \sum_{l=0}^{K_i} p_{ei,k,l}$  and  $p_{i,l} = (b/b_i) \sum_{k=0}^{K_e} p_{ei,k,l}$ . To see why, observe for instance that

$$p_{e,k} = \lim_{\Delta t \rightarrow 0^+} \frac{P_{e,k}}{1 - P_{e,0}} = \lim_{\Delta t \rightarrow 0^+} \sum_{l=0}^{K_i} \frac{P_{ei,k,l}}{1 - P_{ei,00}} \frac{1 - P_{ei,00}}{1 - P_{e,0}} = \left( \sum_{l=0}^{K_i} p_{ei,k,l} \right) \left( \lim_{\Delta t \rightarrow 0^+} \frac{1 - P_{ei,00}}{1 - P_{e,0}} \right) = \frac{b}{b_e} \sum_{l=0}^{K_i} p_{ei,k,l} \quad (\text{B3})$$

where we have used the definitions of the rates  $b$  and  $b_e$  given in Eq. (B1) and Eq. (B2) to establish that

$$\lim_{\Delta t \rightarrow 0^+} \frac{1 - P_{ei,00}}{1 - P_{e,0}} = \frac{\lim_{\Delta t \rightarrow 0^+} (1 - P_{ei,00})/\Delta t}{\lim_{\Delta t \rightarrow 0^+} (1 - P_{e,0})/\Delta t} = \frac{b}{b_e}.$$

### Appendix C: Two examples of limit compound Poisson processes

The probability  $P_{\text{ei},00}$  that plays a central role in Appendix B can be easily computed for zero correlation, i.e.,  $\rho_{\text{ei}} = 0$ , by considering a directing measure under product form  $F_{\text{ei}}(\theta_{\text{e}}, \theta_{\text{i}}) = F_{\text{e}}(\theta_{\text{e}})F_{\text{i}}(\theta_{\text{i}})$ . Then integration with respect to the separable variables  $\theta_{\text{e}}$  and  $\theta_{\text{i}}$  yields

$$P_{\text{ei},kl} = P_{\text{e},k}P_{\text{i},l} = \binom{K_{\text{e}}}{k} \frac{B(\alpha_{\text{e}} + k, \beta_{\text{e}} + K_{\text{e}} - k)}{B(\alpha_{\text{e}}, \beta_{\text{e}})} \binom{K_{\text{i}}}{l} \frac{B(\alpha_{\text{i}} + l, \beta_{\text{i}} + K_{\text{i}} - l)}{B(\alpha_{\text{i}}, \beta_{\text{i}})}.$$

In turn, the limit compound Poisson process can be obtain in the limit  $\Delta t \rightarrow 0^+$  by observing that

$$1 - P_{\text{e},0} = b_{\text{e}}\Delta t + o(\Delta t), \quad 1 - P_{\text{e},0}P_{\text{i},0} = b_{\text{i}}\Delta t + o(\Delta t), \quad \text{and} \quad 1 - P_{\text{e},0}P_{\text{i},0} = (b_{\text{e}} + b_{\text{i}})\Delta t + o(\Delta t),$$

which implies that the overall rate is determined as  $b = \lim_{\Delta t \rightarrow 0^+} (1 - P_{\text{e},0}P_{\text{i},0})/\Delta t = b_{\text{e}} + b_{\text{i}}$ , as expected. To characterize the limit compound Poisson process, it remains to exhibit  $p_{\text{ei},kl}$ , the distribution of the jumps  $k_{\text{e}}$  and  $k_{\text{i}}$ . Suppose that  $k \geq 1$ , then we have

$$\begin{aligned} p_{\text{ei},kl} &= \lim_{\Delta t \rightarrow 0^+} \frac{P_{\text{e},k}P_{\text{i},l}}{1 - P_{\text{e},0}P_{\text{i},0}}, \\ &= \lim_{\Delta t \rightarrow 0^+} \left[ \left( \frac{1 - P_{\text{e},0}}{1 - P_{\text{e},0}P_{\text{i},0}} \right) P_{\text{i},l} \left( \frac{P_{\text{e},k}}{1 - P_{\text{e},0}} \right) \right], \\ &= \left( \lim_{\Delta t \rightarrow 0^+} \frac{1 - P_{\text{e},0}}{1 - P_{\text{e},0}P_{\text{i},0}} \right) \left( \lim_{\Delta t \rightarrow 0^+} P_{\text{i},l} \right) \left( \lim_{\Delta t \rightarrow 0^+} \frac{P_{\text{e},k}}{1 - P_{\text{e},0}} \right). \end{aligned}$$

Then one can use the limit behaviors

$$\lim_{\Delta t \rightarrow 0^+} \frac{1 - P_{\text{e},0}}{1 - P_{\text{e},0}P_{\text{i},0}} = \frac{b_{\text{e}}}{b_{\text{e}} + b_{\text{i}}} \quad \text{and} \quad \lim_{\Delta t \rightarrow 0^+} P_{\text{i},l} = \mathbb{1}_{\{l=0\}}.$$

so that for  $k \geq 1$ , we have

$$p_{\text{ei},kl} = \frac{b_{\text{e}}}{b_{\text{e}} + b_{\text{i}}} \mathbb{1}_{\{l=0\}} p_{\text{e},k} \quad \text{with} \quad p_{\text{e},k} = \lim_{\Delta t \rightarrow 0^+} \frac{P_{\text{e},k}}{1 - P_{\text{e},0}} = \binom{K_{\text{e}}}{k} \frac{B(k, \beta_{\text{e}} + K_{\text{e}} - k)}{\psi(K_{\text{e}} + \beta_{\text{e}}) - \psi(\beta)}.$$

A similar calculation shows that for all  $l \geq 1$ , we have  $p_{\text{ei},kl} = b_{\text{i}}/(b_{\text{e}} + b_{\text{i}}) \mathbb{1}_{\{k=0\}} p_{\text{i},l}$ . Thus  $p_{\text{ei},kl} = 0$  whenever  $k, l \geq 1$ , so that the support of  $p_{\text{ei},kl}$  is  $\{1, \dots, K_{\text{e}}\} \times \{0\} \cup \{0\} \times \{1, \dots, K_{\text{i}}\}$ . This is consistent with the intuition that excitation and inhibition happen at distinct times in the absence of correlations.

Let us now consider the case of maximum correlation for  $F_{\text{e}} = F_{\text{i}} = F$ , where  $F$  is a beta distribution with parameters  $\alpha$  and  $\beta$ . Moreover, let us assume the deterministic coupling  $\theta_{\text{e}} = \theta_{\text{i}}$  such that  $F_{\text{ei}}(\theta_{\text{e}}, \theta_{\text{i}}) = F(\theta_{\text{e}})\delta(\theta_{\text{i}} - \theta_{\text{e}})$ . Then, the joint distribution of the jumps  $(k_{\text{e}}, k_{\text{i}})$  can be evaluated via direct integration as

$$\begin{aligned} P_{\text{ei},kl} &= \binom{K_{\text{e}}}{k} \binom{K_{\text{i}}}{l} \int \theta_{\text{e}}^k (1 - \theta_{\text{e}})^{K_{\text{e}}-k} \theta_{\text{e}}^l (1 - \theta_{\text{i}})^{K_{\text{i}}-l} dF(\theta_{\text{e}}) \delta(\theta_{\text{i}} - \theta_{\text{e}}), \\ &= \binom{K_{\text{e}}}{k} \binom{K_{\text{i}}}{l} \int \theta^{k+l} (1 - \theta)^{K_{\text{e}}+K_{\text{i}}-k-l} dF(\theta), \\ &= \binom{K_{\text{e}}}{k} \binom{K_{\text{i}}}{l} \frac{B(\alpha + k + l, \beta + K_{\text{e}} + K_{\text{i}} - k - l)}{B(\alpha, \beta)}. \end{aligned}$$

As excitation and inhibition are captured separately by the same marginal functions  $F_{\text{e}} = F_{\text{i}} = F$ , we necessarily have  $\alpha/(\alpha + \beta) = \mathbb{E}[X_k] = \mathbb{E}[Y_l] = r_{\text{e}}\Delta t = r_{\text{i}}\Delta t$  and we refer to the common spiking rate as  $r$ . Then the overall rate of synaptic activation is obtained as

$$b = \lim_{\Delta t \rightarrow 0^+} \frac{1 - P_{\text{ei},00}}{\Delta t} = \lim_{\alpha \rightarrow 0^+} \frac{1 - P_{\text{ei},00}}{\alpha} \lim_{\Delta t \rightarrow 0^+} \frac{\alpha}{\Delta t} = (\psi(K_{\text{e}} + K_{\text{i}} + \beta) - \psi(\beta)) \beta r, \quad (\text{C1})$$

and one can check that  $b$  differs from the excitatory- and inhibitory-specific rates  $b_{\text{e}}$  and  $b_{\text{i}}$ , which satisfy

$$b_{\text{e}} = \lim_{\Delta t \rightarrow 0^+} \frac{1 - P_{\text{e},0}}{\Delta t} = (\psi(K_{\text{e}} + \beta) - \psi(\beta)) \beta r \quad \text{and} \quad b_{\text{i}} = \lim_{\Delta t \rightarrow 0^+} \frac{1 - P_{\text{i},0}}{\Delta t} = (\psi(K_{\text{i}} + \beta) - \psi(\beta)) \beta r. \quad (\text{C2})$$

To characterize the limit compound Poisson process, it remains to exhibit  $p_{\text{ei},kl}$ , the joint distribution of the jumps  $(k_{\text{e}}, k_{\text{i}})$ . A similar calculation as for the case of excitation alone yields

$$p_{\text{ei},kl} = \lim_{\Delta t \rightarrow 0^+} \frac{P_{\text{ei},kl}}{1 - P_{\text{ei},00}} = \binom{K_{\text{e}}}{k} \binom{K_{\text{i}}}{l} \frac{B(k + l, \beta + K_{\text{e}} + K_{\text{i}} - k - l)}{\psi(K_{\text{e}} + K_{\text{i}} + \beta) - \psi(\beta)}.$$

Remember that within our model, spiking correlations do not depends on the number of neurons and that by construction we have  $\rho_{ei} \leq \sqrt{\rho_e \rho_i}$ . Thus, for the symmetric case under consideration, maximum correlation corresponds to  $\rho_{ei} = \rho_e = \rho_i = 1/(1 + \beta)$ . In particular perfect correlation between excitation and inhibition can only be attained for  $\beta \rightarrow 0$ . When  $\beta > 0$ , i.e., for partial correlations, the Poisson processes  $N_e$  and  $N_i$  only share a fraction of their times, yielding an aggregate Poisson process  $N$  such that  $\min(b_e, b_i) < b < b_e + b_i$ . The relations between  $b$ ,  $b_e$ , and  $b_i$  can be directly recovered from the knowledge of  $p_{ei,kl}$  by observing that

$$\begin{aligned}\mathbb{P}[k_e = 0, k_i > 0] &= \sum_{l=1}^{K_i} p_{ei,0l} = \frac{\psi(K_e + K_i + \beta) - \psi(K_e + \beta)}{\psi(K_e + K_i + \beta) - \psi(\beta)} \\ \mathbb{P}[k_i = 0, k_e > 0] &= \sum_{k=1}^{K_e} p_{ei,k0} = \frac{\psi(K_e + K_i + \beta) - \psi(K_i + \beta)}{\psi(K_e + K_i + \beta) - \psi(\beta)} \\ \mathbb{P}[k_i > 0, k_e > 0] &= \sum_{k=1}^{K_e} \sum_{l=1}^{K_i} p_{ei,kl} = 1 - \frac{2\psi(K_e + K_i + \beta) - \psi(K_e + \beta) - \psi(K_i + \beta)}{\psi(K_e + K_i + \beta) - \psi(\beta)}.\end{aligned}$$

This implies that the fraction of times with nonzero excitation is given by

$$\mathbb{P}[k_e > 0] = \mathbb{P}[k_e > 0, k_i = 0] + \mathbb{P}_0[k_e > 0, k_i > 0] = \frac{\psi(K_e + \beta) - \psi(\beta)}{\psi(K_e + K_i + \beta) - \psi(\beta)},$$

so that we consistently recover the value of  $b_e$  already obtained in Eq. (8) and Eq. (C2) via

$$b_e T = \mathbb{E}[N_e(T)] = \mathbb{E}[\mathbb{1}_{\{k_e > 0\}} N(T)] = b T \mathbb{E}_{ei}[\mathbb{1}_{\{k_e > 0\}}] = b T \mathbb{P}_0[k_e > 0].$$

#### Appendix D: Continuous-time spiking correlation

Eq. (A1) and Eq. (A3) carry over to the continuous time limit  $\Delta t \rightarrow 0^+$  by observing that for limit compound Poisson processes to emerge, one must have that  $\mathbb{E}[X_k] = \mathbb{E}[\theta_e] = O(\Delta t)$  and  $\mathbb{E}[Y_l] = \mathbb{E}[\theta_i] = O(\Delta t)$ . This directly implies that when  $\Delta t \rightarrow 0^+$ , we have

$$\rho_e = \frac{\mathbb{C}[X_k, X_l]}{\mathbb{V}[X_k]} \sim \frac{\mathbb{E}[X_k X_l]}{\mathbb{E}[X_k^2]} = \frac{\mathbb{E}[X_k X_l]}{\mathbb{E}[X_k]} \quad \text{and} \quad \rho_{ei} = \frac{\mathbb{C}[X_k, Y_l]}{\sqrt{\mathbb{V}[X_k] \mathbb{V}[Y_l]}} \sim \frac{\mathbb{E}[X_k Y_l]}{\sqrt{\mathbb{E}[X_k^2] \mathbb{E}[Y_l^2]}} = \frac{\mathbb{E}[X_k Y_l]}{\sqrt{\mathbb{E}[X_k] \mathbb{E}[Y_l]}}. \quad (\text{D1})$$

All the stationary expectations appearing above can be computed via the jump distribution of the limit point process emerging in the limit  $\Delta t \rightarrow 0^+$  [93]. Because this limit process is a compound Poisson process with discrete bivariate jumps, the resulting jump distribution  $p_{ei,kl}$  is specified over  $\{1, \dots, K_e\} \times \{1, \dots, K_i\} \setminus \{0,0\}$ . Denoting by  $b$  the overall rate of synaptic events, one has  $\lim_{\Delta t \rightarrow 0^+} \mathbb{E}[X_k Y_l] / \Delta t = b \mathbb{E}_{ei}[X_k Y_l]$ . Then by partial exchangeability of the  $\{0, 1\}$ -valued population vectors  $\{X_k\}_{1 \leq k \leq K_e}$  and  $\{Y_l\}_{1 \leq l \leq K_i}$ , we have

$$\mathbb{E}_{ei}[X_k Y_l] = \mathbb{E}_{ei}[\mathbb{E}[X_k Y_l | (k_e, k_i)]] = \mathbb{E}_{ei}\left[\frac{k_e}{K_e} \frac{k_i}{K_i}\right] = \sum_{k=0}^{K_e} \sum_{l=0}^{K_i} \frac{k}{K_e} \frac{l}{K_i} p_{ei,kl} = \frac{\mathbb{E}_{ei}[k_e k_i]}{K_e K_i}. \quad (\text{D2})$$

where the bivariate jump  $(k_e, k_i)$  is distributed as  $p_{ei,kl}$ .

To further proceed, it is important to note the relation between the expectation  $\mathbb{E}_{ei}[\cdot]$ , which is tied to the overall input process with rate  $b$ , and the expectation  $\mathbb{E}_e[\cdot]$  which is tied to the excitatory input process with rate  $b_e$ . This relation is best captured by remarking that  $p_{e,k}$  are not defined as the marginals of  $p_{ei,kl}$ , but as only as conditional marginals on  $\{k_e > 0\}$ . In other words, we have  $p_{e,k} = (b/b_e) \sum_{l=0}^{K_i} p_{ei,kl}$ , which implies that  $b \mathbb{E}_{ei}[X_k X_l] = b_e \mathbb{E}_e[X_k X_l]$  and  $\mathbb{E}[X_k] = b \mathbb{E}_{ei}[X_k] = b_e \mathbb{E}_e[X_k]$  with

$$\mathbb{E}_e[X_k X_l] = \mathbb{E}_e[\mathbb{E}[X_k X_l | k_e]] = \mathbb{E}_e\left[\frac{k_e(k_e - 1)}{K_e(K_e - 1)}\right] = \sum_{k=0}^{K_e} \frac{k(k - 1)}{K_e(K_e - 1)} p_{e,k} = \frac{\mathbb{E}_e[k_e(k_e - 1)]}{K_e(K_e - 1)}, \quad (\text{D3})$$

$$\mathbb{E}_e[X_k] = \mathbb{E}_e[\mathbb{E}[X_k | k_e]] = \mathbb{E}_e\left[\frac{k_e}{K_e}\right] = \sum_{k=0}^{K_e} \sum_{l=0}^{K_i} \frac{k}{K_e} p_{ei,kl} = \frac{\mathbb{E}_e[k_e]}{K_e}, \quad (\text{D4})$$

with similar expressions for the inhibition-related quantities. Injecting (D2), (D3), and (D4) in Eq. (D1) yields

$$\rho_e = \frac{\mathbb{E}_e[k_e(k_e - 1)]}{\mathbb{E}_e[k_e](K_e - 1)} \quad \text{and} \quad \rho_{ei} = \frac{b \mathbb{E}_{ei}[k_e k_i]}{\sqrt{K_e b_e \mathbb{E}_e[k_e] K_i b_i \mathbb{E}_i[k_i]}} = \frac{\mathbb{E}_{ei}[k_e k_i]}{\sqrt{K_e \mathbb{E}_{ei}[k_e] K_i \mathbb{E}_{ei}[k_i]}}.$$

## Appendix E: Marcus jump rule

The goal of this appendix is to justify the Marcus-type update rule given in Eq. (13). To do so let us first remark that given a finite time interval  $[0, T]$ , the number of synaptic activation times  $\{T_n\}_{n \in \mathbb{Z}}$  falling in this interval is almost surely finite. In particular, we have  $\Delta = \inf_{0 \leq T_n \neq T_m \leq T} |T_n - T_m| > 0$  almost surely. Consequently, taking  $\epsilon < \Delta/\tau_s$  ensures that synaptic activation events do not overlap in time, so that it is enough to consider a single synaptic activation triggered with no lack of generality in  $T_0 = 0$ . Let us denote the voltage just before the impulse onset as  $V(T_0^-) = V_0$ , which will serve as initial condition for the ensuing voltage dynamics. As the synaptic conductances remains equals to  $W_e/(\epsilon\tau)$  and  $W_i/(\epsilon\tau)$  for a duration  $[0, \epsilon\tau]$ , the voltage  $V_\epsilon$  satisfies

$$\tau \dot{V}_\epsilon = -V_\epsilon + (W_e/\epsilon)(V_e - V_\epsilon) + (W_i/\epsilon)(V_i - V_\epsilon), \quad 0 \leq t \leq \epsilon\tau,$$

where we assume  $I = 0$  for simplicity. The unique solution satisfying  $V(0^-) = V_0$  is

$$V_\epsilon(t) = V_0 e^{-t/\tau(1+W_e/\epsilon+W_i/\epsilon)} + \frac{W_e V_e + W_i V_i}{\epsilon + W_e + W_i} \left( 1 - e^{-t/\tau(1+W_e/\epsilon+W_i/\epsilon)} \right), \quad 0 \leq t \leq \epsilon\tau.$$

The Marcus-type rule follows from evaluating the jump update as the limit

$$\begin{aligned} \lim_{\epsilon \rightarrow 0^+} V_\epsilon(\epsilon\tau) - V_0 &= \lim_{\epsilon \rightarrow 0^+} \left\{ V_0 \left( e^{-(\epsilon+W_e+W_i)} - 1 \right) + \frac{W_e V_e + W_i V_i}{\epsilon + W_e + W_i} \left( 1 - e^{-(\epsilon+W_e+W_i)} \right) \right\}, \\ &= \left( \frac{W_e V_e + W_i V_i}{W_e + W_i} - V_0 \right) \left( 1 - e^{-(W_e+W_i)} \right), \end{aligned}$$

which has the same form as the rule announced in Eq. (13). Otherwise, at fixed  $\epsilon > 0$ , the fraction of time for which the voltage  $V_\epsilon$  is exponentially relaxing toward the leak reversal potential  $V_L = 0$  is larger than  $1 - N\epsilon/T$ , where  $N$  denotes the almost surely finite number of synaptic activations, which does not depends on  $\epsilon$ . Thus, the voltage  $V = \lim_{\epsilon \rightarrow 0^+} V_\epsilon$  exponentially relaxes toward  $V_L = 0$ , except when it has jump discontinuities in  $\{T_n\}_{n \in \mathbb{Z}}$ .

## Appendix F: Evaluation of $Q_\epsilon(t, s)$ for $\epsilon > 0$

The goal here is to justify the closed-form expression of  $Q_\epsilon(t, s) = \mathbb{E}[e^{H_e(t) + H_i(s)}]$  via standard manipulation of exponential functionals of Poisson processes. By definition, assuming with no loss of generality the order  $0 \geq t \geq s$ , we have

$$\begin{aligned} H_e(t) + H_i(s) &= -\frac{1}{\tau} \left( \int_t^0 h_e(u) \, du + \int_s^0 h_i(u) \, du \right), \\ &= -\frac{1}{\epsilon\tau} \left( \int_t^0 du \sum_{N(u-\epsilon\tau)+1}^{N(u)} W_{e,k} + \int_s^0 du \sum_{N(u-\epsilon\tau)+1}^{N(u)} W_{i,k} \right), \\ &= -\frac{1}{\epsilon\tau} \left( \int_t^0 du \sum_{N(u-\epsilon\tau)+1}^{N(u)} (W_{e,k} + W_{i,k}) + \int_s^t du \sum_{N(u-\epsilon\tau)+1}^{N(u)} W_{i,k} \right). \end{aligned} \quad (\text{F1})$$

We will evaluate  $Q_\epsilon(t, s) = \mathbb{E}[e^{H_e(t) + H_i(s)}]$  as a product of independent integral contributions.

Isolating these independent contributions from Eq. (F1) requires to establish two preliminary results about the quantity

$$I(t, s) = \int_s^t \sum_{k=N(u-\Delta)+1}^{N(u)} X_k \, du, \quad (\text{F2})$$

where  $N$  denotes a Poisson process,  $X_k$  denotes i.i.d. nonnegative random variables, and where  $\Delta$  is positive activation

time. Assume  $t - s \geq \Delta$ , then given some real  $w < u - \Delta$ , we have

$$\begin{aligned}
I(t, s) &= \int_s^t du \sum_{k=N(v)+1}^{N(u)} X_k - \int_s^t du \sum_{k=N(v)+1}^{N(u-\Delta)} X_k, \\
&= \int_s^t du \sum_{k=N(v)+1}^{N(u)} X_k - \int_{s-\Delta}^{t-\Delta} du \sum_{k=N(v)+1}^{N(u)} X_k, \\
&= \int_{t-\Delta}^t du \sum_{k=N(v)+1}^{N(u)} X_k - \int_{s-\Delta}^s du \sum_{k=N(v)+1}^{N(u)} X_k, \\
&= \left( \int_{t-\Delta}^t du \sum_{k=N(v)+1}^{N(t-\Delta)} X_k + \int_{t-\Delta}^t du \sum_{k=N(t-\Delta)+1}^{N(u)} X_k \right) - \left( \int_{s-\Delta}^s du \sum_{k=N(v)+1}^{N(s)} X_k - \int_{s-\Delta}^s du \sum_{k=N(u)+1}^{N(s)} X_k \right), \\
&= \int_{t-\Delta}^t du \sum_{k=N(t-\Delta)+1}^{N(u)} X_k + \Delta \sum_{k=N(s)+1}^{N(t-\Delta)} X_k + \int_{s-\Delta}^s du \sum_{k=N(u)+1}^{N(s)} X_k.
\end{aligned} \tag{F3}$$

One can check that the three terms in Eq. (F3) above are independent for involving independent numbers of i.i.d. draws over the intervals  $(t - \Delta, t]$ ,  $(s, t - \Delta]$ , and  $(s - \Delta, s]$ , respectively. Similar manipulations for the order for  $t - s \leq \Delta$  yields

$$I(t, s) = \int_s^t du \sum_{k=N(s)+1}^{N(u)} X_k + (t - s) \sum_{k=N(t-\Delta)+1}^{N(s)} X_k + \int_{s-\Delta}^{t-\Delta} du \sum_{k=N(u)+1}^{N(t-\Delta)} X_k, \tag{F4}$$

where that three independent contributions corresponds to independent numbers of i.i.d. draws over the intervals  $(s, t]$ ,  $(t - \Delta, s]$ , and  $(s - \Delta, t - \Delta]$ , respectively.

As evaluating  $Q_\epsilon$  only involves taking the limit  $s \rightarrow t^-$  at fixed  $\epsilon > 0$ , it is enough to consider the order  $0 \geq -\epsilon\tau \geq t \geq s \geq t - \epsilon\tau$ . With that in mind, we can apply Eq. (F3) Eq. (F4) with  $\Delta = \epsilon\tau$  and  $X_k = W_{e,k} + W_{i,k}$  or  $X_k = W_{i,k}$ , to decompose the two terms of Eq. (F1) in six contributions

$$\begin{aligned}
I(t, s) &= \int_{-\epsilon\tau}^0 du \sum_{k=N(t-\Delta)+1}^{N(u)} (W_{e,k} + W_{i,k}) + \epsilon\tau \sum_{k=N(t)+1}^{N(-\epsilon\tau)} (W_{e,k} + W_{i,k}) + \int_{t-\epsilon\tau}^t du \sum_{k=N(u)+1}^{N(t)} (W_{e,k} + W_{i,k}) \\
&\quad + \int_s^t du \sum_{k=N(s)+1}^{N(u)} W_{i,k} + (t - s) \sum_{k=N(t-\epsilon\tau)+1}^{N(s)} W_{i,k} + \int_{s-\epsilon\tau}^{t-\epsilon\tau} du \sum_{k=N(u)+1}^{N(t-\epsilon\tau)} W_{i,k}.
\end{aligned} \tag{F5}$$

It turns out that the contribution of the third term overlaps with that of the fourth and fifth terms. Further splitting of that third term produces the following expression

$$\begin{aligned}
I(t, s) &= \underbrace{\int_{-\epsilon\tau}^0 du \sum_{k=N(t-\Delta)+1}^{N(u)} (W_{e,k} + W_{i,k})}_{I_1} + \underbrace{\epsilon\tau \sum_{k=N(t)+1}^{N(-\epsilon\tau)} (W_{e,k} + W_{i,k})}_{I_2(t)} \\
&\quad + \underbrace{\int_s^t du \left( \sum_{k=N(u)+1}^{N(t)} (W_{e,k} + W_{i,k}) + \sum_{k=N(s)+1}^{N(u)} W_{i,k} \right) + (s - t + \epsilon\tau) \sum_{k=N(s)+1}^{N(t)} (W_{e,k} + W_{i,k})}_{I_3(t, s)} \\
&\quad + \underbrace{\left( \int_{t-\epsilon\tau}^s du \sum_{k=N(u)+1}^{N(s)} (W_{e,k} + W_{i,k}) + (t - s) \sum_{k=N(t-\epsilon\tau)+1}^{N(s)} W_{i,k} \right)}_{I_4(s, t)} + \underbrace{\int_{s-\epsilon\tau}^{t-\epsilon\tau} du \sum_{k=N(u)+1}^{N(t-\epsilon\tau)} W_{i,k}}_{I_5(t, s)},
\end{aligned} \tag{F6}$$

where all five terms correspond to independent numbers of i.i.d. draws over the intervals  $(-\epsilon\tau, 0]$ ,  $(t, -\epsilon\tau]$ ,  $(s, t]$ ,  $(t - \epsilon\tau, s]$ , and  $(s - \epsilon\tau, t - \epsilon\tau]$ . Then, we have

$$Q_\epsilon(t, s) = \mathbb{E} \left[ e^{H_e(t) + H_i(s)} \right] = \mathbb{E} \left[ e^{-I_1/(\epsilon\tau)} \right] \mathbb{E} \left[ e^{-I_2(t)/(\epsilon\tau)} \right] \mathbb{E} \left[ e^{-I_3(t,s)/(\epsilon\tau)} \right] \mathbb{E} \left[ e^{-I_4(s,t)/(\epsilon\tau)} \right] \mathbb{E} \left[ e^{-I_5(t,s)/(\epsilon\tau)} \right],$$

where all expectation terms can be computed via standard manipulation of the moment-generating function of Poisson processes [40]. The trick is to remember that for all  $t \geq s$ , given that a Poisson process admits  $K = N(t) - N(s)$  points in  $(s, t]$ , all these  $K$  points are uniformly i.i.d. over  $(s, t]$ . This trick allows one to simply represent all integral terms in terms of uniform random variables, whose expectations are easily computable. To see this, let us consider  $A_3(t, s)$  for instance. We have

$$\begin{aligned} I_3(t, s) &= (t - s) \sum_{k=N(s)+1}^{N(t)} [(1 - U_k)(W_{e,k} + W_{i,k}) + U_k W_{i,k}] + (s - t + \epsilon\tau) \sum_{k=N(s)+1}^{N(t)} (W_{e,k} + W_{i,k}), \\ &= (t - s) \sum_{k=N(s)+1}^{N(t)} U_k W_{e,k} + \epsilon\tau \sum_{k=N(s)+1}^{N(t)} (W_{e,k} + W_{i,k}), \end{aligned}$$

where  $\{U_k\}_{N(s)+1 \leq k \leq N(t)}$  are uniformly i.i.d. on  $[0, 1]$ . From the knowledge of the moment-generating function of Poisson random variables [40], one can evaluate

$$\begin{aligned} \mathbb{E} \left[ e^{-I_3(t,s)/(\epsilon\tau)} \right] &= \mathbb{E} \left[ e^{-\frac{t-s}{\epsilon\tau} \sum_{k=N(s)+1}^{N(t)} U_k W_{e,k} - \sum_{k=N(s)+1}^{N(t)} (W_{e,k} + W_{i,k})} \right], \\ &= \mathbb{E} \left[ \mathbb{E} \left[ e^{-\frac{t-s}{\epsilon\tau} U W_e - (W_e + W_i)} \right]^{N(t) - N(s)} \middle| N(t) - N(s) \right], \\ &= \exp \left( b(t - s) \left( \mathbb{E} \left[ e^{-\frac{t-s}{\epsilon\tau} U W_e - (W_e + W_i)} \right] - 1 \right) \right), \end{aligned} \quad (\text{F7})$$

where  $(W_e, W_i)$  denotes exemplary conductance jumps and  $U$  denotes an independent uniform random variable. Furthermore we have

$$\begin{aligned} \mathbb{E} \left[ e^{-\frac{t-s}{\epsilon\tau} U W_e - (W_e + W_i)} \right] &= \mathbb{E} \left[ \mathbb{E} \left[ e^{-\frac{t-s}{\epsilon\tau} U W_e - (W_e + W_i)} \right] \middle| W_e, W_i \right], \\ &= \mathbb{E}_{ei} \left[ e^{-(W_e + W_i)} \mathbb{E} \left[ e^{-\frac{t-s}{\epsilon\tau} U W_e} \right] \right], \\ &= \mathbb{E}_{ei} \left[ e^{-(W_e + W_i)} \frac{\left(1 - e^{-\frac{t-s}{\epsilon\tau} W_e}\right)}{\frac{t-s}{\epsilon\tau} W_e} \right], \end{aligned} \quad (\text{F8})$$

so that we finally obtain

$$\ln \mathbb{E} \left[ e^{-I_3(t,s)/(\epsilon\tau)} \right] = \epsilon b \tau \left( \mathbb{E}_{ei} \left[ e^{-(W_e + W_i)} \frac{\left(1 - e^{-\frac{t-s}{\epsilon\tau} W_e}\right)}{W_e} \right] - \frac{t - s}{\epsilon\tau} \right). \quad (\text{F9})$$

Similar calculations show that we have

$$\ln \mathbb{E} \left[ e^{-I_1/(\epsilon\tau)} \right] = \epsilon b \tau \left( \mathbb{E}_{ei} \left[ \frac{1 - e^{-(W_e + W_i)}}{W_e + W_i} \right] - 1 \right), \quad (\text{F10})$$

$$\ln \mathbb{E} \left[ e^{-I_2(t)/(\epsilon\tau)} \right] = b(\epsilon\tau + t) \left( 1 - \mathbb{E}_{ei} \left[ e^{-(W_e + W_i)} \right] \right),$$

$$\ln \mathbb{E} \left[ e^{-I_4(s,t)/(\epsilon\tau)} \right] = \epsilon b \tau \left( \mathbb{E}_{ei} \left[ e^{-\frac{t-s}{\epsilon\tau} W_i} \frac{\left(1 - e^{-(1 + \frac{s-t}{\epsilon\tau})(W_e + W_i)}\right)}{W_e + W_i} \right] - \left(1 + \frac{s - t}{\epsilon\tau}\right) \right),$$

$$\ln \mathbb{E} \left[ e^{-I_5(t,s)/(\epsilon\tau)} \right] = \epsilon b \tau \left( \mathbb{E}_{ei} \left[ \frac{1 - e^{-\frac{t-s}{\epsilon\tau} W_i}}{W_i} \right] - \frac{t - s}{\epsilon\tau} \right). \quad (\text{F11})$$

### Appendix G: Expression of $R_\epsilon(t, u, s, v)$ on $\mathcal{O}_\epsilon$ and $\mathcal{D}_\epsilon$

Using the similar calculations as in Appendix (F), we can evaluate the quadrivariate expectation  $R_\epsilon(t, u, s, v)$  on the region  $\mathcal{O}_\epsilon$ , for which the  $O$ -order holds:  $0 \geq -\epsilon\tau \geq t \geq u \geq t - \epsilon\tau \geq u - \epsilon\tau \geq s \geq v \geq s - \epsilon\tau \geq v - \epsilon\tau$ . This requires to isolate consider 9 independent contributions, corresponding to the 9 contiguous intervals specified by the  $O$ -order. We find

$$\ln R_\epsilon(t, u, s, v) = A_1 + A_2(t) + A_3(t, u) + A_4(u, t) + A_5(t, u) + A_6(u, s) + A_7(s, v) + A_8(v, s) + A_9(s, v),$$

where the nonnegative terms making up the above sum are defined as

$$A_1 = \epsilon b \tau \left( \mathbb{E}_{\text{ei}} \left[ \frac{1 - e^{-2(W_e + W_i)}}{2(W_e + W_i)} \right] - 1 \right),$$

$$A_2(t) = b(\epsilon\tau + t) \left( 1 - \mathbb{E}_{\text{ei}} \left[ e^{-2(W_e + W_i)} \right] \right),$$

$$A_3(t, u) = \epsilon b \tau \left( \mathbb{E}_{\text{ei}} \left[ e^{-2(W_e + W_i)} \frac{\left( 1 - e^{-\frac{t-u}{\epsilon\tau} W_e} \right)}{W_e} \right] - \frac{t-u}{\epsilon\tau} \right),$$

$$A_4(u, t) = \epsilon b \tau \left( \mathbb{E}_{\text{ei}} \left[ e^{-W_e - \left( 1 + \frac{t-u}{\epsilon\tau} \right) W_i} \frac{\left( 1 - e^{-\left( 1 + \frac{u-t}{\epsilon\tau} \right) (W_e + W_i)} \right)}{W_e + W_i} \right] - \left( 1 + \frac{u-t}{\epsilon\tau} \right) \right),$$

$$A_5(t, u) = \epsilon b \tau \left( \mathbb{E}_{\text{ei}} \left[ e^{-(W_e + W_i)} \frac{\left( 1 - e^{-\frac{t-u}{\epsilon\tau} W_i} \right)}{W_i} \right] - \frac{t-u}{\epsilon\tau} \right),$$

$$A_6(u, s) = b(s + \epsilon\tau - u) \left( 1 - \mathbb{E}_{\text{ei}} \left[ e^{-(W_e + W_i)} \right] \right)$$

$$A_7(s, v) = \epsilon b \tau \left( \mathbb{E}_{\text{ei}} \left[ e^{-(W_e + W_i)} \frac{\left( 1 - e^{-\frac{s-v}{\epsilon\tau} W_e} \right)}{W_e} \right] - \frac{s-v}{\epsilon\tau} \right),$$

$$A_8(v, s) = \epsilon b \tau \left( \mathbb{E}_{\text{ei}} \left[ e^{-\frac{s-v}{\epsilon\tau} W_i} \frac{\left( 1 - e^{-\left( 1 - \frac{s-v}{\epsilon\tau} \right) (W_e + W_i)} \right)}{W_e + W_i} \right] - \left( 1 - \frac{s-v}{\epsilon\tau} \right) \right),$$

$$A_9(s, v) = \epsilon b \tau \left( \mathbb{E}_{\text{ei}} \left[ \frac{\left( 1 - e^{-\frac{s-v}{\epsilon\tau} W_i} \right)}{W_i} \right] - \frac{s-v}{\epsilon\tau} \right).$$

One can check that  $A_3(t, t) = A_5(t, t) = 0$  and  $A_7(s, s) = A_9(s, s) = 0$  and that  $A_1$ ,  $A_4(u, t)$ , and  $A_8(v, s)$  are all uniformly  $O(\epsilon)$  on the region  $\mathcal{O}_\epsilon$ . This implies that for all  $(t, s)$  in  $\mathcal{O}_\epsilon$ , we have

$$R(t, s) = \lim_{\epsilon \rightarrow 0^+} R_\epsilon(t, t, s, s) = \lim_{\epsilon \rightarrow 0^+} e^{A_2(t) + A_6(t, s)} = e^{2bta_{\text{ei}, 2} - b|t-s|a_{\text{ei}, 1}}.$$

Using the similar calculations as in Appendix (F), we can evaluate the quadrivariate expectation  $R_\epsilon(t, u, s, v)$  on the region  $\mathcal{D}_\epsilon$ , for which the  $D$ -order holds:  $0 \geq -\epsilon\tau \geq t \geq u \geq s \geq v \geq t - \epsilon\tau \geq u - \epsilon\tau \geq s - \epsilon\tau \geq v - \epsilon\tau$ . This requires to isolate consider 9 independent contributions, corresponding to the 9 contiguous intervals specified by the  $O$ -order. We find

$$\begin{aligned} \ln R_\epsilon(t, u, s, v) &= \\ B_1 + B_2(t) + B_3(t, u) + B_4(t, u, s) + B_5(t, u, s, v) + B_6(t, u, s, v) + B_7(t, u, s, v) + B_8(u, s, v) + B_9(s, v) &= \end{aligned} \tag{G1}$$

where the nonnegative terms making up the above sum are defined as

$$B_1 = \epsilon b \tau \left( \mathbb{E}_{\text{ei}} \left[ \frac{1 - e^{-2(W_e + W_i)}}{2(W_e + W_i)} \right] - 1 \right),$$

$$B_2(t) = b(\epsilon \tau + t) \left( 1 - \mathbb{E}_{\text{ei}} \left[ e^{-2(W_e + W_i)} \right] \right),$$

$$B_3(t, u) = \epsilon b \tau \left( \mathbb{E}_{\text{ei}} \left[ e^{-2(W_e + W_i)} \frac{\left( 1 - e^{-\frac{t-u}{\epsilon \tau} W_e} \right)}{W_e} \right] - \frac{t-u}{\epsilon \tau} \right),$$

$$B_4(t, u, s) = \epsilon b \tau \left( \mathbb{E}_{\text{ei}} \left[ e^{-\left( 2 - \frac{t-s}{\epsilon \tau} \right) W_e - \left( 2 - \frac{u-s}{\epsilon \tau} \right) W_i} \frac{\left( 1 - e^{-\frac{u-s}{\epsilon \tau} (W_e + W_i)} \right)}{W_e + W_i} \right] - \frac{u-s}{\epsilon \tau} \right),$$

$$B_5(t, u, s, v) = \epsilon b \tau \left( \mathbb{E}_{\text{ei}} \left[ e^{-\left( 2 - \frac{t-v}{\epsilon \tau} \right) W_e - \left( 2 - \frac{u-v}{\epsilon \tau} \right) W_i} \frac{\left( 1 - e^{-\frac{s-v}{\epsilon \tau} (2W_e + 2W_i)} \right)}{2W_e + 2W_i} \right] - \frac{s-v}{\epsilon \tau} \right),$$

$$B_6(t, u, s, v) = \epsilon b \tau \left( \mathbb{E}_{\text{ei}} \left[ e^{-\left( \frac{t-s}{\epsilon \tau} \right) W_e - \left( \frac{2t-(u+v)}{\epsilon \tau} \right) W_i} \frac{\left( 1 - e^{-\left( 1 - \frac{t-v}{\epsilon \tau} \right) 2(W_e + W_i)} \right)}{2(W_e + W_i)} \right] - \left( 1 - \frac{t-v}{\epsilon \tau} \right) \right),$$

$$B_7(t, u, s, v) = \epsilon b \tau \left( \mathbb{E}_{\text{ei}} \left[ e^{-\left( \frac{u-s}{\epsilon \tau} \right) W_e - \left( \frac{u-v}{\epsilon \tau} \right) W_i} \frac{\left( 1 - e^{-\frac{t-u}{\epsilon \tau} (W_e + 2W_i)} \right)}{W_e + 2W_i} \right] - \frac{t-u}{\epsilon \tau} \right),$$

$$B_8(u, s, v) = \epsilon b \tau \left( \mathbb{E}_{\text{ei}} \left[ e^{-\left( \frac{s-v}{\epsilon \tau} \right) W_i} \frac{\left( 1 - e^{-\frac{u-s}{\epsilon \tau} (W_e + W_i)} \right)}{W_e + W_i} \right] - \frac{u-s}{\epsilon \tau} \right),$$

$$B_9(s, v) = b \epsilon \tau \left( \mathbb{E}_{\text{ei}} \left[ e^{-\left( \frac{s-v}{\epsilon \tau} \right) W_i} \frac{\left( 1 - e^{-\frac{s-v}{\epsilon \tau} W_i} \right)}{W_i} \right] - \frac{s-v}{\epsilon \tau} \right).$$

Observe that  $B_1 = A_1$  and  $B_2(t) = A_2(t)$  and that  $B_3(t, t) = B_7(t, t, s, v) = 0$  and  $B_5(t, u, s, s) = B_9(s, s) = 0$ . Moreover, one can see that  $R(t, s)$  is continuous over the whole negative orthant by checking that:

$$\begin{aligned} \lim_{s \rightarrow (t-\epsilon \tau)^-} B_4(t, t, s) &= \lim_{s \rightarrow (t-\epsilon \tau)^+} A_4(t, s), \\ \lim_{s \rightarrow (t-\epsilon \tau)^-} B_6(t, t, s, s) &= \lim_{s \rightarrow (t-\epsilon \tau)^+} A_6(t, s), \\ \lim_{s \rightarrow (t-\epsilon \tau)^-} B_8(t, s, s) &= \lim_{s \rightarrow (t-\epsilon \tau)^+} A_8(t, s). \end{aligned}$$

Actually, by computing the appropriate limit values of the relevant first- and second-order derivatives of  $R_\epsilon(t, u, s, v)$ , one can check that for  $\epsilon > 0$ , all the integrands involved in specifying the coefficients of the quadratic form Eq. (21) define continuous functions.

## Appendix H: Integrals of the quadratic terms on $\mathcal{D}_\epsilon$

Here, we only treat the quadratic term  $A_e$  as the other quadratic terms  $A_i$  and  $B_{ei}$  involve a similar treatment. The goal here is to compute  $A_e''$ , which is defined as the contribution to  $A_e$  resulting from integrating  $\lim_{(u,v) \rightarrow (t,s)^-} \partial_t \partial_s R_\epsilon(t, u, s, v)$  over the diagonal region  $\mathcal{D}_\epsilon = \{t, s \leq 0 \mid \tau \epsilon \geq |t - s|\}$ , in the limit  $\epsilon \rightarrow 0^+$ . To this end we first remark that

$$\frac{\partial_t \partial_s R_\epsilon(t, u, s, v)}{R_\epsilon(t, u, s, v)} = \partial_t \partial_s \ln R_\epsilon(t, u, s, v) + (\partial_t \ln R_\epsilon(t, u, s, v)) (\partial_s \ln R_\epsilon(t, u, s, v)).$$

Injecting the analytical expression Eq. (G1) into the above relation and evaluating  $I_\epsilon(t, s) = \lim_{(u,v) \rightarrow (t,s)^-} \partial_t \partial_s R_\epsilon(t, u, s, v)$  reveals that  $I_\epsilon(t, s)$  scales as  $1/\epsilon$ , so that one expects that

$$A_e'' = \lim_{\epsilon \rightarrow 0^+} \iint_{\mathcal{D}_\epsilon} e^{\frac{t+s}{\tau}} I_\epsilon(t, s) dt ds > 0.$$

To compute the exact value of  $A_e''$ , we perform the change of variable  $x = (t - s)/(\epsilon \tau) \Leftrightarrow s = t - \epsilon \tau x$  to write

$$\iint_{\mathcal{D}_\epsilon} e^{\frac{t+s}{\tau}} I_\epsilon(t, s) dt ds = 2 \int_{-\infty}^0 \left( \int_0^1 \epsilon \tau e^{-\epsilon x} I_\epsilon(t, t + \epsilon \tau x) dx \right) e^{\frac{2t}{\tau}} dt,$$

where the function  $\epsilon e^{-\epsilon x} I_\epsilon(t, t + \epsilon x)$  remains of order one on  $\mathcal{D}_\epsilon$  in the limit of instantaneous synapses. Actually, one can compute that

$$\lim_{\epsilon \rightarrow 0^+} \epsilon e^{-\epsilon x} I_\epsilon(t, t + \epsilon x) = \frac{b}{2\tau} \mathbb{E}_{ei} \left[ \frac{W_e^2}{W_e + W_i} e^{-x(W_e + W_i)} \left( 1 - e^{-2(1-x)(W_e + W_i)} \right) \right] e^{2bt a_{ei,2}}.$$

Then, for dealing with positive, continuous, uniformly bounded functions, one can safely exchange the integral and limit operations to get

$$\begin{aligned} A_e'' &= 2 \int_{-\infty}^0 \left( \int_0^1 \lim_{\epsilon \rightarrow 0^+} \epsilon \tau e^{-\epsilon x} I_\epsilon(t, t + \epsilon \tau x) dx \right) e^{\frac{2t}{\tau}} dt, \\ &= \left( \int_{-\infty}^0 e^{2\frac{t}{\tau}(1+a_{ei,2})} dt \right) \left( \int_0^1 b \mathbb{E}_{ei} \left[ \frac{W_e^2}{W_e + W_i} e^{-\frac{x}{\tau}(W_e + W_i)} \left( 1 - e^{-2(1-\frac{x}{\tau})(W_e + W_i)} \right) \right] dx \right), \\ &= \frac{b\tau}{2(1+a_{ei,2})} \mathbb{E}_{ei} \left[ \frac{W_e^2}{(W_e + W_i)^2} \left( 1 - e^{-(W_e + W_i)^2} \right) \right]. \end{aligned}$$

A similar calculation for the quadratic cross term  $B_{ei}''$  yields

$$B_{ei}'' = \frac{2c_{ei}}{1+a_{ei,2}} \quad \text{with} \quad c_{ei} = \frac{b\tau}{2} \mathbb{E}_{ei} \left[ \frac{W_e W_i}{(W_e + W_i)^2} \left( 1 - e^{-(W_e + W_i)^2} \right) \right].$$

In order to express  $A_e''$  in term of  $c_{ei}$ , we need to introduce the quantity  $a_{e,12} = a_{e,1} - a_{e,2}$  which satisfies

$$\begin{aligned} a_{e,12} &= b\tau \mathbb{E}_{ei} \left[ \frac{W_e}{(W_e + W_i)} \left( 1 - e^{-(W_e + W_i)} \right) \right] - \frac{1}{2} \mathbb{E}_{ei} \left[ \frac{W_e}{(W_e + W_i)} \left( 1 - e^{-(W_e + W_i)} \right)^2 \right], \\ &= b\tau \mathbb{E}_{ei} \left[ \frac{W_e}{(W_e + W_i)} \left( 1 - e^{-(W_e + W_i)} \right) \left( 1 - \frac{1}{2} \left( 1 - e^{-(W_e + W_i)} \right) \right) \right], \\ &= b\tau \mathbb{E}_{ei} \left[ \frac{W_e}{(W_e + W_i)} \left( 1 - e^{-(W_e + W_i)} \right) \left( \frac{(1 + e^{-(W_e + W_i)})}{2} \right) \right], \\ &= \frac{b\tau}{2} \mathbb{E}_{ei} \left[ \frac{W_e}{(W_e + W_i)} \left( 1 + e^{-(W_e + W_i)} \right)^2 \right], \end{aligned}$$

With the above observation, we remark that

$$\begin{aligned} (1 + a_{ei,2}) A_e'' - a_{e,12} &= \frac{b\tau}{2} \left( \mathbb{E}_{ei} \left[ \frac{W_e^2}{(W_e + W_i)^2} \left( 1 - e^{-(W_e + W_i)} \right)^2 \right] - \mathbb{E}_{ei} \left[ \frac{W_e}{(W_e + W_i)} \left( 1 - e^{-(W_e + W_i)} \right)^2 \right] \right), \\ &= \frac{b\tau}{2} \mathbb{E}_{ei} \left[ \frac{W_e^2 - W_e(W_e + W_i)}{(W_e + W_i)^2} \left( 1 - e^{-(W_e + W_i)} \right)^2 \right], \\ &= -\frac{b\tau}{2} \mathbb{E}_{ei} \left[ \frac{W_e W_i}{(W_e + W_i)^2} \left( 1 - e^{-(W_e + W_i)} \right)^2 \right], \\ &= -c_{ei} \end{aligned}$$

so that we have the following compact expression for the quadratic diagonal term

$$A_e'' = \frac{a_{e,12} - c_{ei}}{1 + a_{ei,2}}.$$

### Appendix I: Compact variance expression

Our goal is find a compact, interpretable formula for the stationary variance  $\mathbb{V}[V]$  from the knowledge of the quadratic form

$$\mathbb{E}[V^2] = A_e V_e^2 + B_{ei} V_e V_i + A_i V_i^2 + (V_e B_{eI} + V_i B_{iI}) (I/G) + A_I (I/G)^2.$$

Let us first assume no current injection,  $I = 0$ , so that one only has to keep track of the quadratic terms. Specifying the quadratic coefficient  $A_e = A'_e + A''_e$ ,  $A_i = A'_i + A''_i$  and  $B_{ei} = B'_{ei} + B''_{ei}$  in Eq. (I1), we get

$$\begin{aligned} \mathbb{E}[V^2] &= \left( \frac{a_{e,1}(2a_{e,2} - a_{e,1})}{(1 + a_{ei,1})(1 + a_{ei,2})} + \frac{a_{e,12} - c_{ei}}{1 + a_{ei,2}} \right) V_e^2 \\ &\quad + \left( \frac{a_{e,1}(2a_{i,2} - a_{i,1}) + a_{i,1}(2a_{e,2} - a_{e,1})}{(1 + a_{ei,1})(1 + a_{ei,2})} + \frac{2c_{ei}}{1 + a_{ei,2}} \right) V_e V_i \\ &\quad + \left( \frac{a_{i,1}(2a_{i,2} - a_{i,1})}{(1 + a_{ei,1})(1 + a_{ei,2})} + \frac{a_{i,12} - c_{ei}}{1 + a_{ei,2}} \right) V_i^2, \\ &= \left( \frac{a_{e,1}(2a_{e,2} - a_{e,1}) + (1 + a_{e,1} + a_{i,1})(a_{e,1} - a_{e,2})}{(1 + a_{ei,1})(1 + a_{ei,2})} \right) V_e^2 \\ &\quad + \left( \frac{a_{e,1}(2a_{i,2} - a_{i,1}) + a_{i,1}(2a_{e,2} - a_{e,1})}{(1 + a_{ei,1})(1 + a_{ei,2})} \right) V_e V_i \\ &\quad + \left( \frac{a_{i,1}(2a_{i,2} - a_{i,1}) + (1 + a_{e,1} + a_{i,1})(a_{i,1} - a_{i,2})}{(1 + a_{ei,1})(1 + a_{ei,2})} \right) V_i^2 - \frac{c_{ei}}{1 + a_{ei,2}} (V_e - V_i)^2, \end{aligned}$$

where we collect separately all the terms containing the coefficient  $c_{ei}$  and where we use the facts that by definition  $a_{e,12} = a_{e,1} - a_{e,2}$ ,  $a_{i,12} = a_{i,1} - a_{i,2}$ , and  $a_{ei,1} = a_{e,1} + a_{i,1}$ . Expanding and simplifying the coefficients of  $V_e^2$  and  $V_i^2$  above yield

$$\begin{aligned} \mathbb{E}[V^2] &= \left( \frac{a_{e,1}a_{e,2} + (1 + a_{i,1})(a_{e,1} - a_{e,2})}{(1 + a_{ei,1})(1 + a_{ei,2})} \right) V_e^2 \\ &\quad + \left( \frac{a_{e,1}(2a_{i,2} - a_{i,1}) + a_{i,1}(2a_{e,2} - a_{e,1})}{(1 + a_{ei,1})(1 + a_{ei,2})} \right) V_e V_i \\ &\quad + \left( \frac{a_{i,1}a_{i,2} + (1 + a_{e,1})(a_{i,1} - a_{i,2})}{(1 + a_{ei,1})(1 + a_{ei,2})} \right) V_i^2 - \frac{c_{ei}}{1 + a_{ei,2}} (V_e - V_i)^2. \end{aligned}$$

Then, we can utilize the expression above for  $\mathbb{E}[V^2]$  together with the stationary mean formula

$$\mathbb{E}[V] = \frac{a_{e,1}V_e + a_{i,1}V_i}{1 + a_{ei,1}}, \quad (\text{I1})$$

to write the variance  $\mathbb{V}[V] = \mathbb{E}[V^2] - \mathbb{E}[V]^2$  as

$$\begin{aligned} \mathbb{V}[V] &= \left( \frac{(a_{e,1} - a_{e,2})(1 + a_{i,1})^2 + (a_{i,1} - a_{i,2})a_{e,1}^2}{(1 + a_{ei,1})^2(1 + a_{ei,2})} \right) V_e^2 \\ &\quad - \left( \frac{(a_{e,1} - a_{e,2})a_{e,1}(1 + a_{e,1}) + a_{i,1}(a_{i,1} - a_{i,2})(1 + a_{i,1})}{(1 + a_{ei,1})^2(1 + a_{ei,2})} \right) V_e V_i \\ &\quad + \left( \frac{(a_{i,1} - a_{i,2})(1 + a_{e,1})^2 + (a_{e,1} - a_{e,2})a_{i,1}^2}{(1 + a_{ei,1})^2(1 + a_{ei,2})} \right) V_i^2 - \frac{c_{ei}}{1 + a_{ei,2}} (V_e - V_i)^2. \end{aligned}$$

To factorize the above expression, let us reintroduce  $a_{e,12} = a_{e,1} - a_{e,2}$  and  $a_{i,12} = a_{i,1} - a_{i,2}$  and collect the terms where these two coefficients occur. This yields

$$\begin{aligned}\mathbb{V}[V] &= \frac{a_{e,12}}{(1+a_{ei,1})^2(1+a_{ei,2})} ((1+a_{i,1})^2V_e^2 - a_{i,1}(1+a_{e,1})^2V_eV_i + (a_{e,1})^2V_i^2) \\ &\quad + \frac{a_{i,12}}{(1+a_{ei,1})^2(1+a_{ei,2})} ((1+a_{e,1})^2V_i^2 - a_{e,1}(1+a_{i,1})^2V_eV_i + (a_{i,1})^2V_e^2) \\ &\quad - \frac{c_{ei}}{1+a_{ei,2}} (V_e - V_i)^2, \\ &= \frac{a_{e,12}}{1+a_{ei,2}} \left( \frac{(1+a_{i,1})V_e - a_{e,1}V_i}{1+a_{ei,1}} \right)^2 + \frac{a_{i,12}}{1+a_{ei,2}} \left( \frac{(1+a_{i,e})V_i - a_{i,1}V_e}{1+a_{ei,1}} \right)^2 \\ &\quad - \frac{c_{ei}}{1+a_{ei,2}} (V_e - V_i)^2.\end{aligned}$$

Finally, injecting the expression of stationary mean Eq. (I1) in both parentheses above produces the compact formula

$$\mathbb{V}[V] = \frac{a_{e,12}}{1+a_{ei,2}} (V_e - \mathbb{E}[V])^2 + \frac{a_{i,12}}{1+a_{ei,2}} (V_i - \mathbb{E}[V])^2 - \frac{c_{ei}}{1+a_{ei,2}} (V_e - V_i)^2, \quad (\text{I2})$$

which is the same as the one given in Eq. (30).

#### Appendix J: Factorized variance expression

In this appendix, we reshape the variance expression given in Eq. (I2) under a form that is clearly nonnegative. To this end, let us first remark that the calculation in Appendix H shows that

$$a_{e,12} - c_{ei} = \frac{b\tau}{2} \mathbb{E}_{ei} \left[ \frac{W_e^2}{(W_e + W_i)^2} \left( 1 + e^{-(W_e + W_i)} \right)^2 \right].$$

Then, setting  $(V_e - V_i)^2 = ((V_e - \mathbb{E}[V]) - (V_i - \mathbb{E}[V]))^2 = (V_e - \mathbb{E}[V])^2 - 2(V_e - \mathbb{E}[V])(V_i - \mathbb{E}[V]) + (V_i - \mathbb{E}[V])^2$  in Eq. (I2), we obtain

$$\begin{aligned}\mathbb{V}[V] &= \frac{1}{1+a_{ei,2}} (a_{e,12}(V_e - \mathbb{E}[V])^2 + a_{i,12}(V_i - \mathbb{E}[V])^2 - c_{ei}(V_e - V_i)^2), \\ &= \frac{1}{1+a_{ei,2}} ((a_{e,12} - c_{ei})(V_e - \mathbb{E}[V])^2 + 2c_{ei}(V_e - \mathbb{E}[V])(V_i - \mathbb{E}[V]) + (a_{i,12} - c_{ei})(V_i - \mathbb{E}[V])^2), \\ &= \frac{b\tau}{1+a_{ei,2}} \mathbb{E}_{ei} \left[ \left( \frac{W_e^2(V_e - \mathbb{E}[V])^2}{2(W_e + W_i)^2} + \frac{2W_e(V_e - \mathbb{E}[V])W_i(V_i - \mathbb{E}[V])}{2(W_e + W_i)^2} + \frac{W_i^2(V_i - \mathbb{E}[V])^2}{2(W_e + W_i)^2} \right) \left( 1 - e^{-(W_e + W_i)} \right)^2 \right], \\ &= \frac{b\tau}{2(1+a_{ei,2})} \mathbb{E}_{ei} \left[ \left( \frac{[W_e(V_e - \mathbb{E}[V]) + W_i(V_i - \mathbb{E}[V])]^2}{(W_e + W_i)^2} \right) \left( 1 - e^{-(W_e + W_i)} \right)^2 \right]. \quad (\text{J1})\end{aligned}$$

Note that the above quantity is clearly non negative as any variance shall be. From there, one can include the impact of the injected current  $I$  by further considering all the terms in Eq. (I1), including the linear and inhomogeneous current-dependent terms. Similar algebraic manipulations confirm that Eq. (J1) remains valid so that the only impact of  $I$  is via altering the expression  $\mathbb{E}[V]$ , so that we ultimately obtain the following explicit compact form:

$$\mathbb{V}[V] = \frac{\mathbb{E}_{ei} \left[ \left( \frac{W_e V_e + W_i V_i}{W_e + W_i} - \mathbb{E}[V] \right)^2 \left( 1 - e^{-(W_e + W_i)} \right)^2 \right]}{2/(b\tau) + \mathbb{E}_{ei} \left[ (1 - e^{-2(W_e + W_i)}) \right]} \quad \text{with} \quad \mathbb{E}[V] = \frac{b\tau \mathbb{E}_{ei} \left[ \left( \frac{W_e V_e + W_i V_i}{W_e + W_i} \right) \left( 1 - e^{-(W_e + W_i)} \right) \right] + I/G}{1 + b\tau \mathbb{E}_{ei} \left[ (1 - e^{-(W_e + W_i)}) \right]}.$$

The above expression shows that as expected  $\mathbb{V}[V] \geq 0$  and that the variability vanishes if and only if  $W_e/W_i = (\mathbb{E}[V] - V_i)/(V_e - \mathbb{E}[V])$  with probability one. In turn plugging this relation into the mean voltage expression and solving for  $\mathbb{E}[V]$  reveals that we necessarily have  $\mathbb{E}[V] = I/G$ . This is consistent with the intuition that variability can only vanish if excitation and inhibition perfectly cancel one another.

## Appendix K: Variance in the small-weight approximation

In this appendix, we compute the simplified expression for the variance  $\mathbb{V}[V]$  obtained via the small-weight approximation. Second, let us compute the small-weight approximation of the second-order efficacy

$$c_{ei} = \frac{b\tau}{2} \mathbb{E}_{ei} \left[ \frac{W_e W_i}{(W_e + W_i)^2} \left( 1 - e^{-(W_e + W_i)} \right)^2 \right] \simeq \frac{b\tau}{2} \mathbb{E}_{ei} [W_e W_i] = \frac{b\tau}{2} w_e w_i \mathbb{E}_{ei} [k_e k_i] ,$$

which amounts to compute the expectation of the crossproduct of the jumps  $k_e$  and  $k_i$ . To estimate the above approximation, it is important to remember that first that  $p_{e,k}$  and  $p_{i,k}$  are not defined as the marginals of  $p_{ei,kl}$ , but as conditional marginals, for which we have  $p_{e,k} = (b/b_e) \sum_{l=0}^{K_i} p_{ei,kl}$  and  $p_{i,l} = (b/b_i) \sum_{k=0}^{K_e} p_{ei,kl}$ . Then by the definition of the correlation coefficient  $\rho_{ei}$  in Eq. (9), we have

$$\rho_{ei} = \frac{b \mathbb{E}_{ei} [k_e k_i]}{\sqrt{K_e b \mathbb{E}_{ei} [k_e] K_i b \mathbb{E}_{ei} [k_i]}} = \frac{b \mathbb{E}_{ei} [k_e k_i]}{\sqrt{K_e b_e \mathbb{E}_e [k_e] K_i b_i \mathbb{E}_i [k_i]}} = \frac{b \mathbb{E}_{ei} [k_e k_i]}{K_e K_i \sqrt{r_e r_i}} ,$$

as the rates  $b_e$  and  $b_i$  are such that  $b_e \mathbb{E}_e [k_e] = K_e r_e$  and  $b_i \mathbb{E}_i [k_i] = K_i r_i$ . As a result, we obtain a simplified expression for the cross-correlation coefficient:

$$c_{ei} = (\rho_{ei} \sqrt{r_e r_i} \tau / 2) (K_e w_e) (K_i w_i) .$$

Observe that as expected,  $c_{ei}$  vanishes when  $\rho_{ei} = 0$ . Second, let us compute the small-weight approximation of the second-order efficacy

$$a_{e,12} = \frac{b\tau}{2} \mathbb{E}_{ei} \left[ \frac{W_e}{W_e + W_i} \left( 1 - e^{-(W_e + W_i)} \right)^2 \right] \simeq \frac{b\tau}{2} \mathbb{E}_{ei} [W_e (W_e + W_i)] = \frac{b\tau}{2} (w_e^2 \mathbb{E}_{ei} [k_e^2] + w_e w_i \mathbb{E}_{ei} [k_e k_i]) .$$

To estimate the above approximation, we use the definition of the correlation coefficient  $\rho_e$  in Eq. (7),

$$\rho_e = \frac{b_e \mathbb{E}_e [k_e (k_e - 1)]}{b_e \mathbb{E}_e [k_e] (K_e - 1)} = \frac{b \mathbb{E}_{ei} [k_e (k_e - 1)]}{K_e (K_e - 1) r_e} ,$$

as the rate  $b_e$  is such that  $b_e \mathbb{E}_e [k_e] = K_e r_e$ . This directly implies that

$$b \mathbb{E}_{ei} [k_e^2] = b \mathbb{E}_{ei} [k_e (k_e - 1)] + b \mathbb{E}_{ei} [k_e] = \rho_e K_e (K_e - 1) r_e + K_e r_e = K_e r_e (1 + \rho_e (K_e - 1)) .$$

so that we evaluate

$$a_{e,12} = \frac{b\tau}{2} (w_e^2 \mathbb{E}_{ei} [k_e^2] + w_e w_i \mathbb{E}_{ei} [k_e k_i]) = \frac{r_e \tau}{2} K_e (1 + \rho_e (K_e - 1)) w_e^2 + \rho_{ei} \frac{\sqrt{r_i r_e} \tau}{2} (K_e w_e) (K_i w_i) ,$$

which simplifies to  $a_{e,12} = (r_e \tau / 2) K_e (1 + \rho_e (K_e - 1)) w_e^2$  when excitation and inhibition act independently. A symmetric expression holds for the inhibitory efficacy  $a_{i,12}$ . Plugging the above expressions for synaptic efficacies in the variance expression Eq. (30) yields the small-weight approximation

$$\begin{aligned} \mathbb{V}[V] \simeq & \frac{(1 + \rho_e (K_e - 1)) K_e r_e w_e^2 (V_e - \mathbb{E}[V])^2 + (1 + \rho_i (K_i - 1)) K_i r_i w_i^2 (V_i - \mathbb{E}[V])^2}{2(1/\tau + K_e r_e w_e + K_i r_i w_i)} \\ & + \frac{\rho_{ei} \sqrt{r_e r_i} (K_e w_e) (K_i w_i) [(V_e - \mathbb{E}[V])^2 + (V_i - \mathbb{E}[V])^2 - (V_e - V_i)^2]}{2(1/\tau + K_e r_e w_e + K_i r_i w_i)} . \end{aligned}$$

Let us note that the first-term in the right-hand side above represents the small-weight approximation of the voltage variance in the absence of correlation between excitation and inhibition, i.e., for  $\rho_{ei} = 0$ . Denoting the latter approximation by  $\mathbb{V}[V] |_{\rho_{ei}=0}$  and using the fact that the small-weight expression for the mean voltage

$$\mathbb{E}[V] = \frac{K_e r_e w_e V_e + K_i r_i w_i V_i}{1/\tau + K_e r_e w_e + K_i r_i w_i} ,$$

is independent of correlations, we observe that as intuition suggests, synchrony-based correlation between excitation and inhibition results in a decrease of the neural variability:

$$\Delta \mathbb{V}[V]_{\rho_{ei}} = \mathbb{V}[V] - \mathbb{V}[V] |_{\rho_{ei}=0} \simeq - \frac{\rho_{ei} \sqrt{r_e r_i} (K_e w_e) (K_i w_i) (V_e - \mathbb{E}[V]) (\mathbb{E}[V] - V_i)}{1/\tau + K_e r_e w_e + K_i r_i w_i} \leq 0 .$$

However, the overall contribution of correlation is to increase variability in the small-weight approximation. This can be shown under the assumptions that  $K_e \gg 1$  and  $K_i \gg 1$ , by observing that

$$\begin{aligned} \Delta \mathbb{V}[V]_{\rho_{ei}, \rho_{e/i}} = \mathbb{V}[V] - \mathbb{V}[V] |_{\rho_{e/i} = \rho_{ei} = 0} &\simeq \frac{(\sqrt{\rho_e r_e} K_e w_e (V_e - \mathbb{E}[V]) - \sqrt{\rho_i r_i} K_i w_i (V_i - \mathbb{E}[V]))^2}{2(1/\tau + K_e r_e w_e + K_i r_i w_i)} \\ &+ (\sqrt{\rho_e \rho_i} - \rho_{ei}) \frac{\sqrt{r_e r_i} (K_e w_e) (K_i w_i) (V_e - \mathbb{E}[V]) (\mathbb{E}[V] - V_i)}{1/\tau + K_e r_e w_e + K_i r_i w_i} \geq 0, \end{aligned}$$

where both terms are positive since we always have  $0 \leq \rho_{ei} \leq \sqrt{\rho_e \rho_i}$ .

### Appendix L: Validity of the small-weight approximation

Biophysical estimates of the synaptic weights  $w_e < 0.01$ ,  $w_i < 0.04$  and the synaptic input numbers  $K_e < 10000$ ,  $K_i < 2500$ , suggest that neurons operates in the small-weight regime. In this regime, we claim that exponential corrections due to finite-size effect can be neglected in the evaluation of synaptic efficacies, as long as the spiking correlations remains weak. Here, we make this latter statement quantitative by focusing on the first-order efficacies in the case of excitation alone. The relative error due to neglecting exponential corrections can be quantified as

$$\mathcal{E} = \frac{\mathbb{E}_e[W_e] - \mathbb{E}_e[1 - e^{-W_e}]}{\mathbb{E}_e[1 - e^{-W_e}]} \geq 0.$$

Let us evaluate this relative error, assumed to be small, when correlations are parametrized via beta distributions with parameter  $\beta_e = 1/\rho_e - 1$ . Assuming correlations to be weak,  $\rho_e \ll 1$ , amounts to assuming large,  $\beta_e \gg 1$ . Under the assumptions of small error, we can compute

$$\mathbb{E}_e[1 - e^{-W_e}] \simeq \mathbb{E}_e[W_e] = w_e \mathbb{E}_e[k_e] \quad \text{and} \quad \mathbb{E}_e[W_e - 1 + e^{-W_e}] \simeq \mathbb{E}_e[W_e^2]/2 = w_e^2 \mathbb{E}_e[k_e^2]/2,$$

By the calculations carried out in Appendix L we have

$$b_e \mathbb{E}_e[k_e] = K_e r_e \quad \text{and} \quad b_e \mathbb{E}_e[k_e^2] = K_e r_e (1 + \rho_e (K_e - 1)).$$

Remembering that  $\beta_e = 1/\rho_e - 1$ , this implies that we have

$$\mathcal{E} \simeq \frac{\mathbb{E}_e[W_e^2]/2}{\mathbb{E}_e[W_e] - \mathbb{E}_e[W_e^2]/2} \simeq \frac{w_e (1 + \rho_e (K_e - 1))/2}{1 - w_e (1 + \rho_e (K_e - 1))/2},$$

For a correlation coefficient  $\rho_e \leq 0.05$ , this means that neglecting exponential corrections incurs less than a  $e = 3\%$  error if the number of inputs is smaller than  $K_e \leq 1000$  for moderate synaptic weight  $w_e = 0.001$  or than  $K_e \leq 100$  for large synaptic weight  $w_e = 0.01$ .

### Appendix M: Infinite-size limit with spiking correlations

The computation of the first two moments  $\mathbb{E}[V]$  and  $\mathbb{E}[V^2]$  requires to evaluate various efficacies as expectations. Upon inspection, these expectations are all of the form  $b \mathbb{E}_{ei}[f(W_e, W_i)]$ , where  $f$  is a smooth positive function that is bounded on  $\mathbb{R}^+ \times \mathbb{R}^+$  with  $f(0, 0) = 0$ . Just as for the Lévy-Khintchine decomposition of stable jump processes [71, 72], this observation allows one to generalize our results to processes that exhibit and countable infinity of jumps over finite, nonzero time intervals. For our parametric forms based on beta distributions, such processes emerge in the limit of an arbitrary large number of inputs, i.e., for  $K_e, K_i \rightarrow \infty$ . Let us consider the case of excitation alone for simplicity. Then, we need to make sure that all expectations of the form  $b_e \mathbb{E}_{ei}[f(W_e)]$  remain well-posed in the limit  $K_e \rightarrow \infty$  for smooth, bounded test function  $f$  with  $f(0) = 0$ . To check this, observe that for all  $0 < k \leq K_e$ , we have by Eq. (6) and Eq. (8) that

$$b_e p_{e,k} = \beta r_e \binom{K_e}{k} B(k, \beta + K_e - k) = \beta r_e \frac{\Gamma(K_e + 1)}{\Gamma(k + 1) \Gamma(K_e - k + 1)} \frac{\Gamma(k) \Gamma(\beta + K_e - k + 1)}{\Gamma(\beta + K_e)},$$

where we have introduce the Gamma function  $\Gamma$ . Rearranging terms and using the fact that  $\Gamma(z + 1) = z\Gamma(z)$  for all  $z > 0$ , we obtain

$$b_e p_{e,k} = \frac{\beta r_e}{k} \frac{K_e \Gamma(K_e)}{\Gamma(\beta + K_e)} \frac{\Gamma(\beta + K_e - k)}{(K_e - k) \Gamma(K_e - k)} = \frac{\beta r_e}{k} \left(1 - \frac{k}{K_e}\right)^{\beta-1} + o\left(\frac{1}{K_e}\right),$$

where the last equality is uniform in  $k$  and follows from the fact that for all  $x > 0$ , we have

$$\lim_{z \rightarrow \infty} \frac{\Gamma(z+x)}{\Gamma(z)} = z^x \left( 1 + \binom{x}{2} \frac{1}{z} + o\left(\frac{1}{z}\right) \right)$$

From there, given a test function  $f$ , let us consider

$$\begin{aligned}
b_e \mathbb{E}_e [f(W_e)] &= \int \sum_{k=1}^{K_e} b_e p_{e,k} \delta \left( W_e - \frac{k\Omega_e}{K_e} \right) f(W_e) dW_e, \\
&= \sum_{k=1}^{K_e} b_e p_{e,k} f \left( \frac{k\Omega_e}{K_e} \right), \\
&= r_e \sum_{k=1}^{K_e} \frac{\beta}{k} \left( 1 - \frac{k}{K_e} \right)^{\beta-1} f \left( \frac{k\Omega_e}{K_e} \right) + o(1).
\end{aligned}$$

The order zero term above can be interpreted as a Riemann sum so that one has

$$\begin{aligned}
\lim_{K_e \rightarrow \infty} b_e \mathbb{E}_e [f(W_e)] &= r_e \lim_{K_e \rightarrow \infty} \frac{1}{K_e} \sum_{k=1}^{K_e} \frac{\beta K_e}{k} \left(1 - \frac{k}{K_e}\right) f\left(\frac{k\Omega_e}{K_e}\right), \\
&= r_e \int_0^1 \beta \theta^{-1} (1-\theta)^{\beta-1} f(\theta\Omega_e) d\theta, \\
&= r_e \int_0^{\Omega_e} \frac{\beta}{w} \left(1 - \frac{w}{\Omega_e}\right)^{\beta-1} f(w) dw.
\end{aligned}$$

Thus, the jump densities is specified via the Lévy-Khintchine measure

$$\nu_e(w) = \frac{\beta}{w} \left(1 - \frac{w}{\Omega_e}\right)^{\beta-1},$$

which is a deficient measure for admitting a pole in zero. This singular behavior indicates that the limit jump process obtained when  $K_e \rightarrow \infty$  has a countable infinity of jumps within any finite, nonempty time interval. Generic stationary jump processes with independent increments, as is the case here, are entirely specified by their Lévy-Khintchine measure  $\nu_e$  [71, 72]. Moreover, one can check that given knowledge of  $\nu_e$ , one can consistently estimate the corresponding pairwise spiking correlation as

$$\rho_e = \lim_{K_e \rightarrow \infty} \frac{\mathbb{E}_e [k_e(k_e - 1)]}{\mathbb{E}_e [k_e] (K_e - 1)} = \lim_{K_e \rightarrow \infty} \frac{b_e \mathbb{E}_e [(k_e/K_e)^2]}{b_e \mathbb{E}_e [k_e/K_e]} = \frac{\int_0^{\Omega_e} w^2 \nu_e(w) dw}{\Omega_e \int_0^{\Omega_e} w \nu_e(w) dw}.$$

- [1] M. M. Churchland, B. M. Yu, J. P. Cunningham, L. P. Sugrue, M. R. Cohen, G. S. Corrado, W. T. Newsome, A. M. Clark, P. Hosseini, B. B. Scott, D. C. Bradley, M. A. Smith, A. Kohn, J. A. Movshon, K. M. Armstrong, T. Moore, S. W. Chang, L. H. Snyder, S. G. Lisberger, N. J. Priebe, I. M. Finn, D. Ferster, S. I. Ryu, G. Santhanam, M. Sahani, and K. V. Shenoy, *Nature Neuroscience* **13**, 369 EP (2010).
- [2] D. Tolhurst, J. A. Movshon, and I. Thompson, *Experimental brain research* **41**, 414 (1981).
- [3] D. J. Tolhurst, J. A. Movshon, and A. F. Dean, *Vision research* **23**, 775 (1983).
- [4] M. M. Churchland, M. Y. Byron, S. I. Ryu, G. Santhanam, and K. V. Shenoy, *Journal of Neuroscience* **26**, 3697 (2006).
- [5] J. Rickert, A. Riehle, A. Aertsen, S. Rotter, and M. P. Nawrot, *Journal of Neuroscience* **29**, 13870 (2009).
- [6] V. Braatenberg and A. Schüz, *Cortex: statistics and geometry of neuronal connectivity* (Springer Science & Business Media, 2013).
- [7] A. Renart, J. de la Rocha, P. Bartho, L. Hollender, N. Parga, A. Reyes, and K. D. Harris, *Science* **327**, 587 (2010).
- [8] A. S. Ecker, P. Berens, G. A. Keliris, M. Bethge, N. K. Logothetis, and A. S. Tolias, *science* **327**, 584 (2010).
- [9] M. R. Cohen and A. Kohn, *Nature neuroscience* **14**, 811 (2011).
- [10] W. R. Softky and C. Koch, *Cortical cells should fire regularly, but do not* (1992).
- [11] A. Bell, Z. F. Mainen, M. Tsodyks, and T. J. Sejnowski,

La Jolla, CA: Institute for Neural Computation Technical Report INC-9502 (1995).

[12] H. Sompolinsky, A. Crisanti, and H. J. Sommers, *Phys. Rev. Lett.* **61**, 259 (1988).

[13] van Vreeswijk C. and S. H., *Science* **274**, 1724 (1996).

[14] D. J. Amit and N. Brunel, *Cerebral cortex* (New York, NY: 1991) **7**, 237 (1997).

[15] C. v. Vreeswijk and H. Sompolinsky, *Neural Computation*, *Neural Computation* **10**, 1321 (1998).

[16] N. Brunel, *Journal of computational neuroscience* **8**, 183 (2000).

[17] A. Y. Y. Tan, S. Andoni, and N. J. Priebe, *Neuroscience* **247**, 364 (2013).

[18] A. Y. Y. Tan, Y. Chen, B. Scholl, E. Seidemann, and N. J. Priebe, *Nature* **509**, 226 EP (2014).

[19] M. Okun, N. A. Steinmetz, L. Cossell, M. F. Iacaruso, H. Ko, P. Barthó, T. Moore, S. B. Hofer, T. D. Mrsic-Flogel, M. Carandini, *et al.*, *Nature* **521**, 511 (2015).

[20] D. Hansel and C. van Vreeswijk, *Journal of Neuroscience* **32**, 4049 (2012).

[21] J. J. Pattadkal, G. Mato, C. van Vreeswijk, N. J. Priebe, and D. Hansel, *Cell reports* **24**, 2042 (2018. PMC6179374).

[22] M. N. Shadlen and W. T. Newsome, *Journal of neuroscience* **18**, 3870 (1998).

[23] Y. Chen, W. S. Geisler, and E. Seidemann, *Nature neuroscience* **9**, 1412 (2006).

[24] A. Polk, A. Litwin-Kumar, and B. Doiron, *Proceedings of the National Academy of Sciences* **10.1073/pnas.1121274109** (2012), <http://www.pnas.org/content/early/2012/03/27/1121274109>.

[25] I. Lampl, I. Reichova, and D. Ferster, *Neuron* **22**, 361 (1999).

[26] J. Yu and D. Ferster, *Neuron* **68**, 1187 (2010).

[27] S. Arroyo, C. Bennett, and S. Hestrin, *Neuron* **99**, 1289 (2018).

[28] M. Okun and I. Lampl, *Nature neuroscience* **11**, 535 (2008).

[29] Y. Zerlaut, S. Zucca, S. Panzeri, and T. Fellin, *Cell reports* **27**, 1119 (2019).

[30] A. Sanzeni, M. H. Histed, and N. Brunel, *Physical Review X* **12**, 011044 (2022).

[31] R. B. Stein, *Biophysical Journal* **5**, 173 (1965).

[32] H. C. Tuckwell, *Introduction to theoretical neurobiology: linear cable theory and dendritic structure*, Vol. 1 (Cambridge University Press, 1988).

[33] S. Marcus, *IEEE Transactions on Information theory* **24**, 164 (1978).

[34] S. I. Marcus, *Stochastics: An International Journal of Probability and Stochastic Processes* **4**, 223 (1981).

[35] A. Destexhe, M. Rudolph, J.-M. Fellous, and T. Sejnowski, *Neuroscience* **107**, 13 (2001).

[36] H. Meffin, A. N. Burkitt, and D. B. Grayden, *Journal of computational neuroscience* **16**, 159 (2004).

[37] B. Doiron, A. Litwin-Kumar, R. Rosenbaum, G. K. Ocker, and K. Josić, *Nature neuroscience* **19**, 383 (2016).

[38] G. K. Ocker, Y. Hu, M. A. Buice, B. Doiron, K. Josić, R. Rosenbaum, and E. Shea-Brown, *Current opinion in neurobiology* **46**, 109 (2017).

[39] W. Rall, *Biophysical Journal* **9**, 1483 (1969).

[40] D. J. Daley and D. Vere-Jones, *An introduction to the theory of point processes. Vol. I. Probability and its Applications* (New York). Springer-Verlag, New York,, 2003).

[41] D. J. Daley and D. Vere-Jones, *An introduction to the theory of point processes: volume II: general theory and structure* (Springer Science & Business Media, 2007).

[42] B. W. Knight, *The Journal of general physiology* **59**, 767 (1972).

[43] B. Knight, *The Journal of general physiology* **59**, 734 (1972).

[44] J. F. Kingman, *The Annals of Probability* **6**, 183 (1978).

[45] D. J. Aldous, in *École d'Été de Probabilités de Saint-Flour XIII—1983* (Springer, 1985) pp. 1–198.

[46] B. De Finetti, in *Atti del Congresso Internazionale dei Matematici: Bologna del 3 al 10 de settembre di 1928* (1929) pp. 179–190.

[47] A. K. Gupta and S. Nadarajah, *Handbook of beta distribution and its applications* (CRC press, 2004).

[48] J. H. Macke, P. Berens, A. S. Ecker, A. S. Tolias, and M. Bethge, *Neural computation* **21**, 397 (2009).

[49] N. L. Hjort, *the Annals of Statistics* , 1259 (1990).

[50] R. Thibaux and M. I. Jordan, in *Artificial intelligence and statistics* (PMLR, 2007) pp. 564–571.

[51] T. Broderick, M. I. Jordan, and J. Pitman, *Bayesian analysis* **7**, 439 (2012).

[52] P. Diaconis, *Bayesian statistics* **3**, 111 (1988).

[53] P. Berkes, F. Wood, and J. Pillow, *Advances in neural information processing systems* **21** (2008).

[54] N. Balakrishnan and C. D. Lai, *Continuous bivariate distributions* (Springer Science & Business Media, 2009).

[55] K. Itô, *Proceedings of the Imperial Academy* **20**, 519 full.pdf+44.

[56] R. Stratonovich, *SIAM Journal on Control* **4**, 362 (1966).

[57] A. Chechkin and I. Pavlyukevich, *Journal of Physics A: Mathematical and Theoretical* **47**, 342001 (2014).

[58] K. Matthes, in *Trans. Third Prague Conf. Information Theory, Statist. Decision Functions, Random Processes (Liblice, 1962)* (Publ. House Czech. Acad. Sci., Prague, 1964) pp. 513–528.

[59] M. J. Richardson and W. Gerstner, *Neural computation* **17**, 923 (2005).

[60] M. J. Richardson and W. Gerstner, *Chaos: An Interdisciplinary Journal of Nonlinear Science* **16**, 026106 (2006).

[61] A. Arieli, A. Sterkin, A. Grinvald, and A. Aertsen, *Science* **273**, 1868 (1996).

[62] Z. Mainen and T. Sejnowski, *Science* **268**, 1503 (1995).

[63] F. Rieke, D. Warland, R. de Ruyter van Steveninck, and W. Bialek, *Spikes*, A Bradford Book (MIT Press, Cambridge, MA, 1999) pp. xviii+395, exploring the neural code, *Computational Neuroscience*.

[64] W. R. Softky and C. Koch, *Journal of neuroscience* **13**, 334 (1993).

[65] R. M. Bruno and B. Sakmann, *Science* **312**, 1622 (2006).

[66] J.-S. Jouhanneau, J. Kremkow, A. L. Dorrn, and J. F. Poulet, *Cell reports* **13**, 2098 (2015).

[67] A. Pala and C. C. Petersen, *Neuron* **85**, 68 (2015).

[68] S. C. Seeman, L. Campagnola, P. A. Davoudian, A. Hoggarth, T. A. Hage, A. Bosma-Moody, C. A. Baker, J. H. Lee, S. Mihalas, C. Teeter, *et al.*, *elife* **7**, e37349 (2018).

[69] L. Campagnola, S. C. Seeman, T. Chartrand, L. Kim, A. Hoggarth, C. Gamlin, S. Ito, J. Trinh, P. Davoudian,

C. Radaelli, M.-H. Kim, T. Hage, T. Braun, L. Alfilier, J. Andrade, P. Bohn, R. Dalley, A. Henry, S. Kebede, A. Mukora, D. Sandman, G. Williams, R. Larsen, C. Teeter, T. L. Daigle, K. Berry, N. Dotson, R. Enstrom, M. Gorham, M. Hupp, S. D. Lee, K. Ngo, P. R. Nicovich, L. Potekhina, S. Ransford, A. Gary, J. Goldy, D. McMillen, T. Pham, M. Tieu, L. Siverts, M. Walker, C. Farrell, M. Schroeder, C. Slaughterbeck, C. Cobb, R. Ellenbogen, R. P. Gwinn, C. D. Keene, A. L. Ko, J. G. Ojemann, D. L. Silbergeld, D. Carey, T. Casper, K. Crichton, M. Clark, N. Dee, L. Ellingwood, J. Gloe, M. Kroll, J. Sulc, H. Tung, K. Wadhwan, K. Brouner, T. Egdorf, M. Maxwell, M. McGraw, C. A. Pom, A. Ruiz, J. Bomben, D. Feng, N. Hejazinia, S. Shi, A. Szafer, W. Wakeman, J. Phillips, A. Bernard, L. Esposito, F. D. D’Orazi, S. Sunkin, K. Smith, B. Tasic, A. Arkhipov, S. Sorensen, E. Lein, C. Koch, G. Murphy, H. Zeng, and T. Jarsky, *Science* **375**, eabj5861 (2022), <https://www.science.org/doi/pdf/10.1126/science.abj5861>.

[70] A. Destexhe, M. Rudolph, and D. Paré, *Nature reviews neuroscience* **4**, 739 (2003).

[71] A. Khintchine, *Mathematische Annalen* **109**, 604 (1934).

[72] P. Lévy and P. Lévy, *Théorie de l’addition des variables aléatoires* (Gauthier-Villars, 1954).

[73] B. F. Qaqish, *Biometrika* **90**, 455 (2003).

[74] E. Niebur, *Neural Computation* **19**, 1720 (2007).

[75] J. H. Macke, L. Buesing, J. P. Cunningham, B. M. Yu, K. V. Shenoy, and M. Sahani, *Advances in neural information processing systems* **24** (2011).

[76] J. W. Pillow, J. Shlens, L. Paninski, A. Sher, A. M. Litke, E. Chichilnisky, and E. P. Simoncelli, *Nature* **454**, 995 (2008).

[77] I. M. Park, E. W. Archer, K. Latimer, and J. W. Pillow, *Advances in neural information processing systems* **26** (2013).

[78] L. Theis, A. M. Chagas, D. Arnstein, C. Schwarz, and M. Bethge, *PLoS computational biology* **9**, e1003356 (2013).

[79] E. Schneidman, M. J. Berry, R. Segev, and W. Bialek, *Nature* **440**, 1007 (2006).

[80] E. Granot-Atedgi, G. Tkačik, R. Segev, and E. Schneidman, *PLoS computational biology* **9**, e1002922 (2013).

[81] S. M. Bohté, H. Spekreijse, and P. R. Roelfsema, *Neural Computation* **12**, 153 (2000).

[82] S.-i. Amari, H. Nakahara, S. Wu, and Y. Sakai, *Neural computation* **15**, 127 (2003).

[83] B. Staude, S. Rotter, and S. Grün, *Journal of computational neuroscience* **29**, 327 (2010).

[84] B. Staude, S. Rotter, *et al.*, *Frontiers in computational neuroscience* , 16 (2010).

[85] M. Shelley, D. McLaughlin, R. Shapley, and J. Wieland, *Journal of computational neuroscience* **13**, 93 (2002).

[86] M. Rudolph and A. Destexhe, *Neural Computation* **15**, 2577 (2003).

[87] A. Kumar, S. Schrader, A. Aertsen, and S. Rotter, *Neural computation* **20**, 1 (2008).

[88] N. G. Van Kampen, *Stochastic processes in physics and chemistry*, Vol. 1 (Elsevier, 1992).

[89] H. Risken, in *The Fokker-Planck Equation* (Springer, 1996) pp. 63–95.

[90] F. Baccelli and T. Taillefumier, *SIAM Journal on Applied Dynamical Systems* **18**, 1756 (2019).

[91] F. Baccelli and T. Taillefumier, *SIAM Journal on Applied Dynamical Systems* **20**, 165 (2021).

[92] L. Yu and T. O. Taillefumier, *PLoS Computational Biology* **18**, e1010215 (2022).

[93] F. Baccelli and P. Brémaud, in *Elements of Queueing Theory* (Springer, 2003) pp. 1–74.

[94] M. J. Richardson and R. Swarbrick, *Physical review letters* **105**, 178102 (2010).

[95] R. Iyer, V. Menon, M. Buice, C. Koch, and S. Mihalas, *PLoS computational biology* **9**, e1003248 (2013).

[96] F. Droste and B. Lindner, *Journal of Computational Neuroscience* **43**, 81 (2017).

[97] M. Tamborrino and P. Lansky, *Physica D: Nonlinear Phenomena* **418**, 132845 (2021).

[98] L. F. Abbott and C. van Vreeswijk, *Phys. Rev. E* **48**, 1483 (1993).

[99] J. Baladron, D. Fasoli, O. Faugeras, and J. Touboul, *The Journal of Mathematical Neuroscience* **2**, 10 (2012).

[100] J. Touboul, G. Hermann, and O. Faugeras, *SIAM Journal on Applied Dynamical Systems* **11**, 49 (2012).

[101] P. Robert and J. Touboul, *J. Stat. Phys.* **165**, 545 (2016).

[102] M. London, A. Roth, L. Beeren, M. Häusser, and P. E. Latham, *Nature* **466**, 123 EP (2010).

[103] B. B. Averbeck, P. E. Latham, and A. Pouget, *Nature Reviews Neuroscience* **7**, 358 EP (2006).

[104] A. S. Ecker, P. Berens, A. S. Tolias, and M. Bethge, *Journal of Neuroscience* **31**, 14272 (2011), <http://www.jneurosci.org/content/31/40/14272.full.pdf>.

[105] Y. Hu, J. Zylberberg, and E. Shea-Brown, *PLOS Computational Biology* **10**, 1 (2014).

[106] B. Scholl, C. I. Thomas, M. A. Ryan, N. Kamasawa, and D. Fitzpatrick, *Nature* **590**, 111 (2021).

[107] J. de la Rocha, B. Doiron, E. Shea-Brown, K. Josić, and A. Reyes, *Nature* **448**, 802 EP (2007).

[108] G. Buzsáki and K. Mizuseki, *Nature Reviews Neuroscience* **15**, 264 (2014).

[109] A. Amarasingham, S. Geman, and M. T. Harrison, *Proceedings of the National Academy of Sciences* **112**, 6455 (2015).

[110] R. Brette, *Frontiers in systems neuroscience* **9**, 151 (2015).

[111] A. Litwin-Kumar and B. Doiron, *Nature neuroscience* **15**, 1498 (2012).

[112] R. Rosenbaum, M. A. Smith, A. Kohn, J. E. Rubin, and B. Doiron, *Nature neuroscience* **20**, 107 (2017).

[113] A.-S. Sznitman, in *École d’Été de Probabilités de Saint-Flour XIX—1989*, Lecture Notes in Math., Vol. 1464 (Springer, Berlin, 1991) pp. 165–251.

[114] X. Erny, E. Löcherbach, and D. Loukianova, *Electronic Journal of Probability* **26**, 1 (2021).